Heterologous expression and characterization of lignocellulose degradation enzymes of wood rotting fungus *Ceriporiopsis subvermispora*, manganese peroxidases and glucuronoyl esterases

Meng-I Lin

Table of contents

Chapter 1. General introduction

1.1 Renewable energy and biomass

Global climate change and rising sea levels make reduction of carbon emissions very necessary. Discovery and development of sustainable and affordable renewable energy sources have become a hot topic. In 2016, nearly 18.2% of global energy consumed was from renewable sources, including hydropower, solar photovoltaic, wind power, geothermal, and biomass ones (1). Among the latter, we focus on application of biomass in this study. Biomass is a source derived from living or recently living organisms, and is composed of carbon, hydrogen, and oxygen. It can be converted to usable sources of energy like methane gas or transportation fuels such as bioethanol and biodiesel. Biofuels can be produced from various sources, for example, starch, sugar, vegetable oil, lignocellulose, algae and so on. Processes for producing biofuels from starch and sugar have been well established and have led to significant achievements. However, it remains a controversial issue because the production of energy from food, such as corn and sugar cane, may lead to a food crisis.

1.2 Wood biomass

Nonfood biomass resources are superior for ensuring food security and thus are being considered for more sustainable feedstocks. Wood biomass, or lignocellulose biomass, is one of the most abundant materials in the world and can be used for producing both fuel and chemicals. However, the efficiency of utilizing wood biomass is problematic due to its recalcitrant structure.

Wood consists of 35-45% cellulose, 25-35% hemicellulose, and 20-30% lignin (**Fig. 1-1**). Cellulose is a beta-linked glucose (a C6 sugar) polymer; hemicellulose is a branched chain of C5 sugars and C6 sugars including xylose, arabinose, glucose, mannose, and galactose; whereas lignin has a stable polymer backbone made from phenolic groups. Lignin links hemicellulose and grips on cellulose, and due to this complex structure in wood, it is much more difficult for cellulose and hemicellulose to be broken down into sugar. Thus, to increase the feasibility of converting cellulose and hemicellulose to biofuels, additional pretreatment to either degrade or separate lignin from polysaccharides is necessary.

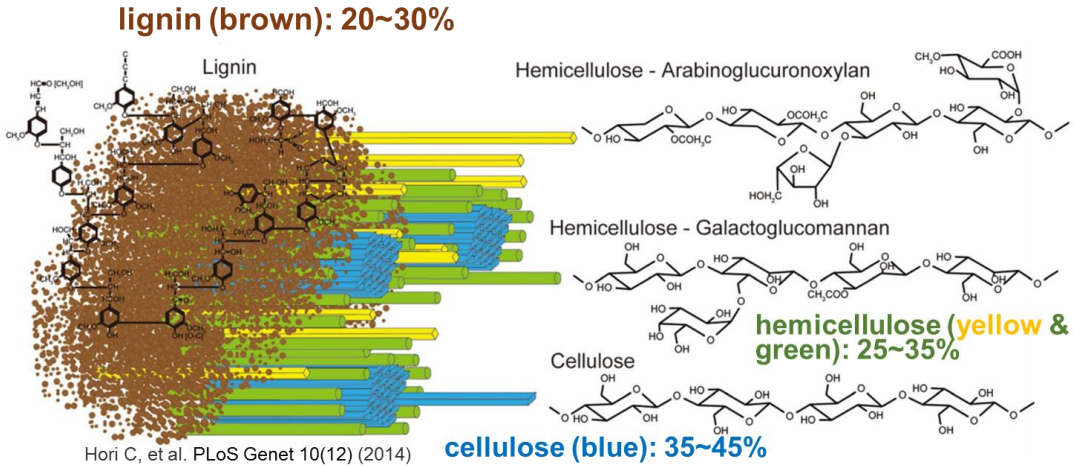

Fig. 1-1. Three main components in wood biomass. This figure is adapted from (2).

Aside from the utilization of cellulose and hemicellulose, the unique structure and chemical properties of lignin make it the only renewable source of aromatic chemicals. To increase the sugar yield and to make full application of all three components in wood biomass, several pretreatment methods have been developed. The various lignin pretreatments involving different conditions alter the chemical structure and linkages of lignin to different extents. A few predominant methods are briefly described below. Kraft lignin, isolated through processes in the pulp and paper industries, is said not to be suitable for producing valuable chemicals. Klason lignin is considered as the standard for measuring the lignin content; however the process involving 72% sulfuric acid changes the lignin structure extensively. Milled wood lignin (MWL) is thought to be the most appropriate and least altered lignin preparation for chemical and biological studies, but it needs further purification, which results in a lower yield. The pyrolysis, steam explosion, ammonia fiber explosion, and hot water processes can also break lignin down to some extent, but the energy demand for these processes is high. In addition to the above mentioned pretreatment processes, biological pretreatment using wood-rotting fungi that are able to degrade cell walls under mild conditions has also received a lot of attention.

1.3 Wood-rotting fungi

For lignocellulose degradation, three types of wood-rotting fungi are being intensively studied, soft rot fungi, brown rot fungi, and white rot fungi.

Soft rot fungi are taxonomically classified into the phylum *Ascomycota* and were

first identified in high moisture-containing wood (3). Soft rot fungi mainly attack low lignin content materials and exhibit a high preference for degrading carbohydrates. Soft rot fungi are much more widespread than the other two types. They have been discovered in not only wet environments but also under dry or extreme environmental conditions, for example, in ancient wooden tomb objects and historic expedition huts in Antarctica (4, 5). Among the three types of wood-rotting fungi, it is reported that soft rot fungi harbor the highest number of genes encoding cellulolytic, hemicellulolytic and pectinolytic enzymes (6).

Both brown rot fungi and white rot fungi are taxonomically classified into the phylum *Basidiomycota*, and many species and characteristics have been studied. Brown rot fungi are ubiquitous on coniferous wood, and intensively break cellulose and hemicellulose down so that the rotted wood has a brown appearance. In addition to degradation of polysaccharides, a high proportion of demethylated lignins is also observed during wood degradation by brown rot fungi (7, 8). The degradation of polysaccharides and the structural modification of lignin, including depolymerization and repolymerization, are considered to be initiated by a non-enzymatic Fenton reaction (9-11).

Differing from soft rot and brown rot fungi, white rot fungi secrete several types of ligninolytic enzymes and are capable of degrading not only polysaccharides but also lignin enzymatically (12, 13). As lignin is being degraded, the rotting wood appears lighter-colored or bleached. Two degradation patterns have been found for white rot fungi, simultaneous degradation of lignin and polysaccharides or selective degradation of lignin prior to polysaccharides. Interestingly, some fungi are reported to exhibit both patterns (14). The number of genes encoding ligninolytic enzymes in white rot fungi is significantly higher than those in the other two types (6). The ability to efficiently degrade lignin or separate lignin from polysaccharides and the variety of lignocellulosic enzymes, especially ligninolytic enzymes, of white rot fungi are expected to provide an efficient way of utilizing wood or lignocellulosic biomass.

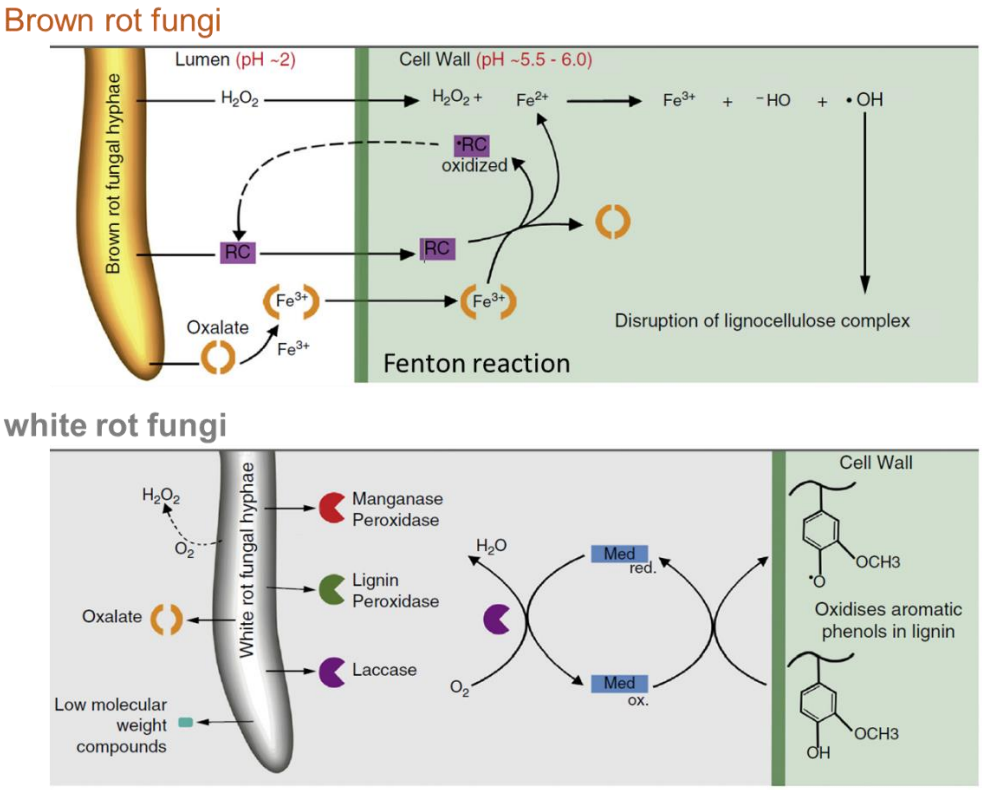

Fig. 1-2. Lignin structure modification by brown rot fungi and lignin degradation by white rot fungi. RC, reducing compounds. Med, mediators. This figure is adapted from (15).

1.4 Lignocellulosic enzymes

Lignocellulosic enzymes include enzymes which are able to degrade cellulose, hemicellulose, pectin, and lignin. These enzymes are categorized into five classes and one associated module in the Carbohydrate-Active Enzymes (CAZy) database (16, 17), glycoside hydrolases (GH), glycosyl transferases (GT), polysaccharide lyases (PL), carbohydrate esterases (CE), auxiliary activities (AA), and carbohydrate-binding domains (CBM).

There are three major groups of cellulose-degrading enzymes from wood-rotting fungi, endo-glucanases (EGs, EC 3.2.1.4), cellobiohydrolases (CBHs, EC 3.2.1.91), and β-glucosidases (BGLs, EC 3.2.1.21) (18, 19). The EGs and CBHs hydrolyze interval and terminal cellulose chains, respectively, and release cellulooligosaccharides and cellobiose. The resulting short oligosaccharide chains can then be cleaved into glucose by the BGLs. The major enzymes converting cellulose to glucose are shown in **Fig. 1-2**. In addition to these three well-characterized enzymes, cellobiose dehydrogenase (CDH, EC 1.1.99.18)

together with lytic polysaccharide monooxygenase (LPMO, EC 1.14.99.54) were recently reported to participate in the degradation of cellulose (20).

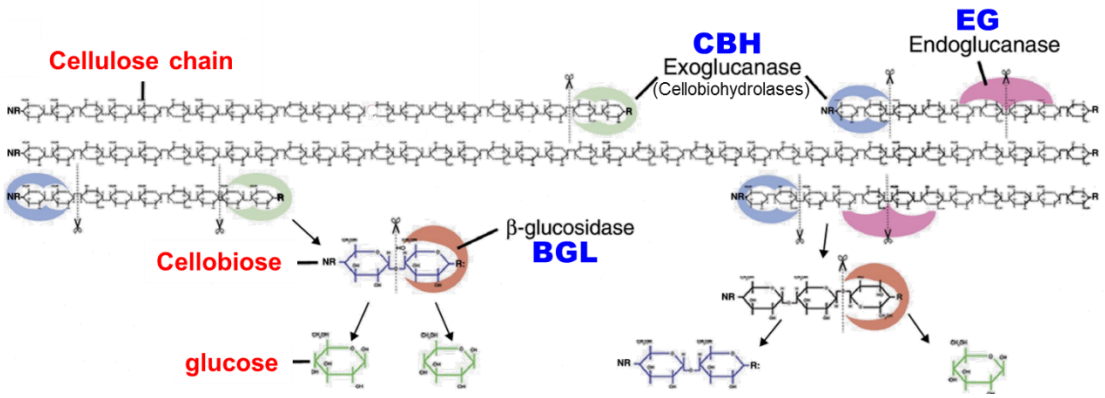

Fig. 1-3. Cellulose degradation by EGs, CBHs, and BGLs. EGs and CBHs catalyze the cleavage of internal and terminal bonds in cellulose chains, respectively. BGLs then break short oligosaccharide chains or cellobiose down into glucose. This figure is adapted from (15) and slightly modified.

Several types of enzymes are involved in the degradation of hemicellulose and most of these hemicellulose-degrading enzymes are glycoside hydrolases (GHs) and carbohydrate esterases (CEs) (**Fig. 1-3**).

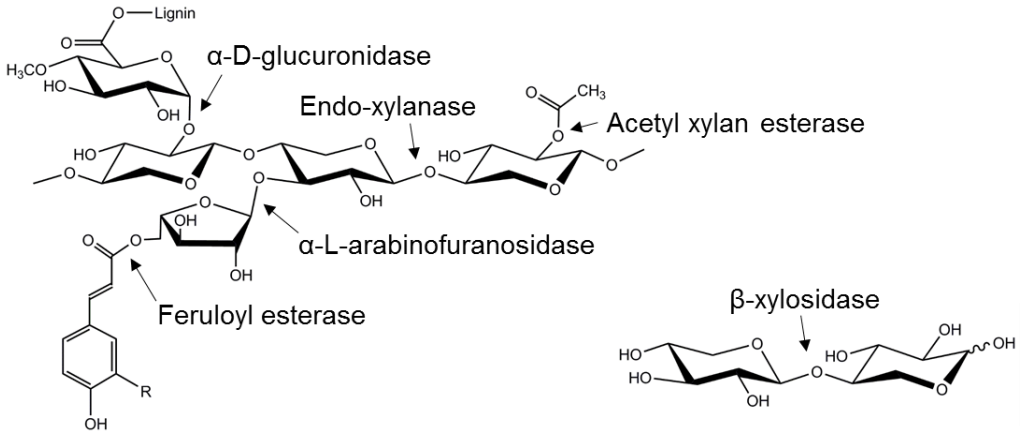

Fig. 1-4. Representative hemicellulose-degrading enzymes.

Ligninolytic enzymes include four major types of oxidizing enzymes, lignin peroxidases (LiP, EC 1.11.1.14), manganese peroxidases (MnP, EC 1.11.1.13), versatile peroxidases (VPs, EC 1.11.1.16), and laccases (EC 1.10.3.1), and some auxiliary enzymes, such as aryl-alcohol oxidases (AAOs, EC 1.1.3.7) and P450 monooxygenases (EC

1.14.14.1). LiPs, MnPs and VPs belong to AA2, and laccases belong to AA1 in the CAZy database. The three AA2 peroxidases are all heme-peroxidases and the degradation of lignin by these peroxidases is initiated by H_2O_2, while laccases are multi-copper oxidases and their activity is induced by copper ions (21). Among these four oxidizing enzymes, LiPs and VPs are able to degrade both non-phenolic and phenolic lignin. On the other hand, although MnPs and laccases are also capable of degrading phenolic lignin, appropriate redox mediators are said to be indispensable for them to degrade non-phenolic lignin (22-26).

1.5 Manganese peroxidases (MnPs)

MnP was first discovered in white rot fungus *Phanerochaete chrysosporium*, which can degrade lignin and polysaccharides simultaneously (27, 28). MnPs were then found in all white rot fungi and hence are considered to play an important role in lignin degradation.

The crystal structure of MnP from *P. chrysosporium* showed that Mn^{2+} could only bind to one heme propionate and the side chains of three amino acids, two Glu and one Asp (**Fig. 1-5**) (29, 30). MnP has five disulfide bonds and two calcium ions, which are important for maintaining the heme environment (31).

MnPs are extracellular heme enzymes that are able to catalyze the peroxide-dependent oxidation of Mn^{2+} to Mn^{3+}. The catalytic cycle of MnPs resembles that of other heme peroxidases but MnPs are the only heme peroxidases that use Mn^{2+} as a substrate. The catalytic oxidation by MnPs is initiated by H_2O_2 and the binding of H_2O_2 to the Fe^{3+} ion in heme leads to the formation of an iron peroxide complex. Then, the electrons transfer from Fe^{3+} to the peroxide results in cleavage of the oxygen-peroxide bond and the formation of a Fe^{4+}-oxo-porphyrin radical complex, MnP-Compound I (**Fig. 1-6**). Then, Mn^{2+} binds and donates an election to MnP-Compound I, and Mn^{3+} and MnP-Compound II are released. MnP-Compound II is able to oxidize the second Mn^{2+} to Mn^{3+} and thereby to be reduced to the native enzyme. The released Mn^{3+} is chelated and stabilized by carboxylic acid, and then is ready to act as a mediator facilitating lignin degradation.

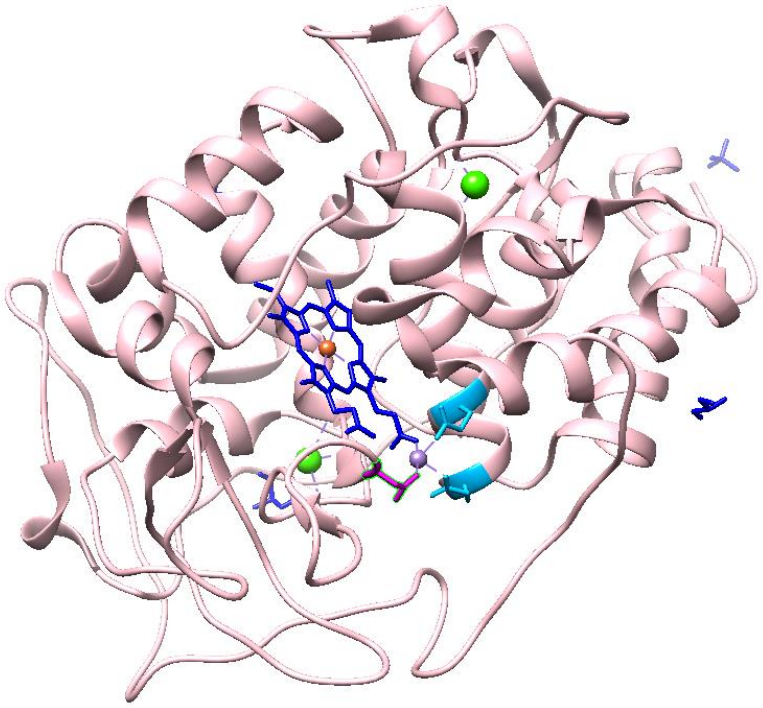

Fig. 1-5. Crystal structure of MnP from *P. chrysosporium* (PDB id: 1YYD).
The colors indicate the heme propionate (navy blue), Fe^{3+} ion in heme (brown), two Ca^{2+} ions (green), Mn^{2+} ion (purple), and two Glu (light blue) and one Asp (magenta) for the binding of Mn^{2+}.

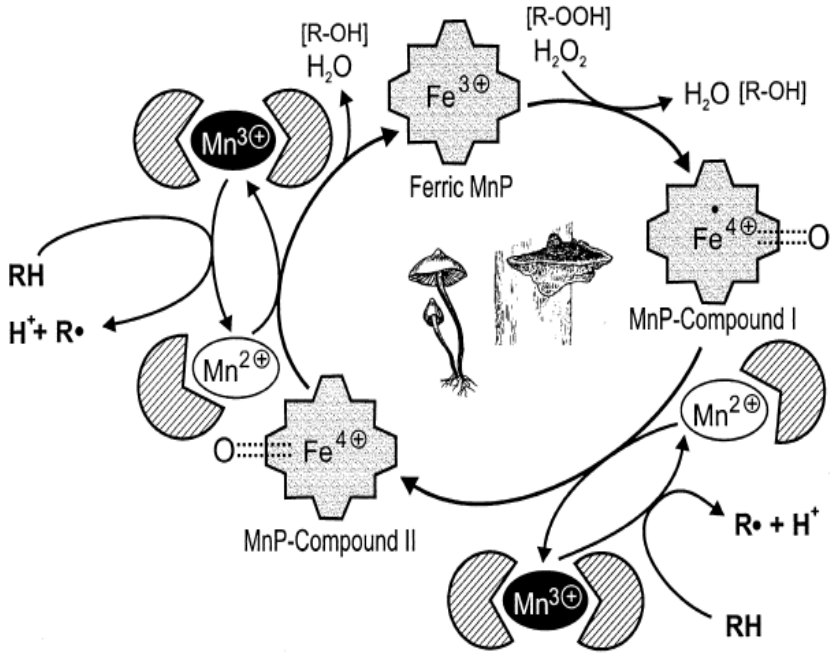

Fig. 1-6. The catalytic cycle of MnP.
This figure is adapted from (32).

1.6 Glucuronoyl esterases (GEs)

The lignin-carbohydrate complex (LCC) found in the recalcitrant woody biomass is a complex of lignin and hemicellulose that are covalently linked through a covalent bond such as γ-ester, benzyl-ether, and phenyl-glycoside bonds. A lignocellulose degrading enzyme that has the ability to hydrolyze the ester bond formed between the lignin alcohol and 4-*O*-methyl-D-glucuronic acid of glucuronoxylans was first discovered for the wood rotting fungus *Schizophyllum commune*, and was named glucuronoyl esterase (GE) (33) (**Fig. 1-7**).

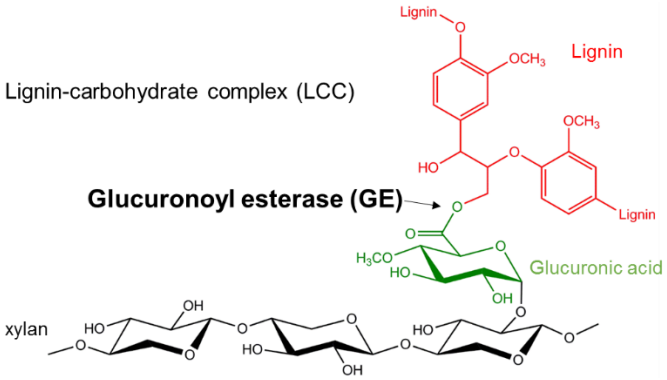

Fig. 1-7. Representative structure of the linkage between glucuronic acid and lignin alcohol which could be cleaved by GE.

After the discovery of this GE of *S. commune* (*Sc*GE), homologous genes were searched for, and many orthologues were found in the genomes of several filamentous fungi and one bacterium (34). The finding of a group containing these orthologues led to the establishment of a new carbohydrate esterase (CE) family, CE15, in the CAZys database (34). GEs of the CE15 family were found to exhibit distant phylogeny from already known acetylxylan esterases (CE1 and CE5 families), feruloyl esterases (CE1 and CE3 families), and pectin methyl esterases (CE8 family) (35). It is appropriate to regard the CE15 family as a new family since the esterase activity of *Sc*GE was shown to be distinct from those of esterases belonging to other families: *Sc*GE was not capable of hydrolyzing the substrates of esterases of other families and *vice versa*. (33). GEs in the CE15 family are mainly found in bacteria, fungi, and plants; GEs of bacteria are suggested to have different properties to those of fungi. In this study, we focus on fungal GEs (FGEs).

The alignment of the amino acid sequences of FGE from *Sporotrichum thermophile* (*St*GE2) with those of several other homologues, all belonging to the CE15 family, has revealed a consensus sequence, G-C-S-R-X-G, in which serine turned out to be a putative nucleophilic catalytic center (36, 37). Substitution of this serine resulted in a complete loss of esterase activity against methyl 4-*O*-methyl-D-glucopyranuronate (36). Later, the first crystal structure of an FGE, i.e., that from *Hypocrea jecorina* (anamorph, *Trichoderma reesei*), was solved and the classical hydrolytic enzyme catalytic triad, Ser-His-Glu, containing the above-mentioned serine, was shown to constitute the active site (38) (**Fig. 1-8**). These studies established that FGE is a serine-type esterase. It has also been reported that some FGEs contain not only a catalytic domain (CE15 domain) but also a carbohydrate binding module (CBM) domain, which is known to increase the enzymatic efficiency as to solid and insoluble substrates.

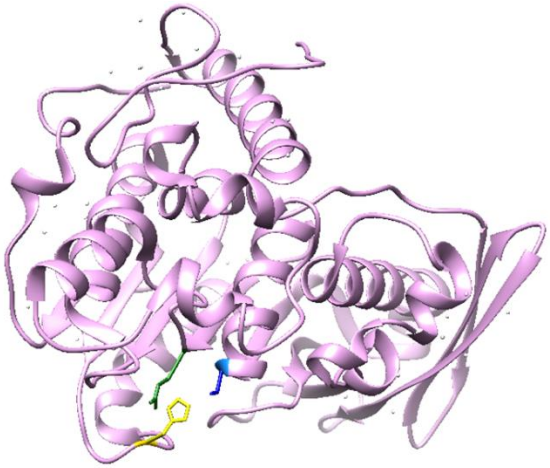

Fig. 1-8. The crystal structure of the GE from *Trichoderma reesei* (PDB id 3pic). The catalytic triad was marked in blue (serine), yellow (histidine) and green (glutamic acid).

1.7 The aim of this study

Biological pretreatments for removing or separating lignin from polysaccharides are expected to improve utilization of wood biomass. Among lignocellulotic enzymes, MnP is the most popular and common one for lignin degradation, and FGE is a newly discovered enzyme that can efficiently cleave the ester bonds between lignin and hemicellulose. To expand knowledge on these two enzymes, in this study we focus on characterization of both the MnPs and FGEs of different groups that have distinct

properties. White rot fungus *Ceriporiopsis subvermispora* was considered as the best candidate for this study because it selectively degrade lignin prior to polysaccharides and is the only white rot fungi that secretes all MnPs in different subfamilies. Moreover, the high abundance of the FGE secreted by *C. subvermispora* on growth in medium containing aspen wood was reported (39). For MnPs, we started by developing a method for their expression and purification. Then, the activities of the MnPs were characterized by using different substrates. For FGEs, we first performed phylogenetic analysis of about four hundred putative FGEs to find out whether the FGEs in different subfamilies have some unique properties. The expression and purification of the selected FGEs were also performed and their activities were characterized.

Chapter 2. Production of MnPs by *E. coli*

2.1 Introduction

The molecular mechanisms of the action of fungal lignin-degrading enzymes have not been well characterized yet, mostly because the low expression levels and/or relatively time-consuming production of those enzymes through homologous expression hindered detailed analysis. Various attempts at heterologous expression have also been made using *P. chrysosporium* (40, 41), *Aspergillus niger* (42), *Aspergillis oryzae* (43), and *Pichia pastoris* (44, 45). For such heterologous expression, however, the same problem was encountered.

E. coli has been the most used host and various kinds of expression systems have been developed for it. However, the reducing environment of the *E. coli* cytoplasm is unfavorable for proteins to form disulfide bonds, which often leads to incorrect folding and aggregation of proteins containing multiple cysteine residues. This may be the reason why fungal peroxidases expressed in *E. coli* often result in inclusion bodies (IBs). *In vitro* refolding would be a way to obtain correctly folded, active proteins (46-48). However, less than 1.5 mg of each active peroxidase was obtained from 1 L culture (49-51). A severe drawback of the refolding procedure is that optimum refolding conditions are often different for individual proteins. Therefore, to avoid the refolding process, many efforts have been made to express peroxidases in soluble form in *E. coli*. For example, expression of VP with a thioredoxin tag (52, 53) was reported to improve solubility. More recently, the first soluble MnP was obtained from *E. coli* by adding Triton X-100, Tween-80, glycerol, and ethanol to the culture (51). However, the Rz values ($\text{Absorbance}_{\text{Soret peak maximum}}/\text{Absorbance}_{280\text{ nm}}$), which are a measure of the heme content in heme proteins, of the soluble enzymes were far lower than those of native peroxidases, which are typically more than 3 (48, 54-56).

So far, there is no promising strategy for expressing soluble MnPs with sufficient heme incorporation in *E. coli*. In this study, we developed a way to overcome the problem of IB formation. We also developed a way to increase the heme content for an *E.coli* heterologous expression system. Here, four MnPs from three MnP subfamilies (extralong, long, and short MnPs) in *C. subvermispora* were selected as model proteins for developing a universal method for MnP production: MnP124076 is the only “short MnP”

found in *C. subvermispora*; MnP157986 is an "extralong MnP", and has the longest amino acid sequence; and MnP50297 and MnP117436 are an "extralong MnP" and a "long MnP", respectively, and they are the most abundantly produced MnPs in each subfamily by *C. subvermispora* grown in aspen wood-containing medium (39) (the MnP numbers refer to those made by the US Department of Energy, Joint Genome Institute) (57).

2.2 Results

2.2.1 *In vitro* refolding

The expression of MnP117436 in *E. coli* BL21(DE3) was induced with IPTG at 16, 20, 25, 30, and 37 °C. The recombinant MnP that was overexpressed under 25-37 °C mainly accumulated in insoluble IBs (**Fig. 2-1**).

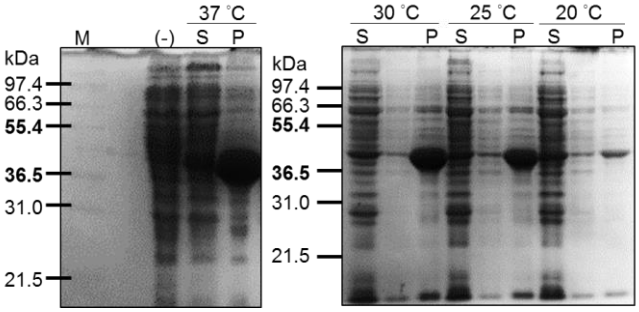

Fig. 2-1. Expression of MnP117436 in *E. coli* as inclusion bodies.
SDS-PAGE analysis of MnP117436 expressed at 20-37 °C. Protein size markers (M), total protein fraction of the cells without induction of MnP expression (-), and soluble (S) and insoluble (P) fractions of the cells after induction of MnP expression are shown.

The IBs were collected and purified for *in vitro* refolding. Calcium chloride was also added to the refolding solution containing urea, DTT, and GSSG. We found that although the formation of a precipitate was effectively suppressed by the presence of arginine during refolding, inactivation of the MnP was observed.

Heme incorporation was allowed to proceed during refolding by supplying hemin to the refolding solution. To determine the optimum conditions as to urea concentration and pH for refolding, we conducted screening experiments, in which we evaluated whether MnP had been folded correctly by checking the activity toward DMP. For example, when the pH was 8.5, 0.25-1.0 M urea provided active MnP117436s (**Table 2-1**). And when 1.0

M urea was used, pH 7.5 provided MnP117436 with the highest activity (**Table 2-1**). By applying the refolding procedure using the optimized conditions, and subsequent purification by SEC and anion exchange chromatography (**Fig. 2-2A and 2-2B**), about 1 mg of an active MnP was obtained from 1 L culture. The SEC analysis showed that the obtained MnP has a molecular weight (Mw) of about 80,000 and the Rz value was lower than 1.

Table 2-1. Activity of MnP-117436 refolded of different pHs and urea concentrations.

(1)	Urea (M)	0	0.25	0.5	0.75	1.0	1.5	2.0
	pH 8.5	-[a]	+[a]	+[a]	+[a]	+[a]	-[a]	-[a]
(2)	pH	6.5	7.0	7.5	8.0	8.5	9.0	9.5
	1 M Urea	-	+	++	+	+[a]	-[a]	-

+, active; -, inactive.
[a] precipitate observed.

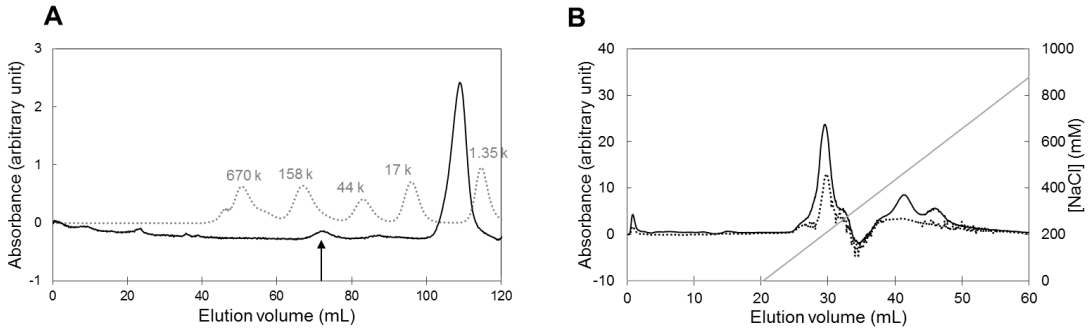

Fig. 2-2. Purification of *in vitro* refolded MnP117436.
(A) Size exclusion chromatography of the refolded MnP. Solid line, refolded MnP; dotted line, standard sample; arrow, dimer peak. (B) Anion exchange chromatography of the dimer fraction. Solid line, protein absorption (280 nm); dotted line, soret absorption of heme (410 nm).

2.2.2 Soluble expression

Instead of in vitro refolding, we tried to find the conditions for expressing the MnPs solubly (**Table 2-2**).

The selected MnPs were expressed as soluble forms in *E. coli* cells at 15 °C ("pCold I alone" panel in **Fig. 2-3C**, "pCold I +, pTf16 -" panel for all the proteins in **Fig. 2-3D**, and "pCold I alone" panel in **Fig. 2-3E**). Finally, we found that expression of MnP117436 under the *csp*A promoter at 15 °C tremendously improved the expression level and the solubility. SDS-PAGE analysis indicated that almost all MnP117436 was expressed as a

soluble form (**Fig. 2-3D**). Notably, expression of MnP157986 under the T7 promoter at 30 °C failed (**Fig. 2-3B**), while the expression was successful under the *csp*A promoter at 15 °C (**Fig. 2-3D**).

Table 2-2. Heterologous expression of *C. subvermispora* MnPs in *E. coli*.

Plasmid	Strain	Coexpression (plasmid)	temp.(°C)	Results[a]
pET15b-*mnp*	BL21(DE3)	-	37	IBs[b]
			30	IBs with little soluble protein
			25	IBs with little soluble protein
			20	low expression
			16	low expression
pET15b-*mnp*	BL21(DE3)	ferrochelatase (pACYC)	30	IBs with little soluble protein
pACYC-*mnp*	BL21(DE3)	ferrochelatase (pACYC)	30	target protein not expressed
pCold1-*mnp*	BL21	-	15	50% soluble high expression level
		dnaK-dnaJ-grpE (pKJE7)	15	> 90% soluble low expression level
		dnaK-dnaJ-grpE groES-groEL (pG-KJE8)	15	target protein not expressed
		groES-groEL (pGro7)	15	> 90% soluble
		tig[c] (pTf16)	15	> 90% soluble
		groES-groEL-tig (pG-Tf2)	15	> 90% soluble low expression level
		DsbC[d]	15	~100% soluble

[a] As judged on SDS-PAGE analysis.
[b] Inclusion bodies
[c] Trigger factor.
[d] Disulfide bond isomerase C.

Among five chaperone sets (**Table 2-2**), dnaK-dnaJ-grpE (the *E. coli* carrying the pKJE7 plasmid), groES-groEL (the *E. coli* carrying the pGro7 plasmid), and trigger factor (the *E. coli* carrying the pTf16 plasmid) provided 90% soluble MnP50297 (**Fig. 2-3C**), while poor growth of the *E. coli* carrying the pG-KJE8 and pG-Tf2 plasmids lowered the total protein amounts of the chaperone and MnP. The trigger factor coexpression showed

high ability as to minimizing IB formation for all four selected MnPs in this study (**Fig. 2-3D and E**). Coexpression of MnP with DsbC resulted in almost all the MnP being soluble. A larger amount of MnP was obtained on coexpression with DsbC than with the trigger factor (**Fig. 2-3E**).

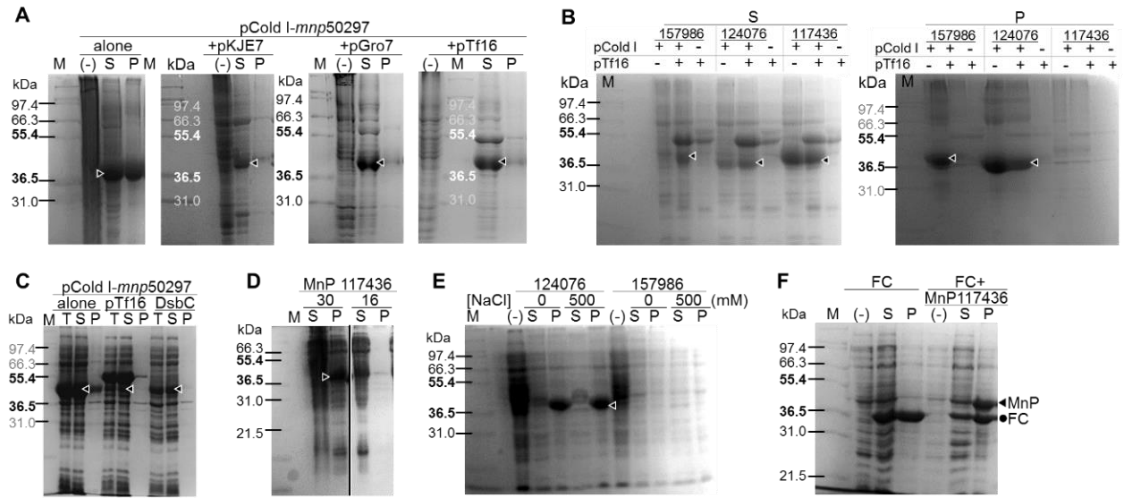

Fig. 2-3. SDS-PAGE analysis of the recombinant MnPs expressed in *E. coli*.
(A) *E. coli* BL21 transformed with pCold I-*mnp*50297, chaperones (pKJE7, pGro7, and pTf16) being coexpressed. (B) MnP-157986, 124076, and 117436 expression either with or without coexpression of the trigger factor. (C) MnP-50297 expression. pTf16, trigger factor coexpression; DsbC, DsbC coexpression in *E. coli* BL21. (D) *E. coli* BL21(DE3) transformed with pET-15b-*mnp*117436, and induced at 30 °C and 16 °C. (E) *E. coli* BL21(DE3) transformed with pET-15b-*mnp*124076 or pET-15b-*mnp*157986, and induced at 30 °C, were lysed in solutions containing 0 or 500 mM NaCl. (F) Ferrochelatase expression and its coexpression with MnP117436. FC, ferrochelatase.
Protein size markers (M), total protein fraction of the cells without induction of MnP expression (-), and the total (T), soluble (S), and insoluble (P) fractions of the cells after induction are shown. Arrowhead (►) and circle (●) indicated the bands of MnP and FC, respectively.

2.2.3 Heme incorporation

When the MnP coexpressed with ferrochelatase, both ferrochelatase and MnP were mostly expressed as IBs (**Fig. 2-3F**). Direct hemin addition to the soluble expressed MnPs was not successful, as judged from the very low Rz value, 0.09 (**Fig. 2-4A**).

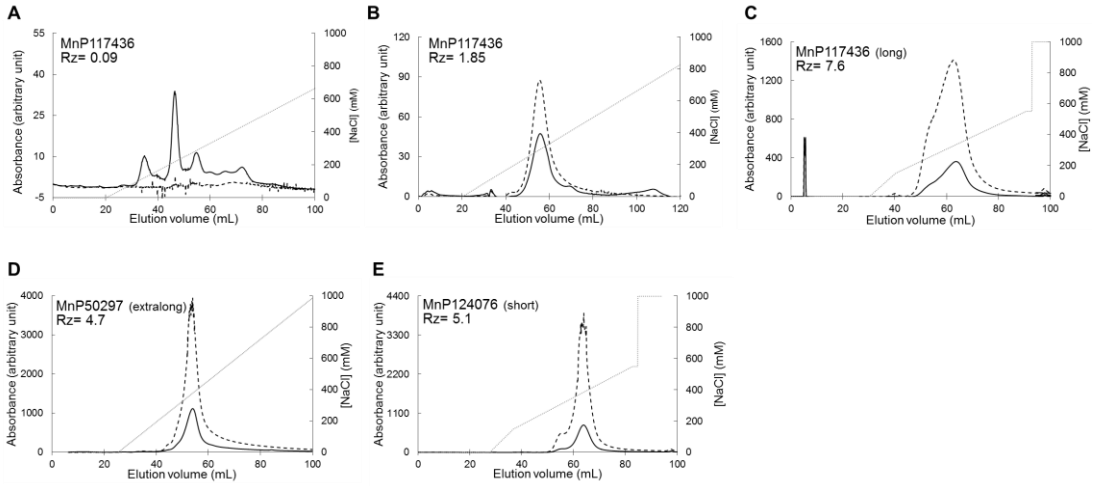

Fig. 2-4. Anion exchange chromatography (Hitrap Q HP 5 mL) of each MnP expressed as soluble forms with R_z values.
Solid line: protein absorption (280 nm); dashed line: Soret absorption of heme (410 nm); dotted line: [NaCl] gradient. (A) Hemin inserted after MnP117436 purification on Ni-affinity column, (B) hemin added to MnP117436 once at the time of induction with IPTG, and (C, D, E) hemin added continuously during expression of MnP117436, MnP50297 and MnP124076, respectively. Rz values i.e., the ratio of Absorbance $_{410\ nm}$/ Absorbance $_{280\ nm}$

MnP117436 was used to investigate whether the addition of hemin to the culture during the expression prompt heme incorporation. When the final concentration of 100 mg/L hemin was added to the culture once at the time of induction with IPTG, the MnP obtained after the purification by Ni and anion exchange chromatography showed an Rz value of ~1.85 (**Fig. 2-4B**). However, when 200 mg hemin/L was added, the amount of total cells decreased. Accordingly, the yield of the purified MnP decreased and the Rz value did not improve either. For further improvement, after the addition of IPTG, we waited for six hours for the MnP to be produced, and then supplied hemin and $CaCl_2$ to culture continuously for 12 hours to reach a final concentration of 100 mg hemin/L and 1 mM $CaCl_2$. As a result, heme incorporation to the MnPs greatly improved as the Rz values reached the range of 3.8-7.6 for each MnP (**Fig. 2-4C-E, and Fig. 2-6**). The full UV/Vis

spectra of MnP50297 and MnP114076 in Tris-HCl were shown in **Fig. 2-5**. Both MnPs exhibited a Soret peak at 413 nm with a shoulder at 358 nm and Q bands at 530 nm and 558 nm. These features are characteristic of the heme coordinated MnPs.

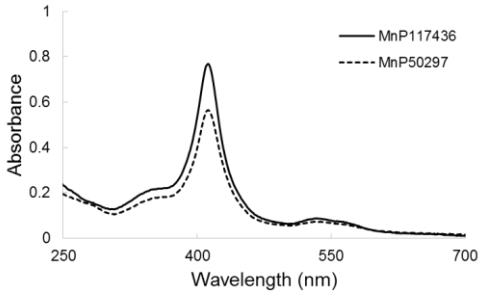

Fig. 2-5. UV/Vis spectra of the purified recombinant MnP50297 and MnP117436.

2.2.4 Purification of the solubly expressed MnPs

Each soluble MnP fused with hexahistidine was firstly subjected to Ni-affinity chromatography. The eluted MnP was subsequently dialyzed against the buffer without imidazole to lower the imidazole concentration. Trace amounts of nonspecifically Ni-bound proteins were completely removed by anion exchange chromatography (**Fig. 2-4C-E**). Although a single band was observed on SDS-PAGE after this two-column purification, subsequent SEC revealed fractions of aggregated MnP (**Fig. 2-6**), which were removed by SEC. The yields after each purification step for three MnPs are listed in **Table 2-3**.

Table 2-3. The yields of the MnPs purified after each step.

Recombinant MnP	Wet cell (g)	Yield (mg)		
		Ni	Anion exchange	Size exclusion
MnP50297	0.70	32.4±1.2	12.6±2.5	3.1±0.4
MnP117436	0.65	29.4±5.1	10.8±3.0	2.7±1.4
MnP124076	0.65	33.7±6.3	17.4±4.6	3.2±0.3

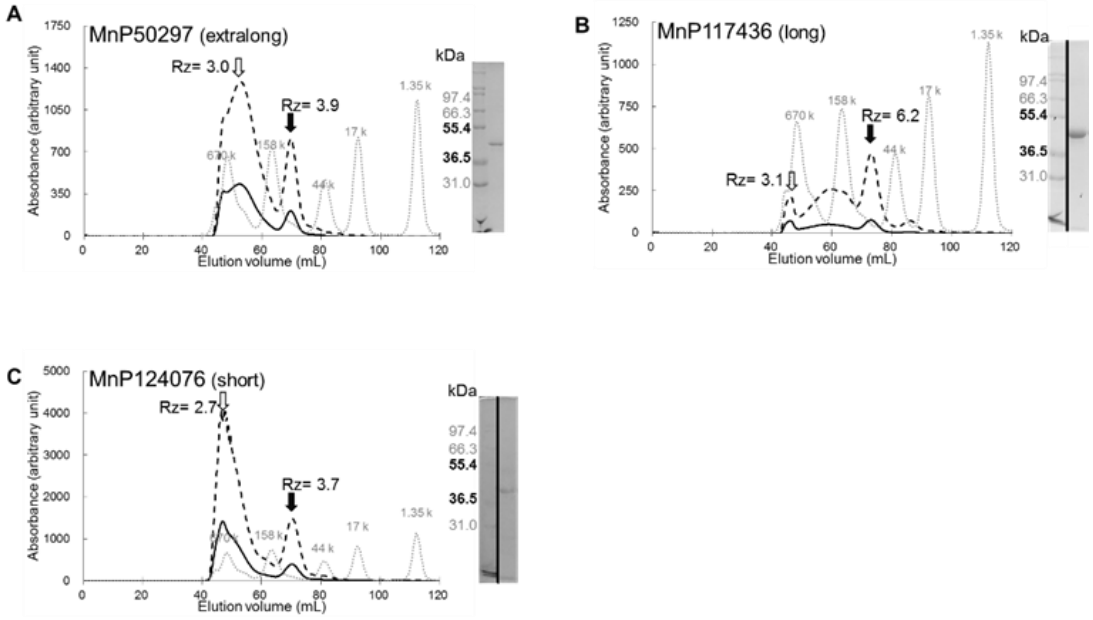

Fig. 2-6. Size exclusion chromatography (HiLoad 16/60 Superdex 200 pg) of MnPs purified from the soluble fraction through continuously addition of hemin during expression, together with Rz values. (A) MnP50297, SDS-PAGE of the peak with the solid arrow is also shown. (B) MnP117436. (C) MnP124076. Solid arrow: dimer fraction; open arrow: aggregation fraction. Solid line: protein absorption (280 nm); dashed line: Soret absorption of heme (410 nm); dotted line: SEC standard.

2.3 Discussion

Recombinant heme-containing ligninolytic peroxidases often form insoluble protein aggregates, known as IB, when expressed in *E. coli*. As the IBs were easily separated and contained only a small amount of impurities, the IBs were collected and purified for *in vitro* refolding. Calcium chloride was added to the refolding solution since it is reportedly essential for refolded MnPs to maintain both structural stability and activity (56, 58). Arginine is frequently used in protein refolding processes to suppress aggregation because it is considered to slow protein-protein association reactions (59). However, the interaction between arginine and heme propionates, and that between arginine and the catalytic Glu residue of MnP results in inhibition of heme peroxidase activity (60). Therefore we decided not to add arginine during refolding. The SEC analysis indicates that a dimer is formed since the theoretical Mw of a monomeric MnP is about 40,000. The purified MnP exhibited the low Rz value, which indicated insufficient incorporation of heme. Finally, even with the optimized refolding condition, the low refolding yield made the production of the MnPs not competitive. These results tempted us to develop an

alternative method for the preparation of MnPs.

Lowering of the temperature of the *E. coli* culture after induction reportedly enhances the formation of soluble recombinant proteins (61). But when protein expressed under the control of the T7 promoter, low temperature induction caused reduction or even inhibition of the expression of MnPs, as shown in Fig. 2A and B. This problem would possibly be alleviated through expression of proteins under the control of cold shock promoter *csp*A (62, 63). In fact, all the selected MnPs were expressed as soluble forms under the control of *csp*A. The formation of IBs was further suppressed by molecular chaperone coexpression. Aside from the molecular chaperones, the effect of another folding accessory protein, disulfide bond isomerase C (DsbC), has also been examined. DsbC was found to facilitate the formation of soluble proteins with correct disulfide bond formation (64). The IB was not observed when MnP50297 was coexpressed with DsbC. Moreover, the use of DsbC gave the highest yield of the MnP as compared with other chaperones. To increase the amounts of the soluble proteins, optimization of the conditions, such as the pH and salt concentration of the lysis solution, turned out also to be important. For example, a large amount of soluble MnP117436 was obtained when lysis buffer of pH 7.5 containing no NaCl was used.

Coexpression of ferrochelatase along with supplementation of $FeCl_3$ and 5-amino levulinic acid, a precursor in the heme biosynthesis pathway, reportedly enables the production of fully heme-incorporated proteins (65). However, in the current study, coexpression of the MnP and ferrochelatase resulted in IB formation of both proteins.

Previously, direct hemin addition to the refolded VP obtained from IBs (58), and aggregated soluble MnP obtained with *E. coli* (51, 58) resulted in Rz values of 2.2 and 1.0, respectively. Likewise, we applied this method to our MnPs purified by Ni column chromatography. Unfortunately, the obtained MnP had very low Rz value, 0.09, indicating the failure of heme incorporation.

Addition of hemin to the culture during the expression of heme proteins is known to prompt heme incorporation (52). Here, we used MnP117436 to investigate whether this is also the case with our MnPs by adding different amounts of hemin to the culture during the expression. We found that an excess amount of hemin lowers not only the growth of the cells but also the overall yield of MnP. Hemin tends to aggregate in an aqueous solution at high concentration because of its hydrophobic nature. This may lower the

intake of hemin into the cells in the first place. Additionally, a high amount of hemin in the cells may cause its aggregation as well as non-specific hydrophobic interactions with proteins in general, both of which may disrupt the proper cell activities. Thus, we attempted to keep the total amount of free hemin both in the culture and inside the cells low. When hemin and $CaCl_2$, which aids the folding of MnP (56, 58), were supplied to culture continuously, the Rz values reached the range of 4.7-7.6 for each purified MnP. These Rz values are comparable to that of the native MnPs, which is higher than 3.0. The Rz values of our MnPs and the previously reported native and recombinant MnPs are listed in Table 2 and are compared. As far as we know, this is the first report showing the expression of the MnPs, in which the hemes are properly incorporated, in soluble form by *E. coli*.

After three-column purification, comprising Ni affinity, anion exchange, and size exclusion chromatography (**Figs. 2-4 and 2-6**), about 3 mg of pure protein was obtained from 0.1 L culture for each MnP. The SEC analysis of the obtained MnP gave results consistent with those obtained for refolding, namely the MnP was a dimer. It was noticed that MnP dimer had no tendency to form oligomers or aggregates after concentration.

The full UV/Vis spectra of MnP50297 and MnP117436 under slightly basic conditions (**Fig. 2-5**) resemble those of the other heme peroxidases (53, 66). The shoulder at 358 nm and the Q band at 530 nm indicate that the ferric MnPs adopted a hexacooridinate low-spin state under the basic conditions; the same features were reported for the native MnP from *P. chrysosporium* (67). The absorbance at two Q bands, 530 nm and 558 nm, suggests that the heme irons of our MnPs are coordinated with two histidine residues (68), which is consistent with the crystal structure of *P. chrysosporium* MnP (PDB ID 3M5Q) (69).

2.4 Conclusion

Heterologous expression of fungal ligninolytic enzymes by *E. coli* expression system often results in the formation of insoluble aggregates or IBs. The conditions of *in vitro* refolding of IBs need to be individually optimized for each protein and even then the yield is still low. Here, we have developed the method that overcomes these drawbacks. Four MnPs from three different MnP subfamilies were all successfully expressed in *E. coli* as soluble and active forms, resulting in 20-fold higher yield than that

from IBs refolding. The way to properly incorporate heme into MnPs has also been figured out, heme-to-protein ratio being as high as native MnPs. The method could accelerate the study and the utilization of fungal ligninolytic enzymes in wood biomass industry.

2.5 Experimental procedures

2.5.1 Bacterial strains and plasmids

The coding sequences for four MnPs (MnP50297, MnP157986, MnP117436, and MnP124076) from *C. subvermispora* were codon-optimized for *E. coli* and synthesized by Thermo Fisher Scientific. The codon-optimized genes of four MnPs, MnP50297, MnP117436, MnP124076, MnP157986, were deposited in the NCBI GenBank under the accession numbers of MG190335, MG190336, MG190337, and MG190338, respectively.

Table 2-3. The sequence of the primers.

Gene	Vector	F/R[a]	RE[b]	primer sequences 5′-3′ [c]
*mnp*50297	pCold I	F	*Nde*I	GGAATTCCATATGGCACCGACCACCATTTGC
		R	*Bam*HI	CGGGATCC(TCATTA)GCTATCATCCTCACCGG
*mnp*117436	pET-15b	F	*Nde*I	GGAATTCCATATGGCACCGACCACCATTTGTC
	pCold I	R	*Bam*HI	CGGGATCC(TCATTA)TGCCGGACCATCAAAC
*mnp*124076	pCold I	F	*Nde*I	GGAATTCCATATGGCCATTACCCGTCGTGTTAC
		R	*Bam*HI	CGGGATCC(TCATTA)GCTACCCGGAACAGG
*mnp*157986	pCold I	F	*Nde*I	GGAATTCCATATGGCACCGGCAAGCAGCAG
		R	*Bam*HI	CGGGATCC(TCATTA)ATCGGTGCCATTAAAAC CTGTTGC
DsbC	pTf16[d]	F	*Nde*I	GGAATTCCATATGGATGACGCGGCAATTCAAC
		R	*Xho*I	CCGCTCGAG(TCATTA)TTTACCGCTGGTCATT TTTTG
TEE (deletion)	pCold I	R	-	GGTGTATTACCTCTTAATAATTAAGTGTGCC
		F	-	ATGGCACCGACCACCATTTG
His-tag (deletion)	pCold I	R	-	CACTTTGTGATTCATGGTGTATTACCTC
		F	-	GCACCGACCACCATTTGCCCGGATG

[a] Forward (F) or reverse (R) primer.
[b] Restriction enzyme site.
[c] Underlined, restriction enzyme sites. Parentheses, stop codon.
[d] The gene sequence of trigger factor in pTf16 plasmid was replaced by the gene sequence of DsbC.

Each of these genes was amplified by polymerase chain reaction (PCR), and subcloned into pET-15b (Novagen) and pCold I (Takara Bio Inc.) vectors via restriction sites *Nde*I and *Bam*HI, and into a pACYCDuet-1 vector (Novagen) via restriction sites *Nco*I and *Bam*HI. The obtained plasmids were named pET-15b-*mnp*50297, -*mnp*157986, -*mnp*117436, and -*mnp*124076, pCold I-*mnp*50297, -*mnp*157986, -*mnp*117436, and -

*mnp*124076, and pACYCDuet-1-*mnp*117436. The chaperone plasmids, pKJE7, pG-KJE8, pGro7, pTf16, and pG-Tf2, were purchased from Takara Bio Inc. *E. coli* strain DH5α was used for subcloning, while strains BL21 and BL21(DE3) were used as hosts for recombinant protein production. The plasmids and *E. coli* strains used in this study are listed in **Table 2-2**. The primers, containing the restriction enzyme sites, used for gene amplification and plasmids construction are listed in **Table 2-3**.

2.5.2 Expression of a MnP as IB, and its solubilization and refolding

E. coli BL21(DE3) cells carrying pET-15b-*mnp*117436 were grown at 37 °C in Luria Broth (LB) containing 100 μg/mL ampicillin. When the optical density at 590 nm (OD_{590}) reached 0.8, protein expression was induced with 1.0 mM isopropyl β-D-1-thiogalactopyranoside (IPTG), and then the cells were further cultivated for 3.5 hours. Cells were harvested by centrifugation, and the obtained cell pellet was resuspended in 50 mM Tris-HCl (pH 8.0) containing 10 mM EDTA, 5 mM DTT, 2.0 mg/mL lysozyme, 5 unit/mL DNase I (Invitrogen), and 1.0 μg/mL RNase (Nippon Gene). The mixture was sonicated and IB were collected after removal of the soluble fraction by centrifugation. The collected IB were washed three times with 50 mM Tris-HCl (pH 8.0) containing 1 mM EDTA and 5 mM DTT. The resulting IB were solubilized using 8 M urea and further purified using Ni-NTA agarose (Qiagen).

Refolding conditions were screened on a small-scale using 200 μL of 50 mM Tris-HCl (pH 6.5-9.5) containing 0.1 mM DTT, 0.5 mM glutathione disulfide (GSSG), 5 mM $CaCl_2$, 10 μM hemin, 0-2 M urea, and 0-0.5 M arginine. The protein solution was rapidly diluted to 1.25 μM (10-fold dilution) in the refolding solution and then incubated at 15 °C for 12 hours. Then, the clear supernatant was collected by centrifugation.

Subsequently, the obtained solution containing a refolded MnP was subjected to activity measurement. The activity of Mn-mediated oxidation of DMP (detailed description in section 2.6) was measured and used to evaluate the success of refolding. Large scale refolding was performed using 200 mL of 50 mM Tris-HCl (pH 7.5) containing 0.1 mM DTT, 0.5 mM GSSG, 5 mM $CaCl_2$, 10 μM hemin, and 0.75 M urea with a final protein concentration of 0.13 μM. After incubation at 15 °C for 20 hours, the clear supernatant was collected by removing the precipitate by centrifugation. The protein solution was then concentrated from 200 mL to 10 mL. The molecular weight of the

obtained protein was determined on a HiLoad 16/60 Superdex 200 pg size exclusion column (SEC) (GE Healthcare Life Sciences), Bio-Rad gel filtration standards being used for calibration.

2.5.3 Soluble MnP expression: low temperature protein expression under a cold shock promoter

E. coli BL21 cells carrying each of the pCold I-*mnp* constructs were grown at 37 °C in LB containing 100 μg/mL ampicillin. When OD_{590} reached 0.4, the culture medium was rapidly chilled to 15 °C by soaking the culture flask in a water-ice bath, followed by standing still at 15 °C for 30 min. IPTG was then added to the final concentration of 0.2 mM and the cells were grown for 24 hours at 15 °C. During expression, $CaCl_2$ and hemin were added to the culture (detailed description in section 2.5.10). When hemin was not added to the culture, heme incorporation was performed at a later stage, which is described in section 2.5.9.

2.5.4 Soluble MnP expression: coexpression with chaperones

MnP50297 were coexpressed with chaperones. Here, *E. coli* BL21 cells carrying pCold I-*mnp*50297 was cotransformed with one of the chaperone plasmids, pKJE7, pG-KJE8, pGro7, pTf16, or pG-Tf2, individually. The resulting cells were grown at 37 °C in LB containing 100 μg/mL ampicillin and 20 μg/mL chloramphenicol, and the expression of each chaperone was induced with either 1 mg/mL L-arabinose (for pGro7, pKJE7, and pTf16), 1 ng/mL tetracycline (for pG-Tf2), or both 1 mg/mL L-arabinose and 1 ng/mL tetracycline (for pG-KJE8). When OD_{590} reached 0.4, the MnP expression was induced by the procedure described in section 2.5.3.

2.5.5 Soluble MnP expression: cloning and coexpression of disulfide bond isomerase C (DsbC)

Genomic DNA of *E. coli* BL21(DE3) was extracted with a QuickExtract™ Bacterial DNA Extraction Kit (Epicentre). The DsbC gene, excluding the secretion signal sequence, was amplified from genomic DNA of *E. coli* BL21(DE3) by PCR using a forward primer (5′- CAT GCC ATG GAT GAC GCG GCA ATT CAA CAA-3′) and a reverse primer (5′-GGA ATT CTT ATT TAC CGC TGG TCA TTT TTT GGT-3′), the restriction sites for

*Nco*I and *Eco*RI being underlined, respectively. The amplified DsbC gene was cloned into the pTf16 vector, from which the gene encoding the trigger factor was intentionally deleted. Coexpression of MnP and DsbC was performed by the same procedure as in the case of MnP and trigger factor (pTf16) coexpression section 2.5.4.

2.5.6 Purification of the recombinant MnPs expressed as soluble forms

The purification steps were all performed at 4 °C. The cell pellet harvested from 100 mL of culture medium described in section 2.5.3 was resuspended in 10 mL of 50 mM Tris-HCl buffer (pH 7.5 for MnP50297 and MnP157986, pH 8.0 for MnP117436, and pH 8.5 for MnP124076), and then homogenized by sonication. The supernatant containing soluble MnPs were collected by 30 minutes centrifugation at 50,000 × g, and nucleic acids were then digested with 5 units/mL DNase I and 1.0 μg/mL RNase. Subsequently, the protein solution was applied to a Ni affinity column containing Cosmogel His-Accept (Nacalai Tesque) resin, and the bound His-tagged MnPs were washed with 50 mM Tris-HCl (pH 7.5) containing 500 mM NaCl, 1 mM $CaCl_2$, and 5 mM imidazole to remove the nonspecifically bound proteins. His-tagged MnPs were eluted with 50 mM Tris-HCl (pH7.5) containing 500 mM NaCl, 1 mM $CaCl_2$, and 250 mM imidazole, and then dialyzed against 50 mM Tris-HCl (pH7.5). This protein solution was further purified with an anion exchange column (Hitrap Q HP 5 mL) (GE Healthcare Life Sciences), concentrated using an Amicon Ultra-15 centrifugal filter (molecular weight cutoff 10,000) (Millipore), and applied to a size exclusion column (HiLoad 16/60 Superdex 200 pg) (GE Healthcare Life Sciences). The protein concentration was determined with a Pierce BCA Protein Assay Kit (Thermo Fisher Scientific), following the manufacturer's instructions.

2.5.7 Heme incorporation assessment

The extent of heme incorporation was assessed by obtaining Rz values (Reinheitszahl value) (70, 71), i.e., the ratio $\text{Absorbance}_{\text{Soret peak maximum}} / \text{Absorbance}_{\text{protein at 280 nm}}$. The full UV/Vis spectra of the purified MnPs were recorded by Shimadzu UV-2450.

2.5.8 Heme incorporation: subcloning and coexpression of MnPs with ferrochelatase

A plasmid expressing ferrochelatase was constructed according to the reported

method (65). A forward primer (5′-GGA ATT CCA TAT GCG TCA GAC TAA AAC CGG TAT C-3′) and reverse primer (5′-CCG CTC GAG TCA TTA GCG ATA CGC GGC AAC AAG-3′) were used for PCR amplification, the underlined sequences being the restriction sites for *Nde*I and *Xho*I, respectively. The obtained gene was inserted into the same restriction sites of pACYCDuet-1. The obtained plasmid was named pACYCDuet-1-*ferrochelatase* and introduced into *E. coli* BL21(DE3) cells carrying pET-15b-*mnp*117436. The protocols for cultivating the cells and inducing the expression of proteins were as previously reported (65). The temperature was set to 30 °C and cells were harvested 6 hours after induction.

2.5.9 Heme incorporation: incorporation of heme to MnP after purification

MnPs that had been purified with Ni affinity resin (section 2.5.6) were mixed with 100 mg/mL hemin and then stood at 4 °C. After 12 hours, excess heme was removed by centrifugation at 50,000 × g for 10 minutes. The resulting protein solution was then subjected to anion exchange chromatography (Hitrap Q HP 5 mL) (GE Healthcare Life Sciences).

2.5.10 Heme incorporation: hemin supplementation during MnP expression

The hemin supplementation procedure was added to the low temperature expression procedure described in section 2.5.3. Six hours after IPTG had been added, 1 M $CaCl_2$ and 10 mg/L hemin (dissolved in 0.1 M NaOH) were supplied continuously for another 12 hours during cultivation at rates of 84 µL/hr and 840 µL/hr, respectively.

Chapter 3. Activities of expressed MnPs

3.1 Introduction

In chapter 2, we have developed the method to solubly express *Cs*MnPs using *E. coli*. All three purified *Cs*MnPs have moderate Rz values and thus are expected to possess the MnP activity. Therefore, we performed the activity assays for the purified MnPs using Mn^{2+}, 2,6-dimethoxyphenol (DMP), 2,2'-azino-bis(3-ethylbenzothiazoline-6-sulphonic acid) (ABTS), and guaiacyl glycerol-β-guaiacyl ether (GOG-OH) as substrates (**Fig.3-1**).

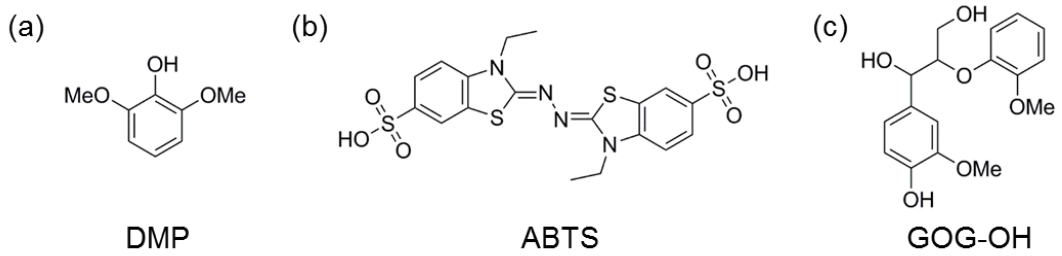

Fig. 3-1. The substrates used for activity assays.
(a) DMP, (b) ABTS, and (c) GOG-OH.

3.2 Results

3.2.1 Kinetic properties of the MnPs and activities toward dimethoxyphenol (DMP)

The oxidation of DMP by Mn^{3+} produced by MnPs results in formation of the quinone dimer (**Fig. 3-2**), which shows a strong absorbance at 469 nm ($\varepsilon_{469\ nm}$= 49.6 $mM^{-1}cm^{-1}$). As a result, the oxidation of DMP is commonly used for the activity assay of MnPs. The oxidative activities toward DMP of two forms, aggregated and dimer forms, of MnPs obtained on SEC (**Fig. 2-6**) were investigated. It was clearly shown that the aggregated form possesses very weak activity toward DMP compared to dimer forms (**Fig. 3-3B and D**). The activity of MnP 124076 toward DMP was only one-tenth of those of the other two MnPs (**Fig. 3-3A, C** and **E**). No oxidized product was detected in the absence of $MnSO_4$. The effect of pH on oxidation of DMP by each MnP from three subfamilies turned out to be similar, the optimum pH being 3.5 (**Fig. 3-3A, C** and **E**). Additionally, the thermal inactivation effects of three MnPs were also examined. The results showed that about 50% (for MnP50297) and 20% (for MnP117436) of the activity remained even when the MnPs were heated at 95 °C for 10 minutes (**Fig. 3-3A** and **C**, solid circles).

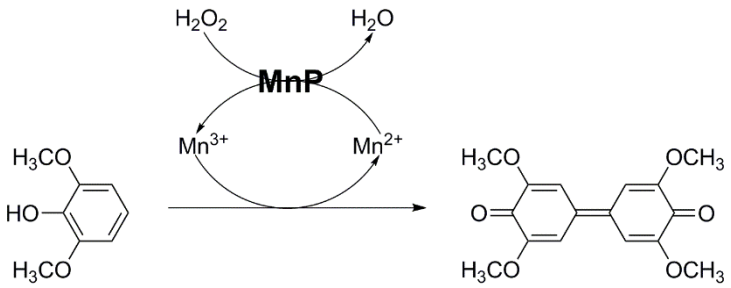

Fig. 3-2. The oxidation of DMP by MnP.

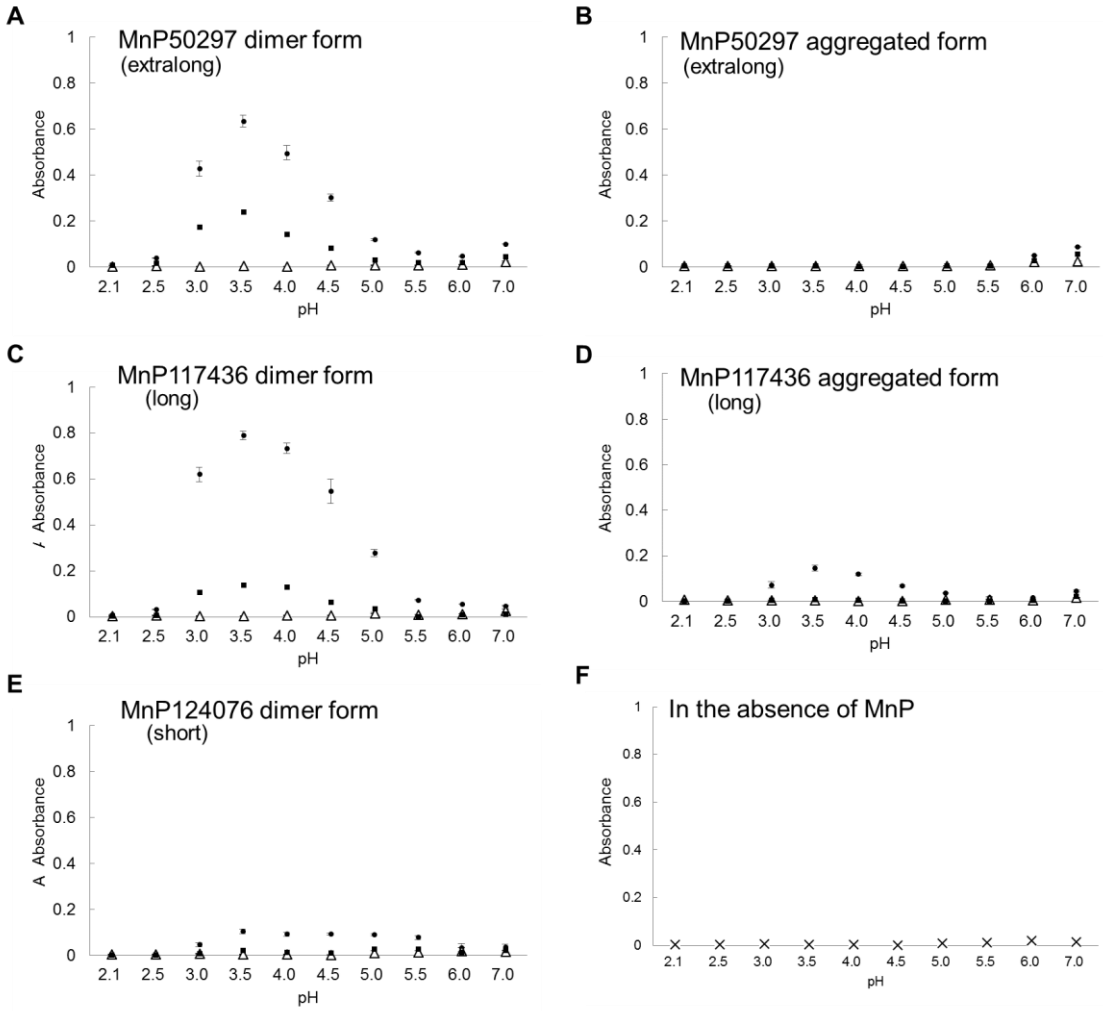

Fig. 3-3. Effect of pH on the activity of MnPs in either an aggregated form or a dimer form toward DMP.

(A) MnP50297 dimer form. (B) MnP50297 aggregated form. (C) MnP117436 dimer form. (D) MnP117436 aggregated form. (E) MnP124076 dimer form. (F) Negative control, in the absence of MnP. (●), in the presence of Mn^{2+}; (△), in the absence of Mn^{2+}; (■), MnPs heated at 95 °C for 10 minutes.

It is cleared that the aggregated MnPs have very low activity. Hence, only the dimer form of the MnPs were used for determining kinetic parameters. The K_M values of MnP50297 and MnP117436 for Mn^{2+} in sodium malonate buffer were 22.6 μM and 12.2 μM, respectively. k_{cat} values of MnP50297 and MnP117436 were 9.1 s^{-1} and 5.3 s^{-1}, respectively. The activity of MnP124076 toward Mn^{2+} was too low to obtain reliable kinetic parameters. The kinetic parameters are summarized in **Table 3-1**.

Table 3-1. Comparison of the MnP properties.

Fungi	Enzyme	MnP preparation	Rz	K_M (μM)	k_{cat}/K_M ($s^{-1}mM^{-1}$)	Reference
C. subvermispora	50297	*E. coli*, soluble	3.8-3.9	22.6 ± 3.3	406	This study
	117436	*E. coli*, soluble	4.8-6.2	12.2 ± 3.7	435	This study
	117436	*E. coli*, refolded	4[a]	58.5 ± 8.5	5600	(49, 57)
I. lacteus CD2	MnP1	*E. coli*, refolded	1.0	193.8	36.6	(66)
	MnP2	*E. coli*, refolded	2.4	152.2	43.4	(66)
I. lacteus F17		native		100.7± 0.87	9620	(51)
		E. coli, refolded	3.1	148 ± 7.1	930	(51)
		E. coli, soluble	0.3-1.0	336 ± 8.0	76	(51)
P. chrysosporium	MnP1	native	6.0	73.2	4322	(41)
	MnP1	homologous expression	4.0	69.4	3952	(41)
	MnP1	native		80	1300	(44)
	MnP1	*P. pastoris*		74	1400	(44)
P. ostreatus	MnP1	*E. coli*, refolded		7±1	1200	(72)
	MnP2	*E. coli*, refolded		92±5	1730	(72)
	MnP3	*E. coli*, refolded		101±12	1610	(72)
	MnP4	*E. coli*, refolded		88±4	1410	(72)
	MnP5	*E. coli*, refolded		22±2	1930	(72)
	MnP6	*E. coli*, refolded		73±9	1500	(72)
B. adusta UAMH 8258		native	4.3	17		(73)

[a] The A_{410}/A_{280} ratio was similar for all the refolded enzymes, with an average value of 4 (49, 57).

3.2.2 Activities toward ABTS

We have also examined the activities of dimer form MnPs toward ABTS. ABTS is a substrate usually used to detect the activities of laccases and peroxidases, and it can act as a mediator for the oxidation of non-phenolic lignin compounds by laccases. ABTS is a useful substrate for assaying because it can be oxidized to the stable cation radical $ABTS^{\cdot+}$ (**Fig. 3-4**), which shows high absorbance at 420 nm (ε_{420nm} = 36.0 $mM^{-1}cm^{-1}$).

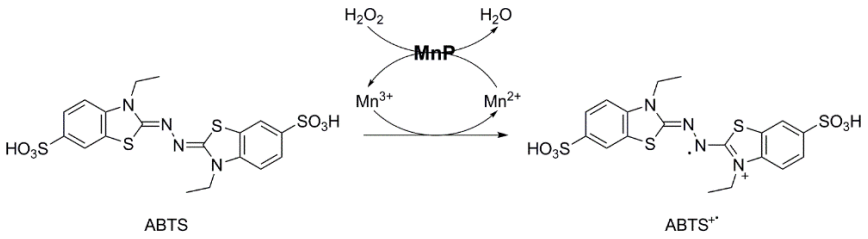

Fig. 3-4. The oxidation of ABTS by MnPs.

Here, MnP117436 exhibited the highest activity toward both DMP and ABTS among the three MnPs (**Fig. 3-5**). On the other hand, MnP124076 showed higher activity than MnP50297, which was opposite to the case of DMP. The optimum pH for MnP124076 is pH 4, i.e., slightly higher than those of MnP117436 and MnP50297. It was also observed that after being heated at 95 °C for ten minutes, MnP117436 and MnP50297 still retained their activities to some extent. However, heating seems to cause full deactivation of MnP124076. Surprisingly, we observed the activity of MnP124076 even when the manganese ions were not included in the reaction mixture. This unique manganese-independent activity is further examined and discussed in the next chapter.

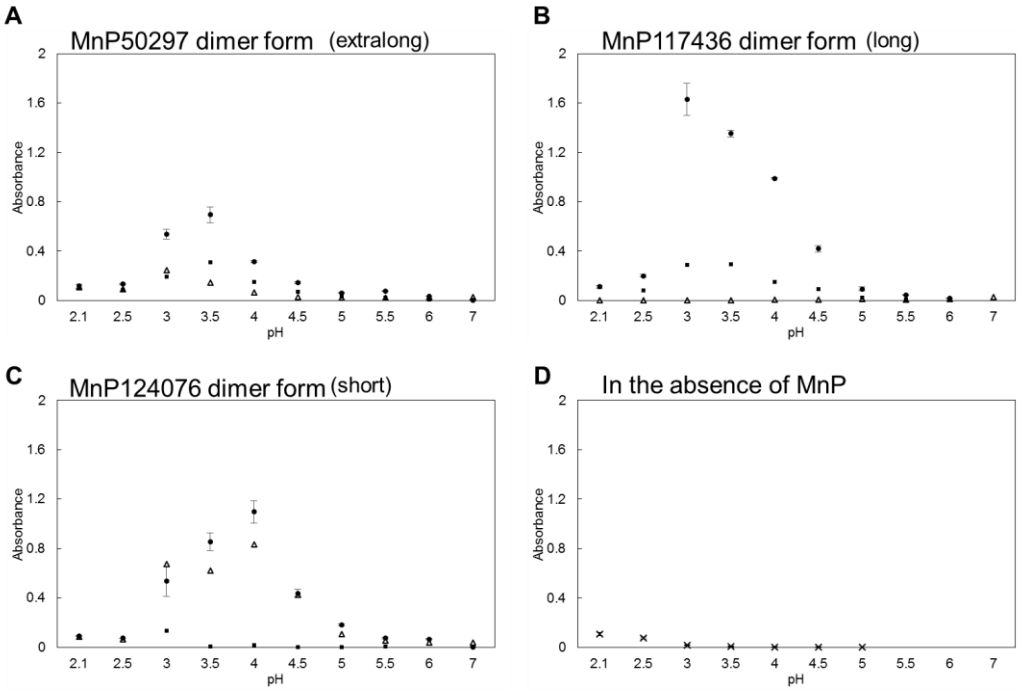

Fig. 3-5. Effect of pH on the activities of dimer form MnPs toward ABTS.
(A) MnP50297. (B) MnP117436. (C) MnP124076. (D) Negative control, in the absence of MnP. (●), in the presence of Mn^{2+}; (△), in the absence of Mn^{2+}; (■), MnPs heated at 95 °C for 10 minutes.

3.2.3 Reactions of the MnPs and phenolic lignin dimer model

According to the results in sections 3.2.1 and 3.2.2, it has been demonstrated that MnP117436 exhibits the highest activity toward both DMP and ABTS in the presence of the manganese ions. Therefore, we considered that MnP117436 would be the best candidate for performing and studying other model reactions. Instead of a simple aromatic monomer substrate, in this section, we tried to monitor the reaction between MnP117436 and a phenolic lignin dimer compound, GOG-OH.

At first, we applied NMR for detecting the reactions. After reaction for eleven hours, a major product was observed (**Fig. 3-6**). When the reactions were extended to twenty-four hours, an increasing number of signals was observed and the intensity of the original signal of GOG-OH became weaker. This indicated an enzymatic reaction had occurred. However, we failed to find any new signals when we subjected the sample at eleven hours to gas chromatography-mass spectrometry, though a decrease in the amount of GOG-OH was observed.

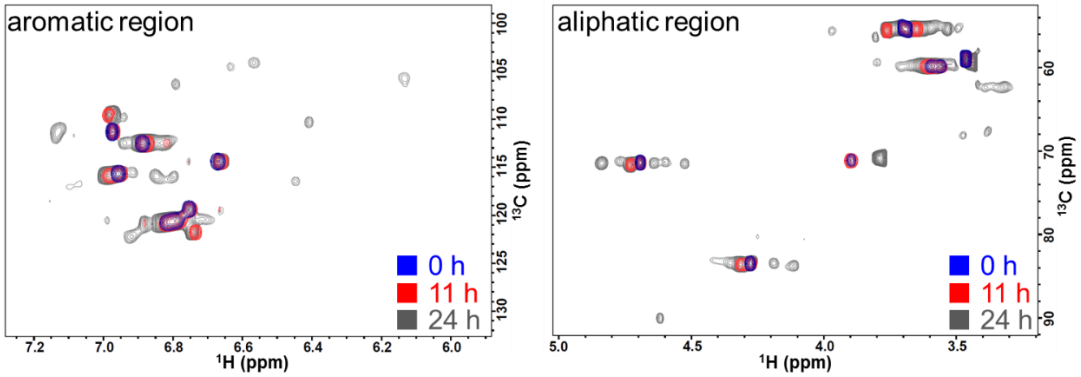

Fig. 3-6. Monitoring of the enzymatic reaction between MnP117436 and the phenolic lignin dimer model, GOG-OH, by means of ^{1}H-^{13}C HSQC spectra.
Blue, red and gray correspond to the reaction times of 0, 11 and 24 hours, respectively.

To detect the products formatted through the reaction, liquid chromatography and gel permeation chromatography were also performed (**Fig. 3-7** and **Fig. 3-8**). The spectra showed the consistency to the results obtained on NMR. After reaction for six hours, one major product was detected, and after reaction for twenty-four hours, several products were detected. We expected to see degradation but, however, it seems that dimerization of the starting material took place in the first stage. The reaction conditions, including the concentrations of the enzyme, substrate, and hydrogen peroxide, may possibly affect the

result. Suitable conditions are still under investigation.

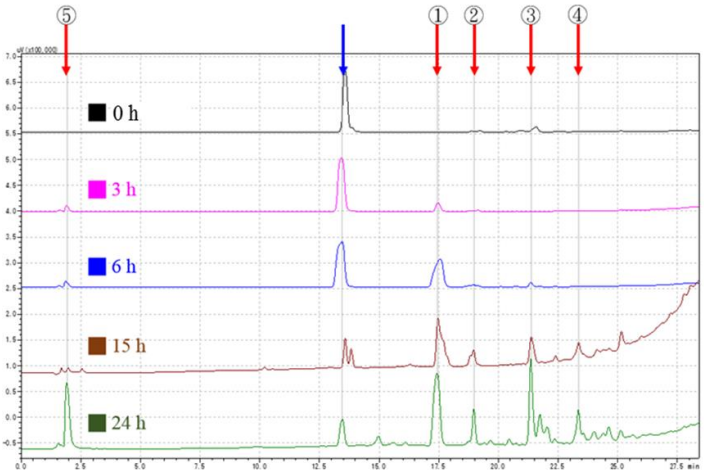

Fig. 3-7. Monitoring of the enzymatic reaction between MnP117436 and the phenolic lignin dimer model, GOG-OH, by liquid chromatography.
Blue arrow, GOG-OH. Red arrows, products formed on reaction for three to twenty-four hours.

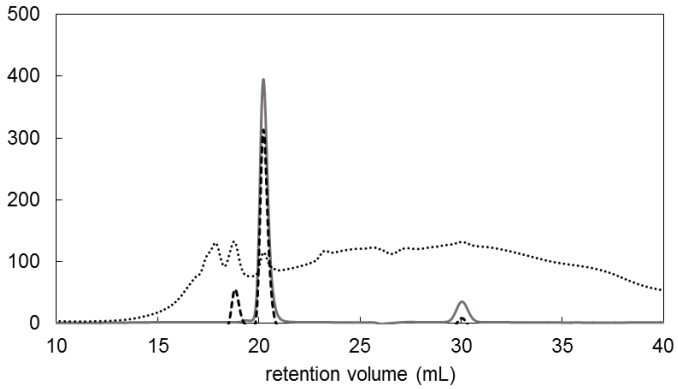

Fig. 3-8. Monitoring of the enzymatic reaction between MnP117436 and the phenolic lignin dimer model, GOG-OH, by GPC.
Gray line, GOG-OH. Dashed line, the reaction mixture at six hours. Dotted line, the reaction mixture at twenty-four hours.

3.3 Discussion

The K_M and k_{cat}/K_M values of MnP50297 and MnP117436 toward Mn^{2+} were comparable to those values previously reported for native and recombinant MnPs (**Table 3-1**). It was noticed, however, that k_{cat}/K_M values of the two MnP117436, soluble (this study) and refolded (4) ones, appeared rather different. In the experiments to determine kinetic constants, the malonate buffer was finally used in our case, as explained below,

while the tartrate buffer was used in the previous report. We performed the kinetic experiments using the malonate buffer and monitored the UV absorbance at 270 nm of the formed Mn^{3+}-malonate complex. The usage of the malonate buffer and monitoring the UV absorbance at 270 nm has two advantages over the usage of the tartrate buffer and monitoring the UV absorbance at 238 nm of the formed Mn^{3+}-tartrate complex. (i) Higher signal-to-noise ratio is achieved, because the molar absorption coefficient of the Mn^{3+}-malonate complex (ε_{270}= 11,590 $M^{-1}cm^{-1}$) is larger than that of the Mn^{3+}-tartrate complex (ε_{238}= 6,500 $M^{-1}cm^{-1}$) (**Table 3-2**), which is critical especially in the case when the concentration of Mn^{3+} is low. (ii) UV absorbance at 270 nm of the Mn^{3+}-malonate complex does not overlap with that of H_2O_2 at 240 nm, while the UV absorbance at 238 nm of the Mn^{3+}-tartrate complex overlaps severely with that of H_2O_2 at 240 nm (ε_{240}= 39.4 $M^{-1}cm^{-1}$). Although ε_{240} of H_2O_2 is hundred times smaller than ε_{238} of the Mn^{3+}-tartrate complex, the concentration of H_2O_2 could be hundred times higher than that of the Mn^{3+}-tartrate complex under the standard experimental conditions used for the determination of kinetic constants; this situation continues during the initial time period after the reaction is initiated by adding H_2O_2 to the concentration of 0.1 mM (74). In fact, initially, we also used the tartrate buffer as used in the previous report. We found, however, it is almost impossible to obtain reproducible kinetic data, possibly due to the disadvantages of using the tartrate buffer. In our experience, the use of the malonate buffer seems more appropriate to obtain the reliable kinetic constants.

Table 3-2. UV-visible absorbance and coefficients of Mn^{3+} complexes.

	UV-visible absorbance	ε ($M^{-1}cm^{-1}$)
Mn^{3+}·malonate	270 nm	11590
Mn^{3+}·tartrate	290 nm	2860
	238 nm	6500
Mn^{3+}·lactate	290 nm	5890
Mn^{3+}·malate	290 nm	4310
Mn^{3+}·oxalate	500 nm	290

In the enzymatic assay with DMP, it was observed that the aggregated form had almost no activity toward DMP, despite the high heme incorporation. In the absence of $MnSO_4$, the oxidation reaction was not detected, which convinced us that the obtained

MnPs possess Mn-dependent activities. Surprisingly, the activity of MnP 124076 toward DMP was very low. This low enzymatic activity of MnP 124076 may be due to two reasons: one is that MnP124076 is shorter in length in the C-terminal region than the other two and the other is that MnP 124076 exhibits relatively low sequence similarity with the other two. The activity remained to some extent when the MnPs were heated at 95 °C for 10 minutes. The remaining activity may be due to that the MnPs are just partially denatured even at 95 °C and/or the MnPs were renatured to some extent after complete denaturation at 95 °C. It is suggested that the length difference in the C-terminal regions may also affect the thermal stability. MnP50297 and MnP117436 are the most and fifth most expressed proteins among all proteins in *C. subvermispora*, respectively (39). We revealed that they exhibit higher activity, which suggests that they play key roles in the degradation of lignin in the wood biomass.

3.4 Conclusion

The results of the obtained kinetic parameters and the activity assays toward DMP and ABTS strongly support the notion that our method described here, in which refolding process is not used, is a promising way to obtain recombinant fungal extracellular enzymes that can be used for both basic enzyme characterization and application. Although eukaryotic expression systems can be directly transferred into actual enzyme production for biomass utilization, *E. coli* expression system is relatively time-saving compared with eukaryotic expression systems, and thereby a quite efficient option for mutant construction and their activity screening. Our study should pave the way for the application of the recombinant MnPs not only for a use in lignin degradation but also for a use in environmental remediation.

3.5 Experimental procedures

3.5.1 Kinetic properties of the MnPs

The kinetic constants for the MnP activity were determined by performing the reactions in 50 mM sodium malonate (pH 5.0) at 25 °C with a varying amount of Mn^{2+} (5-2000 μM) as a substrate. The reactions were initiated by 0.1 mM H_2O_2. The formation of Mn^{3+}-malonate was monitored at 270 nm (ε_{270}= 11,590 $M^{-1}cm^{-1}$) (55), while the

concentration of H_2O_2 was quantified using ε_{240}= 39.4 $M^{-1}cm^{-1}$ (74). The K_M and k_{cat}/K_M parameters were calculated by using the Graph Pad Prism 5 software.

3.5.2 Oxidation of DMP by the MnPs

MnP activity toward 2,6-dimethoxyphenol (DMP) was measured by the method established by Wariishi et al (55). Oxidation of DMP by MnP results in the formation of coerulignone, which can be monitored spectroscopically by measuring the increase in absorbance at 469 nm (Infinite® 200 PRO, TECAN). Reactions were carried out at 30 °C in 200 µL of 50 mM sodium tartrate (pH 2.5-7.0) containing 5 µg/mL MnP, 0.5 mM DMP, 1 mM $MnSO_4$, and 0.1 mM H_2O_2. Manganese independent activity was also examined in the absence of $MnSO_4$. The effect of thermal inactivation was checked by heating the MnP solution at 95 °C for 10 minutes.

3.5.3 Oxidation of ABTS by the MnPs

Reactions were carried out at 30 °C in 200 µL of 50 mM sodium tartrate (pH 2.5-7.0) containing 5 µg/mL MnP, 0.5 mM ABTS, 1 mM $MnSO_4$, and 0.1 mM H_2O_2. Manganese independent activity was also examined in the absence of $MnSO_4$. The effect of thermal inactivation was checked by heating the MnP solution at 95 °C for 10 minutes. The product was monitored spectroscopically by measuring the increase in absorbance at 420 nm (Infinite® 200 PRO, TECAN).

3.5.4 Reactions of the MnP and phenolic lignin dimer model

For the sample of NMR, reactions were carried out at room temperature in 60 mL of 50 mM sodium tartrate (pH 4.5) containing 0.25 µM MnP117436, 0.5 mM GOG-OH, 1 mM $MnSO_4$, and 10 mM H_2O_2 was supplied with flow rate 1.05 µL/min. For sampling at different time period, each time 10 mL of the reaction mixture was taken and flash-frozen with liquid nitrogen to quench the reaction immediately. The samples were then freeze-dried (freeze-dryer FDU-2200, EYELA) and dissolved in DMSO-d6. ^{1}H-^{13}C HSQC NMR spectra were recorded at 25 °C with either DRX600 or Avance III 600 spectrometer, both being equipped with a cryogenic probe and a Z-gradient (Bruker Biospin). After acquiring the NMR spectra, the samples were collected and used for GC-MS, LC (Agilent, Eclipse Plus Phenyl Hexyl, particle size 5 µm), and GPC (Asahipak GF-310HQ).

Chapter 4. Unique activity of the short MnP

4.1 Introduction

In chapter 3, we demonstrated that the short MnP (MnP124076) of *C. subvermispora* exhibited the lowest activity toward DMP in the presence of the manganese ions among the three purified MnPs. For another substrate, ABTS, MnP124076 showed lower activity in the presence of manganese than long MnP117436 as well. Surprisingly, manganese-independent activity was observed in the case of reaction of ABTS with MnP124076. On comparison of the amino acid sequences of all MnPs of *C. subvermispora*, it is obvious that the short MnP exhibits lower similarity to all other long and extralong MnPs. On the other hand, the existence of short MnPs has also been discovered in other white rot fungi and those short MnPs exhibits high identity in amino acid sequences. However, the unique activities of short MnPs have not been well discussed. In this chapter, we focus on the activity of the short MnP, including low activity toward DMP, manganese-independent activity, and the ability to react with a non-phenolic substrate.

4.2 Results

4.2.1 Unique activities of short MnP mutants toward DMP and ABTS

In the previous chapter, we focused on activity comparison between the three types of MnPs, and found the optimum pHs for three purified MnPs. In **Fig. 4-1**, it is shown that long MnP117436 exhibits the highest activity toward ABTS in the presence of the manganese ions. Surprisingly, when the manganese ions were not included in the reaction system, short MnP124076 could still oxidize ABTS to almost the same extent as when the manganese ions were included. Whereas manganese-independent activity was not observed in the case of oxidation of DMP (**Fig. 3-1**).

To study the relationship between the short MnP and the two substrates, DMP and ABTS, we tried to add both substrates to the reaction system, and monitor the absorbance at both 420 nm (ABTS) and 469 nm (DMP). Regarding the oxidation of ABTS, when only ABTS was included in the reaction mixture, the presence of the manganese ions increase the yield of the oxidized product (column 2 and 5 in **Fig. 4-2A**). Interestingly, it was observed that when both DMP and ABTS were included in the reaction mixture, the absorbance at 420 nm decreased by about 90% whether the manganese ions were included

in the system or not (columns 2 and 3, and columns 5 and 6 in **Fig. 4-2A**).

On the other hand, the UV-visible absorbance at 469 nm, i.e., the absorbance of the oxidized product of DMP, slightly increased when ABTS was added to the system containing the manganese ions (columns 1 and 3 in **Fig. 4-2B**). We reported in chapter 3 that all three purified MnPs tend not to react with DMP when there are no manganese ions in the reaction mixture. However, even in the absence of the manganese ions, we observed an increase in absorbance at 469 nm when ABTS was added (column 6 in **Fig. 4-2B**).

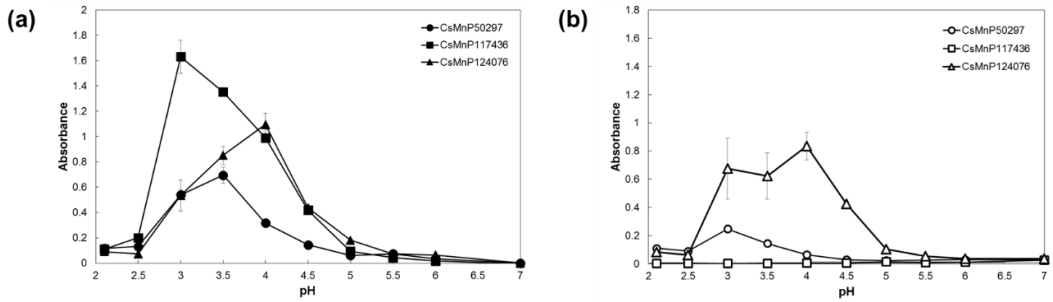

Fig. 4-1. Activities of three *Cs*MnPs toward ABTS at pH 2.1 to 7.0.
(a) In the presence of 5 mM $MnSO_4$. **(b)** In the absence of $MnSO_4$. *Cs*MnP50297 (● and ○), *Cs*MnP117436 (■ and □), and *Cs*MnP124076 (▲ and △).

Table 4-1. Reaction conditions used for studying the characteristics of MnP124076.

1	In the presence of Mn^{2+}	DMP
2		ABTS
3		DMP and ABTS
4	In the absence of Mn^{2+}	DMP
5		ABTS
6		DMP and ABTS

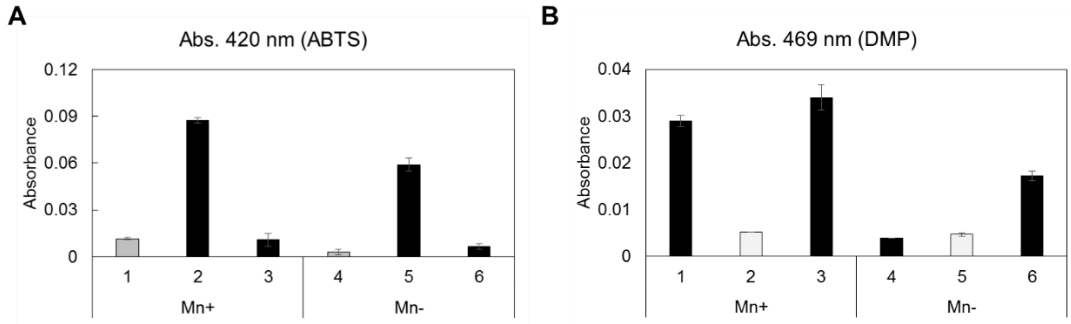

Fig. 4-2. The activities of MnP124076 under different conditions. (A) The absorbance detected at 420 nm. (B) The absorbance detected at 469 nm. Numbers 1-6 correspond to the reaction conditions listed in **Table 4-1**.

4.2.2 Structure modeling and mutations

To identify the factors responsible for the unique activities of short MnPs, we compared the amino acid sequences of some reported short MnPs and the MnPs of *C. subvermispora* (**Table 4-2** and **Fig. 4-3**). Two distinct characteristics of short MnPs were easily recognized on the sequence alignment, an about 14 amino acid deficiency in the C-terminal region and an about 11 amino acid deficiency in the middle region.

Table 4-2. Comparison of *Cs*MnPs with other short MnPs.

Organism	Accession number	Enzyme	kDa[a]	#aa[a]	pI[a]	MnP type	Reference
C. subvermispora	JGI Cersu1|50297	*Cs*MnP2	39.1	369	4.37	extra long	This study
	JGI Cersu1|117436	*Cs*MnP10	38.2	360	4.71	long	
	JGI Cersu1|124076	*Cs*MnP13	35.9	343	4.42	short	
I. lacteus CD2	JGI Irplac1|1291806 Genbank KX620478	*Il*MnP1	36.1	340	4.87		(66)
	Genbank KX620479	*Il*MnP2	35.6	338	4.67		
A. praecox	Genbank HQ336221	*Ap*MnP1	34.9	332	4.82		(75)
I. lacteus Fr. 238	-[b]		37				(76)
I. lacteus CCBAS Fr. 238	-[b]		37				(77)
P. radiata	EMBL AJ310930	*Pr*MnP3	35.4	339	4.23		(78)
A. bisporus ATCC62459	Genbank AJ699058	*Ab*MnP1	35.4	333	4.14		(79)

[a] Signal sequence not included, estimated with ExPASy.
[b] Sequences not provided.

Because the crystal structures of *Cs*MnPs have not yet been determined, we then performed homology modeling to construct the structures of the short and long MnPs for a comparison. The C-terminal region and middle region, which are lacking in short MnP (*Cs*MnP13, also annotated as MnP124076 in this study), were present as loops in the long MnP (*Cs*MnP10, also annotated as MnP117436 in this study). We found that the manganese binding site of the short MnP seems to be blocked compared to in the long MnP (**Fig. 4-4a** and **Fig. 4-4b**). It was also noticed that the amino acids near the manganese binding site are hydrophilic in the case of the long MnP. On the contrary, the amino acids near the manganese binding site are hydrophobic in the case of the short MnP (**Fig. 4-4c**). It was also found that the internal loop present in the long MnP but missing in the short MnP, is composed of hydrophilic amino acids and located close to the manganese binding site (**Fig. 4-4c**).

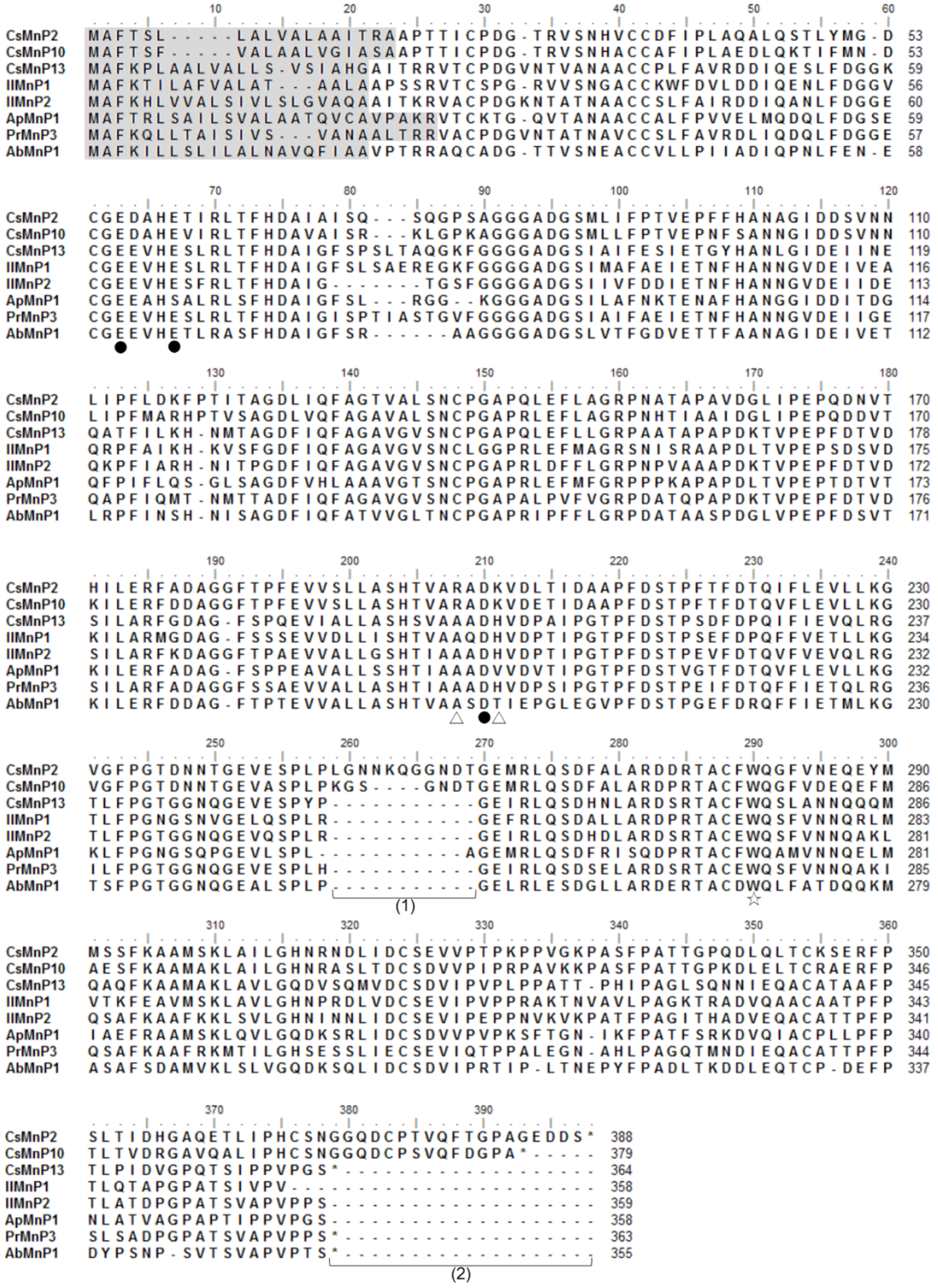

Fig. 4-3. Alignment of the amino acid sequences of two long MnPs and the reported short MnPs.

Signal sequences ■, internal loops near active site (1), C-terminal loops (2), Mn^{2+} binding residues ●, hydrophobic residues near the active site △, Trp residue ☆.

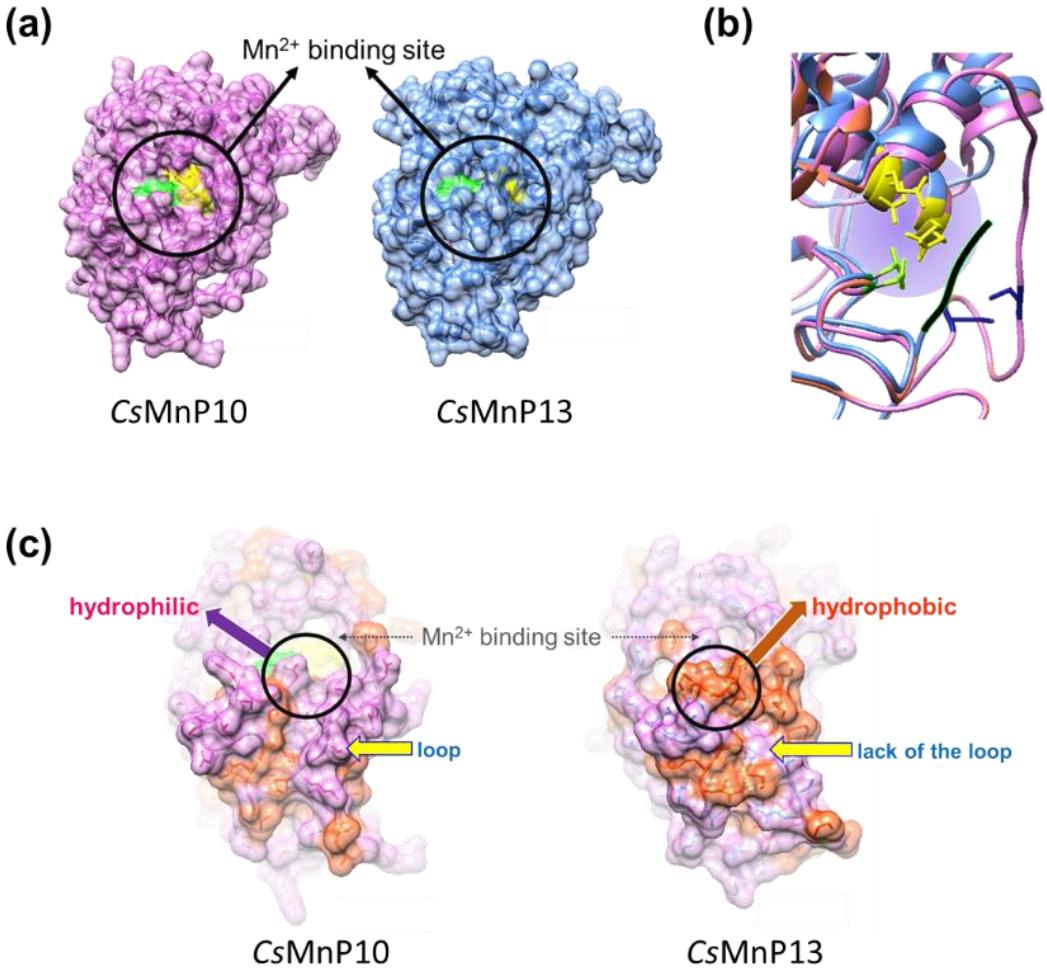

Fig. 4-4. Structure modeling and comparison between *Cs*MnP117436 (*Cs*MnP10) and *Cs*MnP124076 (*Cs*MnP13).
(a) The environment near the manganese binding site. (b) The C-terminal regions of *Cs*MnP10 (pink) and *Cs*MnP13 (blue). (c) The hydrophilic amino acid residues (pink) and hydrophobic amino acid residues (orange) near the manganese binding sites of *Cs*MnP10 and *Cs*MnP13.

Based on the structure modeling, five mutants of short MnP124076 were designed (**Table 4-3**). In addition to the above mentioned structural difference, we also performed mutation of the only Trp residue of short MnP124076. The Trp residue facilitates electron transportation by lignin peroxidases (LiP), but is not regarded as an active site in the case of MnPs. However, as we have observed manganese-independent activity of short MnP124076, it is also essential to confirm the function of the Trp residue in short MnP124076.

Table 4-3. Mutants of short MnP124076 constructed in this study.

(1) C-terminal sequence mutations		
*Cs*MnP13	WT	…GPQTSIPPVPGS*
	M1 (C-ter deletion)	…GPQTSIP*****
	M2 (C-ter mutation)	…GPQTSIP**HCSNG***
	M3 (C-ter extension)	…GPQTSIP**HCSNGGQDCP***
*Cs*MnP10	WT	…GAVQALIPHCSNGGQDCPA*
(2) Internal sequence addition		
*Cs*MnP13	WT	…SPYP - - - - - - - GE…
	M4 (loop addition)	…SPYP**KGSGNDT**GE…
*Cs*MnP10	WT	…SPLPKGSGNDTGE…
(3) Hydrophobic residues near active site		
*Cs*MnP13	WT	…ASHSVAAA<u>D</u>HVDPAIP…[a]
	M5 (A205R H208K)[b]	…ASHSVA**R**AD**K**VDPAIP…[a]
*Cs*MnP10	WT	…ASHTVARA<u>D</u>KVDETID…[a]
(4) Tryptophan		
*Cs*MnP13	WT	…RTACFWQSLANNQ…
	M6 (W276A)[b]	…RTACF**A**QSLANNQ…

[a] Underlining: manganese binding residue.
[b] The numbers of amino acid residues were determined on the basis of **Fig. 4-3**.

All six mutants were prepared by the method described in chapter 2, and the activities toward both DMP and ABTS were assayed by the same method as that described in chapter 3. For the activity toward DMP, all mutants showed almost no activity in the absence of the manganese ions (**Fig. 4-5a**). The modifications made at the positions of the missing loops in short MnP124076 did not yield better activity than that of the wild type. Although the deficiencies of the internal and C-terminal loops are the most obvious structural differences between the short MnPs and the long MnP, it seems that the weak activity toward DMP is not the result of those two missing loops. Instead, we found that increasing the hydrophilicity near the manganese binding site improved the activity of short MnP124076 toward DMP (**Fig 4-5a**, M5). Mutant M6 (W276A) of short MnP124076 did not exhibit a clear difference in the oxidation of DMP.

For the activity toward ABTS, the mutations made at the loops (M1-M4) all led to decreases in the activity (**Fig 4-5b**). Again, the increasing hydrophilicity of short MnP124076 gave rise to increases in both the manganese-dependent and manganese-independent activities (**Fig 4-5b**, M5). Whereas, the mutation at the Trp of short MnP124076 resulted in 80% losses of both the manganese-dependent and manganese-independent activities (**Fig 4-5b**, M6).

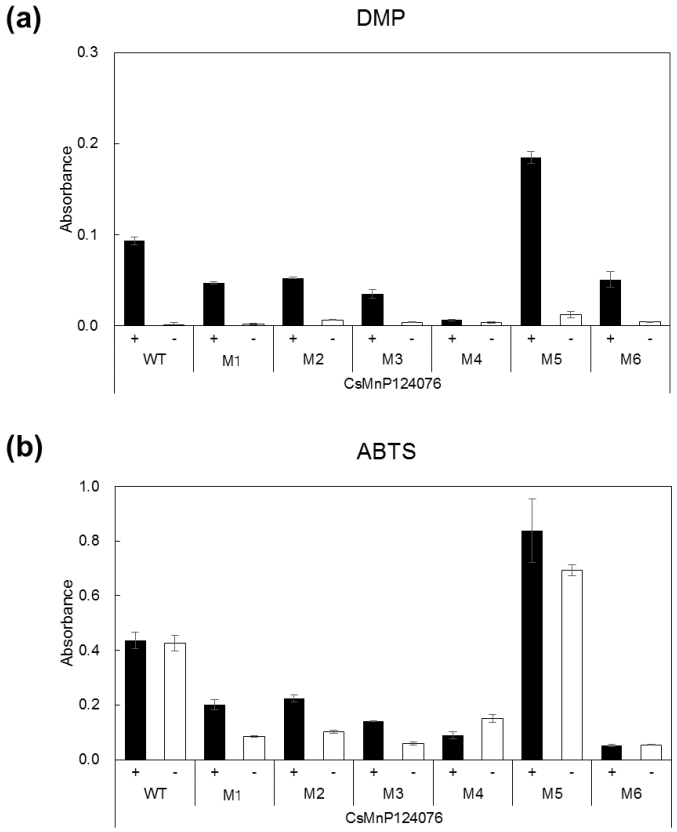

Fig. 4-5. Comparison of mutated MnPs activities.
(a) Activity toward DMP. **(b)** Activity toward ABTS. In the presence of Mn^{2+} (+, black bar), in the absence of Mn^{2+} (-, white bar). Wild-type (WT) and mutated (M1-M6) *Cs*MnP124076 are listed in **Table 4-3**.

4.2.3 Reaction on phenolic lignin dimer model

Although short MnP124076 exhibits the lowest activity toward the phenolic monomer compound DMP among the three MnPs, its unique activity prompted us to exam the reactivity of it with the lignin dimer model, GOG-OH. The previous section (section 3.2.3) showed that the dimerized product was possibly formed at the first stage and, thus, GPC was used to estimate the molecule weight of the product formed in the reaction between short MnP124076 and GOG-OH.

On mixing short MnP124076 with GOG-OH in the presence of the manganese ions, almost the same amount of GOG-OH remained (**Fig. 4-6B**). The manganese-dependent oxidation ability of the short MnP124076 was much lower than that of MnP117436, as we expected. According to the results in section 4.2.1, it was predicted that ABTS may

be able to act as a mediator for MnP124076. Therefore, instead of the manganese ions, we added ABTS to the reaction system. In **Fig. 4-6C**, a small amount of a product with a higher molecular weight than the starting material, GOG-OH, can be observed. Again, the undesired polymerization occurred under these conditions. Meanwhile, a strong peak having a retention time near twenty-three minutes was also observed for the reaction mixture with the same components as in Fig. 4-6C but in the absence of the MnP124076. Thus, it can be deduced that the peak is originated from ABTS. However, because the signal was too strong, it was difficult to judge if there has any degraded product formed or not. We also found that when both the manganese ions and ABTS were included in the reaction mixture, the reaction, no matter whether depolymerization or repolymerization, became slower than that when no manganese ion supplied (**Fig 4-6D**).

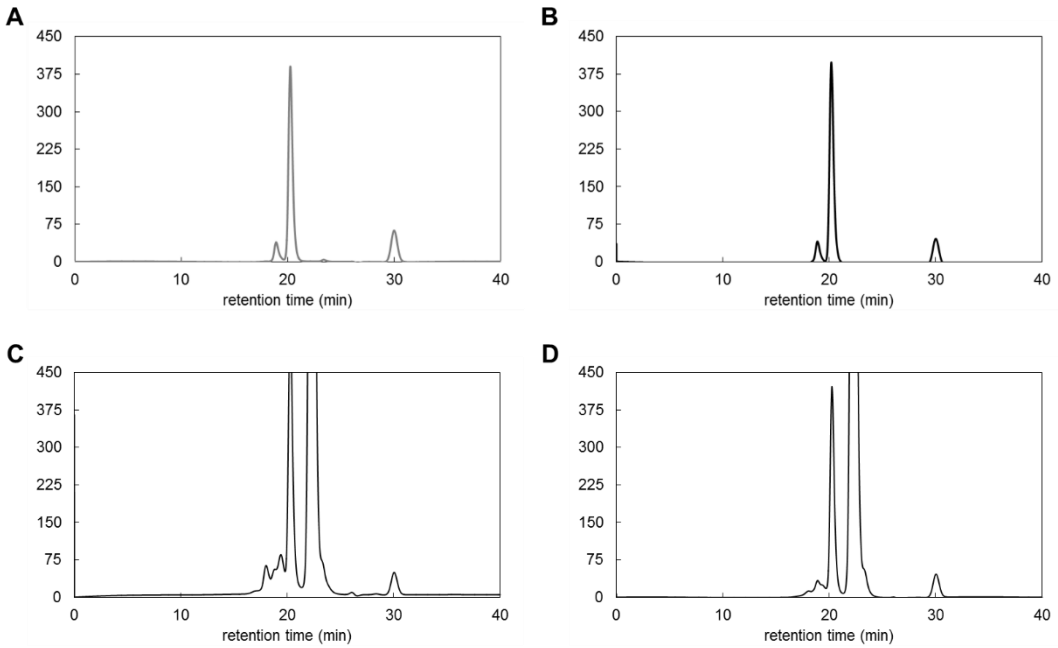

Fig. 4-6. The reaction of MnP124076 with the phenolic lignin dimer model detected by GPC.
(A) The spectrum of substrate GOG-OH without reaction with MnP124076. (B) GOG-OH reacted with MnP124076 in the presence of Mn^{2+}. (C) GOG-OH reacted with MnP124076 in the absence of Mn^{2+} but in the presence of ABTS. (D) GOG-OH reacted with MnP124076 in the presence of both Mn^{2+} and ABTS.

4.2.4 Unique activity toward veratryl alcohol

Previously, in the presence of the manganese ions, MnPs were reported to oxidize phenolic lignin and to be able to oxidize non-phenolic lignin only when unsaturated fatty

acid was included in the reaction system. However, as the short MnP (*Cs*MnP124076) was found to possess different characteristics compared to other MnPs, we performed experiments to confirm whether the short MnP possessed the ability to oxidize the non-phenolic lignin model in the absence of unsaturated fatty acids. For this purpose, veratryl alcohol (VA), a common non-phenolic substrate for assaying of the activities of LiP, was used as the substrate (**Fig. 4-6a**). According to our previous results, the manganese ions are required for the short MnP to oxidize the phenolic compound DMP. Hence, the oxidation of non-phenolic VA proceeded in the presence of the manganese ions.

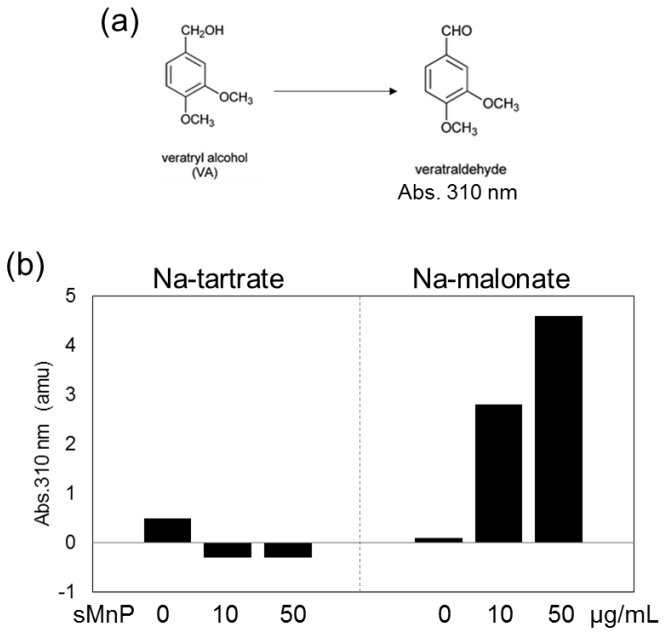

Fig. 4-7. The activity of the short MnP (MnP124076) toward VA.
(a) The formation of veratraldehyde can be detected by observing the UV-visible absorbance at 310 nm. (b) The oxidation activity of MnP124076 toward VA in tartrate or malonate buffer.

When the reactions were performed in sodium tartrate buffer, the absorbance of the VA oxidized product, veratraldehyde, was not observed even when the concentration of the short MnP was increased to 50 μg/mL (**Fig. 4-6b**, left panel). Unexpectedly, the oxidation of VA by the short MnP was observed in sodium malonate buffer (**Fig. 4-6b**, right panel). This finding implied that in the case of the short MnP, some specific carboxylic acids, instead of unsaturated fatty acids, could possibly facilitate the oxidation of non-phenolic lignin models.

4.3 Discussion

The genomic study of white rot fungus *C. subvermispora* showed that there is only one gene encoding the short MnP, and the gene encoding LiP or VP has not been reported (57). In this study, we demonstrated that short MnP124076 exhibited lower activity toward the phenolic substrate DMP. However, manganese-independent activity was observed in the case of oxidation of ABTS (**Fig. 4-8**).

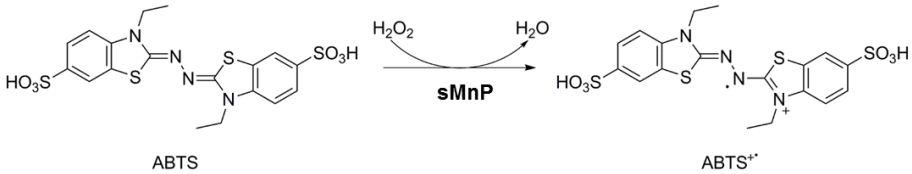

Fig. 4-8. The oxidation of ABTS by the short MnP in the absence of Mn^{2+}.

To further investigate the relationship between MnP124076 and its substrates, we mixed both DMP and ABTS together in the reaction system. In the presence of Mn^{2+}, the oxidized product of ABTS was almost not detectable when DMP was added to the reaction. While in the absence of Mn^{2+}, the oxidized product of DMP was not observed under the original reaction conditions but was detected when ABTS was included in the reaction system. This finding may infer that the ABTS is able to act as a mediator in the presence of Mn^{2+} and as a substrate that can be used to oxidize other substrates in the absence of Mn^{2+} for the short MnP (**Fig. 4-9**). We have further demonstrated that in the presence of ABTS, the short MnP exhibits higher reactivity toward the phenolic lignin dimer model than in the presence of Mn^{2+}. However, unexpected polymerization occurred, which suggests that the reaction conditions need to be carefully examined.

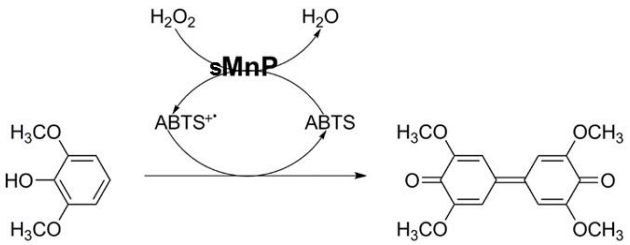

Fig. 4-9. ABTS acts as a mediator for sMnP to oxidize DMP in the absence of Mn^{2+}.

The most apparent difference between the short MnP, and the long and extralong MnPs is the length of the C-terminal loop. Indeed, our structure modeling results showed that the manganese ion binding site may be blocked in the case of the short MnP, which could result in the low activity of the short MnP. However, the mobility of the shortened C-terminal loop of the short MnP is not clear and the mutations of the C-terminal loop did not result in increasing activity. Instead of focusing on the C-terminal loops, we demonstrated that the hydrophobicity near the manganese binding site may be the main reason for the low activity toward the manganese ions. The manganese-independent activity increased as well when the hydrophilicity increased near the manganese binding site. This indicated that ABTS may share the same active site as the manganese ions in the short MnP. On the other hand, the replacement of only Trp with Ala in the short MnP led to a severe decrease in the activity toward ABTS. The Trp, in addition to manganese, should play an important role in the short MnP as to oxidation of substrates.

Previously, it was reported that MnPs could oxidize non-phenolic substrates only in the presence of certain unsaturated fatty acids. We have observed the ability to oxidize a non-phenolic substrate, VA, of the short MnP in the absence of any unsaturated fatty acid. Nevertheless, this unique activity was detected in malonate buffer but not in tartrate buffer. Here we concluded that the short MnP is able to oxidize the non-phenolic lignin model in the presence of a certain carboxylic acid. However, it is still not clear whether the long and extralong MnPs share the same characteristic or not.

4.4 Conclusion

The short MnP of *C. subvermispora* exhibits activity that is not observed in the other two sub-families of MnPs. Also, it seems that the shorter C-terminal loop of the short MnP does not account for the unique activity. Mutant A205R H208K showed increases in both manganese-dependent and manganese-independent activities. Here we demonstrated that ABTS alone could be used together with the short MnP for eliciting enzymatic activity. In addition, we showed that in the presence of malonate, a carboxylic acid that can be produced by fungi, even the non-phenolic substrate could be oxidized. Because these unique characteristics have been observed for the short MnP, it might be suitable to consider the short MnP is in a different group to classical MnPs.

4.5 Experimental procedures

4.5.1 Oxidation of DMP and/or ABTS by the MnP124076

Reactions were carried out at 30 °C for 10 minutes in 200 μL of 50 mM sodium tartrate containing 5 μg/mL MnP, 0.5 mM DMP and/or ABTS, 1 mM $MnSO_4$, and 0.1 mM H_2O_2. Manganese independent activity was also examined in the absence of $MnSO_4$. The product was monitored spectroscopically by measuring the increase in absorbance at 420 and 469 nm (Infinite® 200 PRO, TECAN).

4.5.2 Plasmid construction and preparation of the mutants

The primer pairs used for inverse PCR were listed in **Table 4-4**. The expression and purification were performed followed the same procedures in section 2.5.6.

Table 4-4. The primer pairs used for constructing plasmids for the mutants.

Mutant	For./Rev.	primer sequences 5′-3′
M1	Forward	TAATGAGGATCCGAATTCAAGCTTGTC
	Reverse	CGGAATGCTGGTCTGCGGACCAACATCAATC
M3	Forward	GGCCAGGATTGTCCGTAATGAGGATCCGAATTC
	Reverse	CGGACAATCCTGGCCACCATTGCTACAATG
M4	Forward	GCGGTAATGATACCGGTGAAATTCGTCTGCAG
	Reverse	TACCTTTCGGATACGGGCTTTCAACTTCAC
M5	Forward	GCAACGTGCAGATAAAGTTGATCCGGCAATTC
	Reverse	ACTTTATCTGCACGTGCAACGCTATGGCTTG
M6	Forward	GCTCTGTGCAAAACATGCGGTAC
	Reverse	ATGTTTTGCACAGAGCCTGGCAAATAATC

4.5.3 Oxidation of DMP or ABTS by the mutants of the MnP124076

These experiments were performed by the same processes in section 3.5.2 and 3.5.3.

4.5.4 Reactions of the MnP124076 and phenolic lignin dimer model

The reactions were carried out at room temperature in 2.5 mL of 20 mM sodium tartrate (pH 4.5) containing 0.25 μM MnP124076, 0.5 mM GOG-OH, 5 mM $MnSO_4$ and/or ABTS, and 0.25 mM H_2O_2. The reaction mixtures were extracted with $CHCl_3$ for three times, dried, and dissolved in DMF containing 30 mM LiBr then applied to GPC (Asahipak GF-310HQ).

4.5.5 Oxidation of VA by the MnP124076

Reactions were carried out at 30 °C for 5 minutes in 200 µL of 50 mM sodium tartrate or sodium malonate (pH 5.0) containing 0-100 µg/mL MnP124076, 1 mM VA, 1 mM $MnSO_4$, and 0.1 mM H_2O_2. The product was monitored spectroscopically by measuring the increase in absorbance at 310 nm (Infinite® 200 PRO, TECAN).

Chapter 5. Phylogenetic analysis of GE

5.1 Introduction

To date, only eleven FGEs have been isolated and enzymatically characterized (**Table 5-1**). Six of the characterized FGEs are from Ascomycete and the rest are from Basidiomycete. As FGEs have been discovered relatively late than other lignocellulosic enzymes, the classification toward FGEs has not been reported yet. In order to recognize additional FGEs and find suitable candidates for further study, we conducted phylogenetic analysis of about four hundred putative FGEs in this chapter.

Table 5-1. Theoretical pI values calculated for the characterized FGEs.

Organism	JGI protein ID	Protein	Protein length [a]	Reference
Ascomycete				
Sporotrichum thermophile	2308381	*St*GE2	397	(80)
Neurospora crassa	9686	*Nc*GE	366	(81)
Acremonium alcalophilum	1078265	*Aa*GE1	496	(82)
Podospora anserina	2637	*Pa*GE1	481	(80)
Hypocrea jecorina	123940	Cip2/*Tr*GE	460	(34)
Aspergillus fumigatus	8491	*Af*GE	372	(37)
Basidiomycete				
Cerrena unicolor	364105	*Cu*GE	474	(83)
Phanerochaete chrysosporium	2918304	*Pc*GE1	452	(35)
Phanerochaete chrysosporium	2912243	*Pc*GE2	407	(35)
Schizophyllum commune	2754043	*Sc*GE	411	(33)
Wolfiporia cocos	23632	*Wc*GE	408	(82)

[a] Signal peptide not included.

5.2 Results

5.2.1 Construction of the phylogenetic tree

The *Ascomycota* and *Basidiomycota* are the two largest phyla of the kingdom of fungi. We conducted BLAST analyses using the amino acid sequences of FGEs, Cip2/*Tr*GE and *Sc*GE, which were characterized for the first time for *Ascomycota* and *Basidiomycota*, respectively (33, 34), as queries against the JGI *Ascomycota* and *Basidiomycota* databases. Here, we obtained as many as four hundred putative FGEs, which were then subjected to phylogenetic tree analysis. As a result, these ca. four hundred putative FGEs were classified into at least six clades, clade I to VI (**Fig. 5-1**).

The putative FGEs of *Ascomycota* (A-FGEs) showed close phylogeny and most of them clustered in clades I-IV (**Fig. 5-1**). Both clades I and IV contain only A-FGEs. There were 43 FGEs in clade II, of which nine were A-FGEs and the others were FGEs from *Basidiomycota* (B-FGEs). Clade III comprises twenty-eight members, of which twenty-seven were A-FGEs and only one was a B-FGE. Six A-FGEs that were characterized previously in the literature were shown to belong to clades I, III and IV: *St*GE2 and *Nc*GE (originating from *Neurospora crassa*) in clade I, *Aa*GE and *Pa*GE1 (originating from *Podospora anserina*) in clade III, and Cip2/*Tr*GE and *Af*GE (originating from *Aspergillus fumigatus*) in clade IV.

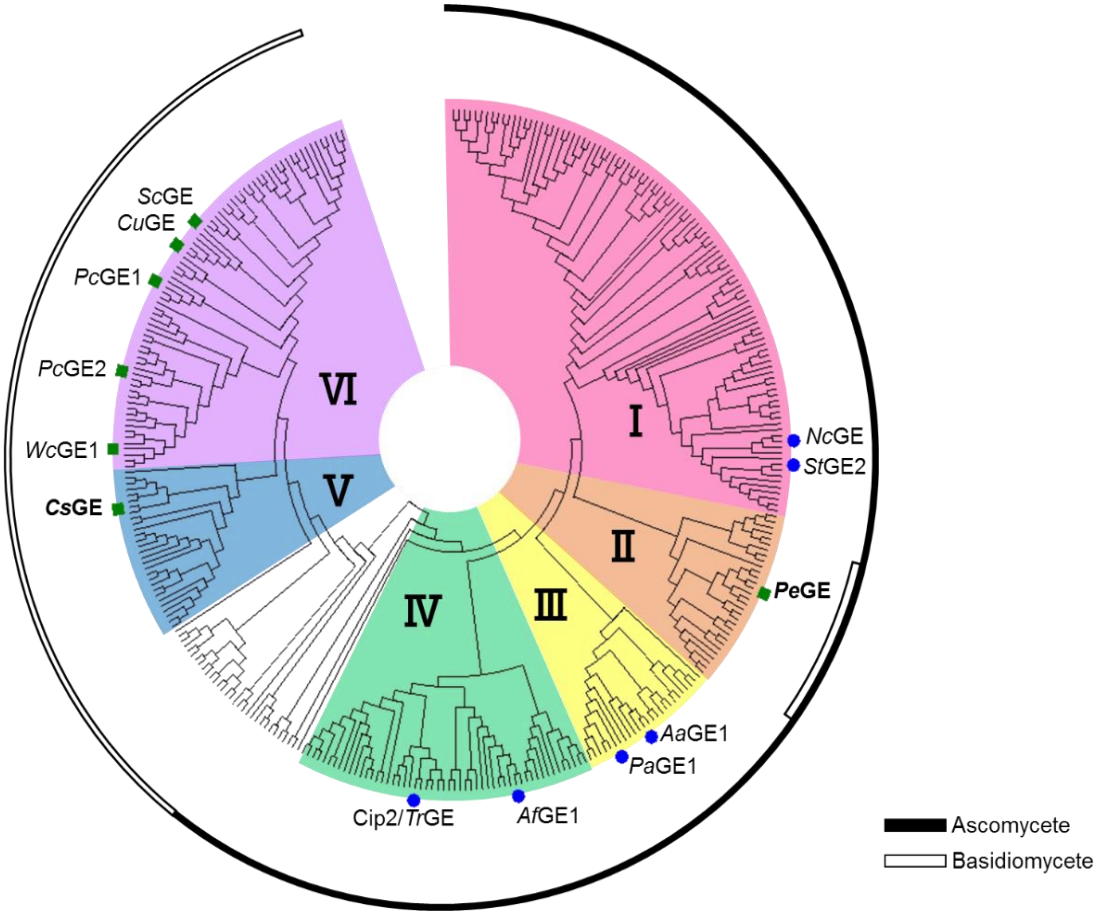

Fig. 5-1. Phylogenetic analysis of putative and characterized fungal GEs using the maximum likelihood method. About four hundred putative FGEs were collected by means of BLAST analyses against the JGI Ascomycota and Basidiomycota databases. The two GEs selected for this study, *Cs*GE and *Pe*GE, are given in bold letters. Evolutionary analysis was conducted in MEGA7. ●, Ascomycota. ■, Basidiomycota.

On the other hand, putative B-FGEs were found in clades II, V and VI. In clades V and VI, all members originated from basidiomycete fungi, while thirty-four putative B-FGEs showed distant phylogeny from other B-FGEs and clustered with a small number of A-FGEs in clade II. Five B-FGEs, four of which were from white rot fungi *S. commune* (*Sc*GE), *C. unicolor* (*Cu*GE), and *Phanerochaete chrysosporium* (*Pc*GE1 and *Pc*GE2), and the other one from brown rot fungus *Wolfiporia cocos* (*Wc*GE1), were studied and characterized previously. All of them were found to belong to clade VI, and importantly none of the putative FGEs belonging to clades II and V have been studied so far. Thus, we chose FGEs, originating from two frequently studied fungi, *Ceriporiopsis subvermispora* and *Pleurotus erygii*, in clades V and II, respectively, for further characterization.

Notably, *Pe*GE, one of the clade II FGEs, was found to have a relatively high theoretical pI, 7.30, compared with most of the studied FGEs in other clades (**Table 5-2**). We then calculated the theoretical pIs of all the B-FGEs in clade II to determine whether a high pI value is a common feature of B-FGEs in clade II. Interestingly, we found that the pI values of most of the putative B-FGEs in clade II were higher than 7.0, and eleven of B-FGEs in clade II had pI values even higher than 8.0 (**Table 5-3**). Moreover, the CE15 domain of most B-FGEs in clade II exhibited a higher pI value than in the cases of full-length proteins, even reaching 9.03. As none of the B-FGEs in clade V had been studied previously, we also calculated the theoretical pIs of B-FGEs in clade V (**Table 5-4**). The pI values of most of the B-FGEs in clade V were in the range of 4.5-5.3, and the pI values of the CE15 domains of B-FGEs in clade V were just slightly higher (between 4.5 and 5.9). The pI values of the five characterized B-FGEs in clade VI were also in the similar range (**Table 5-2**). Thus, we conclude that the high pI values of the B-FGEs in clade II are a unique feature; this special property of B-FGEs in clade II had not been noticed previously.

Table 5-2. Theoretical pI values calculated for the characterized FGEs.

Organism	JGI protein ID	Protein	Clade	Protein length	CBM domain[a]	CE15 domain[a]	pI[b]			Reference
							full length[c]	CBM domain	CE15 domain	
Ascomycete										
Sporotrichum thermophile	2308381	*St*GE2	I	397	-	44-366	5.76	-	6.33	(80)
Neurospora crassa	9686	*Nc*GE	I	366	-	42-364	8.82	-	8.76	(81)
Acremonium alcalophilum	1078265	*Aa*GE1	III	496	23-51	143-463	6.81	5.08	6.32	(82)
Podospora anserina	2637	*Pa*GE1	III	481	27-55	122-448	8.33	3.80	6.66	(80)
Hypocrea jecorina	123940	Cip2/*Tr*GE	IV	460	22-49	110-431	6.70	5.50	6.71	(34)
Aspergillus fumigatus	8491	*Af*GE	IV	372	-	34-359	6.05	-	6.04	(37)
Basidiomycete										
Pleurotus eryngii	**1593200**	***Pe*GE**	**II**	**462**	**23-50**	**108-429**	**7.30**	**5.08**	**8.38**	**This study**
Ceriporiopsis subvermispora	**21396**	***Cs*GE**	**V**	**380**	**-**	**25-352**	**4.48**	**-**	**4.56**	**This study**
Cerrena unicolor	364105	*Cu*GE	VI	474	23-51	111-440	5.97	5.50	5.97	(83)
Phanerochaete chrysosporium	2918304	*Pc*GE1	VI	452	25-52	91-418	5.40	5.50	5.87	(35)
Phanerochaete chrysosporium	2912243	*Pc*GE2	VI	407	-	43-371	4.87	-	4.91	(35)
Schizophyllum commune	2754043	*Sc*GE	VI	411	-	54-377	4.34	-	4.58	(33)
Wolfiporia cocos	23632	*Wc*GE	VI	408	-	45-373	4.05	-	4.10	(82)

[a] The domains of the FGEs were identified with dbCAN (84).

[b] Theoretical pI values were calculated with the ExPASy ProtParam tool (85).

[c] Signal peptide not included.

Table 5-3. The putative B-FGEs in clade II that have high pI values.

Organism	JGI protein ID	Protein length	CBM domain[a]	CE15 domain[a]	pI[b]		
					full length[c]	CBM domain	CE15 domain
Aporpium caryae	672976	465	22-49	110-433	7.11	3.80	8.30
Auricularia subglabra	1151471	464	22-49	111-432	7.08	5.81	8.63
Auricularia subglabra	1150552	464	22-49	110-432	7.11	5.81	8.75
Coprinellus micaceus	839747	394	-	38-359	8.73	-	8.81
Coprinellus micaceus	1876306	466	24-51	111-432	7.15	5.81	8.29
Coprinellus pellucidus	495275	464	26-53	112-433	8.30	5.81	8.27
Coprinopsis cinerea	5049	464	23-51	110-430	8.08	6.31	8.32
Coprinopsis cinerea	5050	463	24-50	110-429	8.34	5.81	8.87
Coprinopsis marcescibilis	704457	390	-	37-357	8.93	-	9.03
Exidia glandulosa	720300	465	22-46	111-433	7.65	7.96	8.29
Lepista nuda	239945	453	23-50	98-419	8.07	5.81	8.86
Lepista nuda	1306438	458	23-50	101-424	7.07	5.81	8.31
Panaeolus papilionaceus	1417416	469	23-51	114-434	8.29	5.50	8.96
Panaeolus papilionaceus	1356968	407	-	52-373	7.24	-	8.30
Pleurotus eryngii	**1593200**	**462**	**23-50**	**108-429**	**7.30**	**5.08**	**8.38**
Pluteus cervinus	816223	471	24-51	115-438	8.06	5.81	8.85
Pluteus cervinus	894910	468	24-51	113-435	8.34	5.82	9.03
Sebacina vermifera	80942	467	22-49	113-435	7.62	5.81	8.50
Sebacina vermifera	111216	466	21-49	112-433	8.02	5.50	8.90
Sebacina vermifera	694308	468	21-49	115-436	8.28	5.81	8.24
Volvariella volvacea	114383	905	467-494	550-871	-	5.82	8.90

[a] The domains of the FGEs were identified with dbCAN (84).

[b] Theoretical pI values were calculated with the ExPASy ProtParam tool (85).

[c] Signal peptide not included.

Table 5-4. The putative B-FGEs in clade V.

Organism	JGI protein ID	Protein length	CBM domain[a]	CE15 domain[a]	pI[b]		
					full length[c]	CBM domain	CE15 domain
Botryobasidium botryosum	35624	472	439-466	34-360	8.06	5.81	8.61
Ceriporiopsis subvermispora	**118322**	**408**	**-**	**44-371**	**4.4**	**-**	**4.51**
Clavicorona pyxidata	1801462	476	26-53	113-441	5.26	5.5	5.58
Clavicorona pyxidata	1837391	335	-	38-300	4.75	-	5.57
Clavicorona pyxidata	1919872	405	-	44-370	5.02	-	5.18
Clavicorona pyxidata	166255	404	-	43-369	4.98	-	5.21
Dendrothele bispora	368841	473	26-53	108-436	5.87	7.94	5.86
Dentipellis sp.	83524	474	26-53	111-439	4.97	5.81	5.16
Gloeopeniophorella convolvens	564372	483	27-55	120-448	5.04	3.80	5.59
Gymnopus androsaceus	989777	405	-	42-369	4.40	-	4.53
Gymnopus earleae	1118812	406	-	43-370	4.49	-	4.57
Gymnopus earleae	21086	472	27-54	110-437	4.68	4.00	5.05
Gymnopus luxurians	245004	405	-	42-369	4.44	-	4.75
Gymnopus luxurians	150683	444	-	82-409	(5.19)	-	5.33
Lentinellus vulpinus	890711	471	26-53	108-436	5.20	4.00	5.61
Lentinellus vulpinus	251035	405	-	38-366	6.58	-	6.13
Obba rivulosa	762191	408	-	44-371	4.54	-	4.7
Phlebia brevispora	125019	418	-	55-383	4.66	-	4.94
Rhodocollybia butyracea	1383016	354	-	40-318	4.53	-	4.64
Tulasnella calospora	4221	484	25-53	121-449	5.74	5.50	5.96
Tulasnella calospora	210406	487	26-61	124-452	6.57	4.53	7.10
Vuilleminia comedens	398242	476	26-53	113-441	4.84	5.5	5.32
Vuilleminia comedens	947964	406	-	43-369	4.57	-	4.79

[a] The domains of the FGEs were identified with dbCAN (84).

[b] Theoretical pI values were calculated with the ExPASy ProtParam tool (85).

[c] Signal peptide not included.

5.2.2 Sequences alignment of CsGE, PeGE and previously characterized FGEs

Alignment of the amino acid sequences of *Cs*GE and *Pe*GE with previously characterized FGEs revealed the presence of the consensus sequence V-T-G-C-S-R-X-G-K-G-A (36, 37), and the catalytic triad Ser-His-Glu in both *Cs*GE and *Pe*GE (**Fig. 5-2a**). The Cys residues that are highly conserved among FGEs and reportedly form disulfide bonds were conserved in *Cs*GE (Cys197-Cys332 and Cys228-Cys304 of *Cs*GE correspond to residues Cys328-Cys464 and Cys360-Cys436 in **Fig. 5-2a**). We noticed that one of the Cys residues of *Pe*GE (Ser306 of *Pe*GE corresponds to residue 360 in **Fig. 5-2a**) was replaced with Ser. To determine whether the Cys to Ser substitution is a common feature of clade II FGEs, we further examined the conservation of the amino acid sequences of the clade II FGEs (**Fig. 5-2b**). This substitution, however, was not observed in any other listed proteins. Additionally, the consensus sequence, catalytic triad, and the Cys residue (Ser306 of *Pe*GE corresponds to residue 360 in **Fig. 5-2a** and residue 766 in **Fig. 5-2b**) were all conserved in all the other FGEs (**Fig. 5-2b**). Thus, *Pe*GE turned out to be an exception.

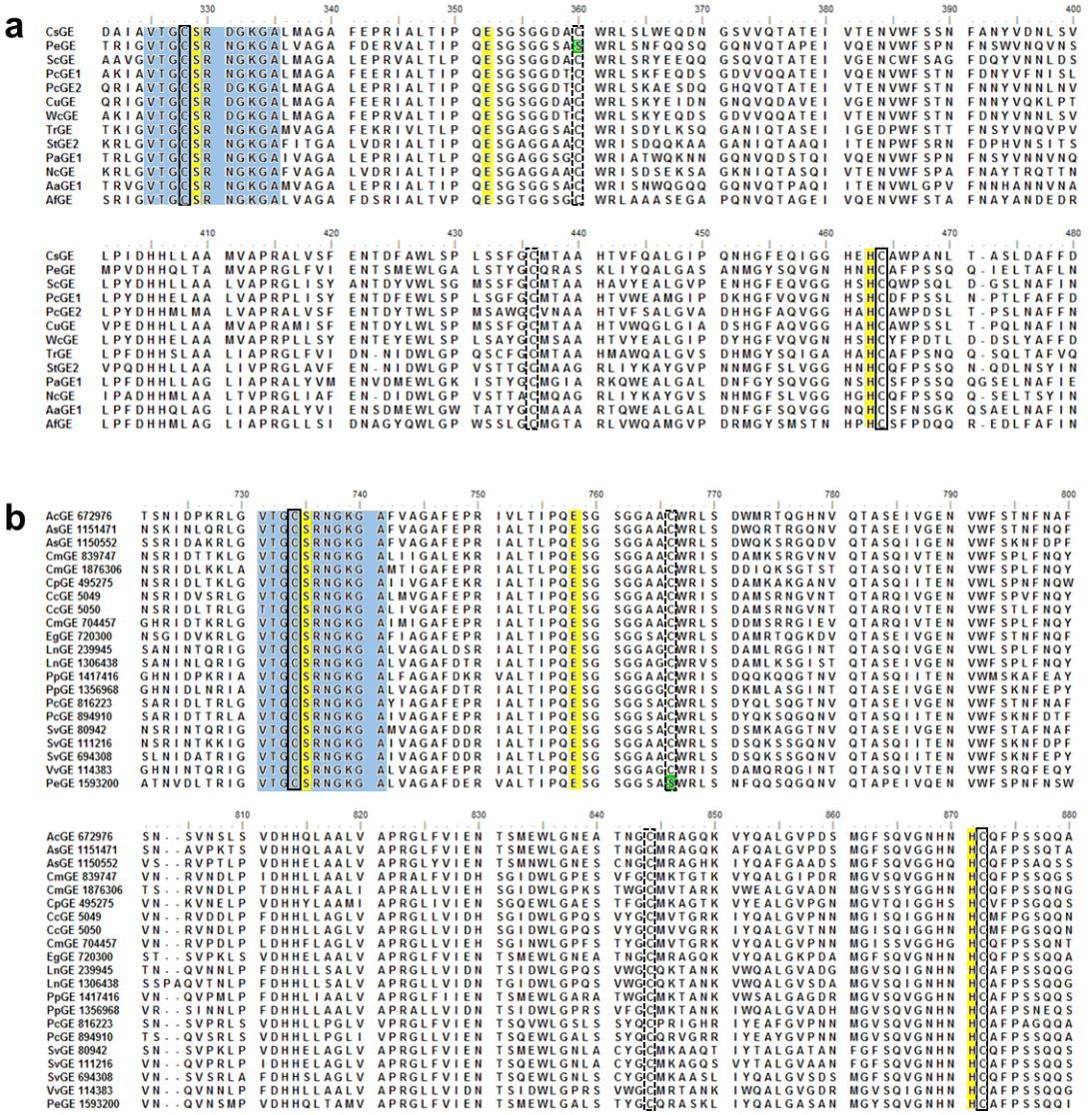

Fig. 5-2. Alignment of amino acid sequences involving the consensus sequence and the catalytic triad of the FGEs.

(a) FGEs studied in this study (*Cs*GE and *Pe*GE) and previously studied FGEs. (b) FGEs in clade II. The blue shaded region indicates the consensus sequence VTGCSRXGKGA. The catalytic triad residues (Ser-His-Glu) are marked in yellow, and the conserved cysteine residues that form disulfide bonds are framed, the pairs being indicated by solid or dotted boxes. The Cys to Ser mutation of *Pe*GE is colored green.

5.3 Discussion

GEs are a relatively new group of lignocellulosic enzymes, and only a few GE members have been studied and characterized so far. Recently, classification of GEs of both bacteria and fungi by peptide pattern recognition (PPR) was reported (86). PPR analysis suggested that the number of CE15 proteins is less in bacteria than in fungi. Meanwhile, high diversity of CE15 genes of Basidiomycota was predicted (86). Because of the novelty of CE15, we conducted phylogenetic analysis of putative GEs of fungi (FGEs). It can be imagined that FGEs originating from the same phylum exhibit closer phylogeny. Indeed, all the putative FGEs of *Ascomycota* (A-FGEs) were closely clustered and so did most of the putative FGEs of *Basidiomycota* (B-FGEs). Interestingly, we found a small group of B-FGEs that exhibit close phylogeny to a group of A-FGEs and form one taxonomical group, clade II, in the phylogenetic tree. This may be consistent with the previously predicted high diversity of CE15 genes in *Basidiomycota* (86).

We noticed that all the characterized B-FGEs belong to clade VI and that the B-FGEs in two other clades, clades II and V, remained unexplored. Hence, to characterize the B-FGEs in these two unexplored clades, we chose a *Pe*GE of clade II and a *Cs*GE of clade V for further investigation. Both *P. eryngii* and *C. subvermispora* are widely distributed white rot fungi and have been extensively studied due to their conspicuous ability to degrade lignocellulosic materials. *P. eryngii* is regarded as either saprobic or weakly parasitic, and lives on the roots of herbaceous plants, while *C. subvermispora* grows on wood aggressively. *P. eryngii* had been cultivated in several types of agriculture waste, and the putative CE15 protein of *P. eryngii* was found to be secreted to some extent under several conditions (87). It has also been reported that when *C. subvermispora* was grown aspen wood-containing medium for 5-7 days, the putative CE15 protein was the third abundant enzyme secreted by *C. subvermispora* (39). Thus, previous secretome profiles of fungal enzymes indicated that *Pe*GE and *Cs*GE may play important roles in wood degradation.

When the amino acid sequences and the protein properties of the selected *Pe*GE and *Cs*GE were compared with those of all other previously characterized FGEs, we found that *Pe*GE has a higher pI than most of the reported FGEs. Moreover, FGEs in clade II turned out to exhibit this property in general. It is worth mentioning that the pI values of the catalytic CE15 domains of most of the clade II B-FGEs are higher than 8.30. Unlike

those of other B-FGEs of different clades, those B-FGEs of clade II are expected to be positively charged under acidic, neutral, and even weak alkali conditions. This feature of B-FGEs of clade II may have unique effects on their enzymatic functions.

5.4 Conclusion

We constructed a phylogenetic tree from nearly four hundred FGEs and defined six clades, four of which were mainly composed of A-FGEs, the other two containing only B-FGEs. Then, two B-FGEs in the unexplored clades, *Pe*GE in clade II and *Cs*GE in clade V, were chosen as the targets of further characterization. We also discovered that most B-FGEs in clade II have higher theoretical pI values than all other B-FGEs in different clades, which suggests that the clade II FGEs may potentially degrade LCC complexes in a different pH range to other FGEs in different clades.

5.5 Experimental procedures

The fungal genomic database of the Department of Energy Joint Genome Institute (JGI) was used to search for putative FGEs. The full length amino acid sequences of Cip2/*Tr*GE (JGI protein ID: Trire2 123940) and *Sc*GE (JGI protein ID: Schco3 2754043) were used as query sequences against the JGI *Ascomycota* and *Basidiomycota* databases, respectively, using BLASTP with default parameters. The protein sequences of hypothetical FGEs exhibiting similarity higher than 50% were aligned using ClustalW. Then a phylogenetic tree was constructed by the maximum likelihood method of MEGA7 based on the above alignment. Signal sequences were identified with SignalP 4.1 (88). The domains of the FGEs were identified with dbCAN (84). Theoretical molecular masses and pI values were calculated by ExPASy ProtParam tool (85).

Chapter 6. Expression and characterization of the *Cs*GE and *Pe*GE

6.1 Introduction

In chapter 5, we have defined six clades and it was found that no FGE of either clade II or V has been characterized yet. Subsequently, we focused on two putative FGEs of two white rot basidiomycetes, *Ceriporiopsis subvermispora* (*Cs*GE) and *Pleurotus eryngii* (*Pe*GE), which belong to clades V and II, respectively. We then expressed the catalytic domain of *Cs*GE by means of the *E. coli*, *Brevibacillus choshinensis* and *Pichia pastoris* expression systems. Finally, *P. pastoris* expression system was used for preparing both CsGE and PeGE, and purification methods were subsequently established for *Cs*GE and *Pe*GE.

The esterase activity and its tolerance to several reagents of both *Cs*GE and *Pe*GE were estimated by the previously described UDH-coupled spectrophotometric assay method (**Fig. 6-1**) (80) using BnGlcA as the substrate.

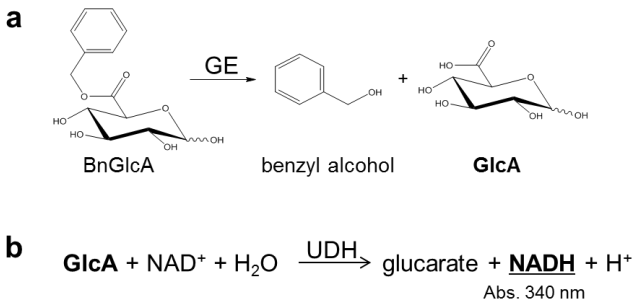

Fig. 6-1. UDH-coupled spectrophotometric assaying of GE enzymatic reaction. (a) Hydrolysis of BnGlcA catalyzed by GE. (b) Spectrophotometric assaying by NAD^+-dependent oxidation of GlcA using uronate dehydrogenase (UDH).

6.2 Results

6.2.1 Soluble expression by *E. coli*

A popular host, *E. coli*, was selected as our first bacteria candidate to express *Cs*GE. Although the target protein formed as inclusion bodies in most of the cases, an adequate amount of soluble recombinant *Cs*GE has been successfully provided by the use of cold shock expression system. CHAPS was included in the protein solution for increasing the solubility of *Cs*GE. The natural *Cs*GE may be a glycosylated protein thus the molecular mass may not be unitary, but that is not an issue in the use of *E. coli* expression system.

The N-terminal hexa-His tag fused *Cs*GE having predicted molecular mass of 42.8 kDa was confirmed by SDS-PAGE (**Fig. 6-2**). Glycerol was added to the solution containing target *Cs*GE to 10% for diminishing the hydrophobic interaction. The resulted *Cs*GE containing solution was then loaded to Ni-affinity column. The *Cs*GE eluted with a relatively low concentration of imidazole, 50-100 mM, and this special property has also been observed in other FGEs (89). About 2.9 mg of purified *Cs*GE was obtained from 0.5 L LB culture (about 13 g wet cell) after this one step purification. To prepare the sample for activity assay, the use of desalting column has an advantage over prompt imidazole removal and pH adjustment of the buffer at the same time (**Fig. 6-2**).

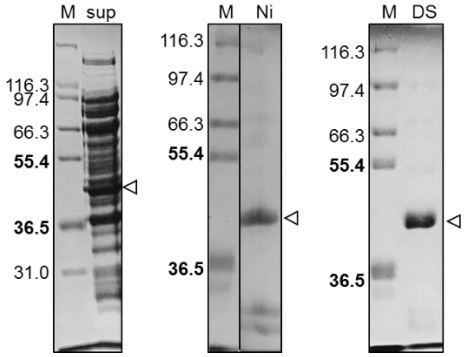

Fig. 6-2. Purification of *Cs*GE expressed in *E. coli*.
The protein expressed in soluble fraction (sup) was purified by Ni affinity column (Ni), and then the imidazole removal and buffer exchange were performed by desalting column (DS). "Arrowheads", the bands of the target *Cs*GE; "M", Molecular weight maker (M).

6.2.2 Secrete expression by *B. choshinensis*

Three vectors (pBIC2, pBIC3, and pNC-HisT) and three types of growth media (2SY, LB, and TM) were used to examine the expression of His-tagged *Cs*GE by *B. choshinensis*. Compared with the empty plasmid, the results of SDS-PAGEs clearly showed that the *Cs*GE was successfully secreted to the culture media in all the conditions whereas the use of pNC-HisT resulted in the highest expression level among the three plasmids in all the growth media (**Fig. 6-3**). Therefore, we further monitored the growth of *B. choshinensis* carrying pNC-HisT-csge plasmid and the *Cs*GE expression in LB and TM media over 72 hours at 30 °C and 120 hours at 25 °C (**Fig. 6-4**). The growth and the expression in LB and TM shared a similar pattern while incubation over 72 hours under 30 °C provided a higher amount of the *Cs*GE than 120 hours under 25 °C. We did not

proceed the same investigation toward 2SY medium because it is known that the components in the 2SY medium may cause the removal of Ni from the column resin during purification.

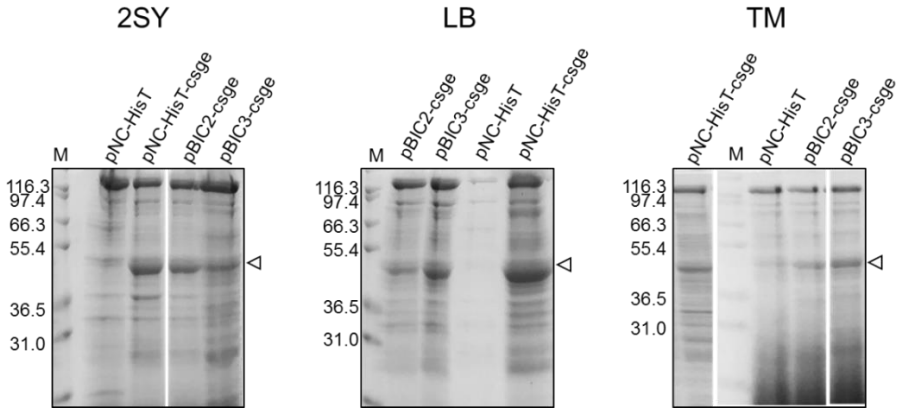

Fig. 6-3. *B. choshinensis* secretion expression of *Cs*GE over 72 hours at 30 °C. SDS-PAGEs are presented to show the amounts of the His-tagged *Cs*GEs expressed from *B. choshinensis* harboring different plasmids, and secreted into media. "2SY", "LB", and "TM" indicate the media used. The labels of the lanes indicate the samples for His-tagged CsGE expressing plasmids, pNC-HisT-csge, pBIC2-csge, and pBIC3-csge, as well as that for the empty plasmid pNC-HisT as a negative control. Arrowheads indicate the bands of His-tagged *Cs*GE.

The culture supernatants containing secreted *Cs*GE were dialyzed for the purification by using of Ni^{2+} sepharose. In spite of the protein precipitation which may due to disulfide bond mediated aggregation, a sufficient amount of *Cs*GE for activity assay was obtained after the purification by Ni^{2+} sepharose. The target *Cs*GE was eluted with 50-100 mM of imidazole, which was consistent with the one prepared from *E. coli* expression system. We noticed that some *Cs*GE did not bind to the Ni^{2+} sepharose, perhaps due to the fouling of Ni^{2+} sepharose by components which come from culture medium or precipitation of the protein.

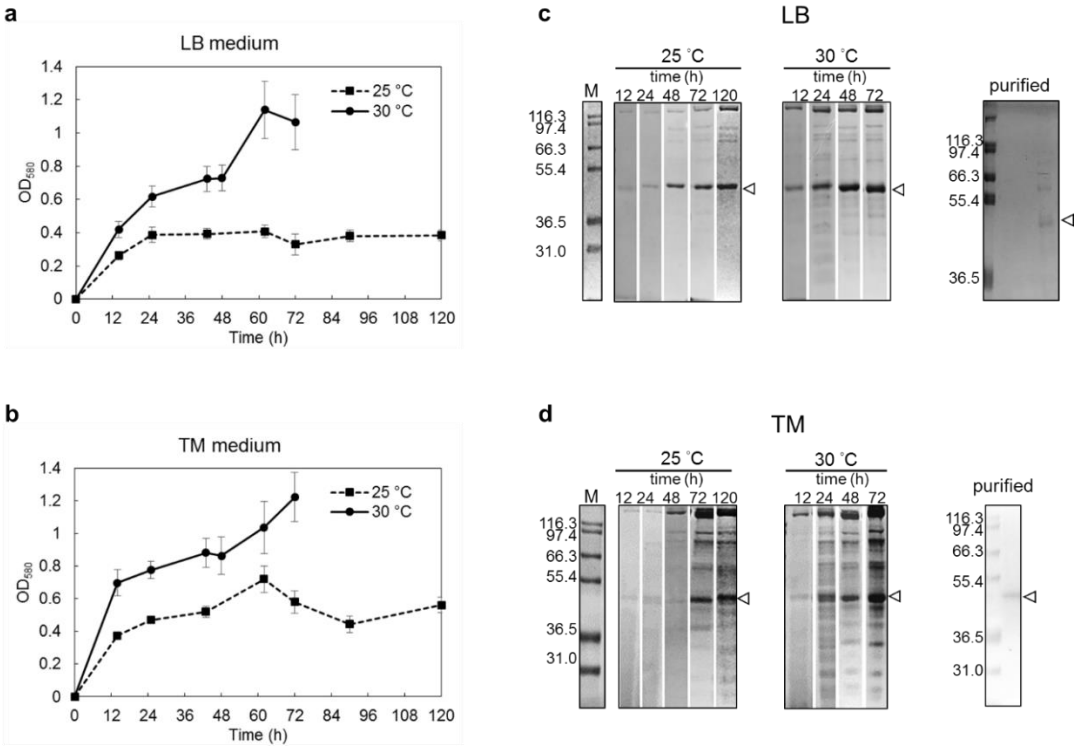

Fig. 6-4. Time course of *B. choshinensis* growth and expression of *Cs*GE in different media and temperatures.
Growth curves of *B. choshinensis* grown either in LB medium (**a**) or TM medium (**b**), which were incubated either at 25 °C (solid line, ●) or 30 °C (broken line, ■) are presented. (**c, d**) SDS-PAGEs of the expressed and purified *Cs*GEs sampled at different time points of the growth curves in (a) and (b).

6.2.3 Secrete expression by *P. pastoris*

To confirm the FGE activity of the putative *Cs*GE and *Pe*GE, we constructed a plasmid containing the gene of the CE15 domain. Production of recombinant *Cs*GE and *Pe*GE was successfully achieved with the *P. pastoris* expression system. For *Cs*GE, *P. pastoris* X-33 carrying the *csge* gene produced the target protein of 46 kDa in the culture supernatant (**Fig. 6-5a**). To adapt the secreted *Cs*GE for purification on Ni^{2+} Sepharose, we concentrated the culture supernatant. After adjusting the pH to 7.0, the resulting solution containing *Cs*GE was loaded on to Ni^{2+} Sepharose and the target *Cs*GE was eluted with 50-250 mM imidazole (**Fig. 6-5b**). Each fraction was collected and concentrated, after which we examined the molecular mass of the protein by SDS-PAGE. All the fractions contained the target protein of 46 kDa. The activity of the *Cs*GE in each fraction was then checked using BnGlcA as a substrate. Fraction 4 showed the highest activity (**Fig. 6-5c**), and was thus used for the following analysis. The same process was

applied to *Pe*GE. Fraction 2 exhibited higher activity (**Fig. 6-5d-f**), and was thus used for the following analysis. Finally, after purification, about 1.1 mg of active *Cs*GE and 160 μg of active *Pe*GE were obtained from 1.2 L culture media.

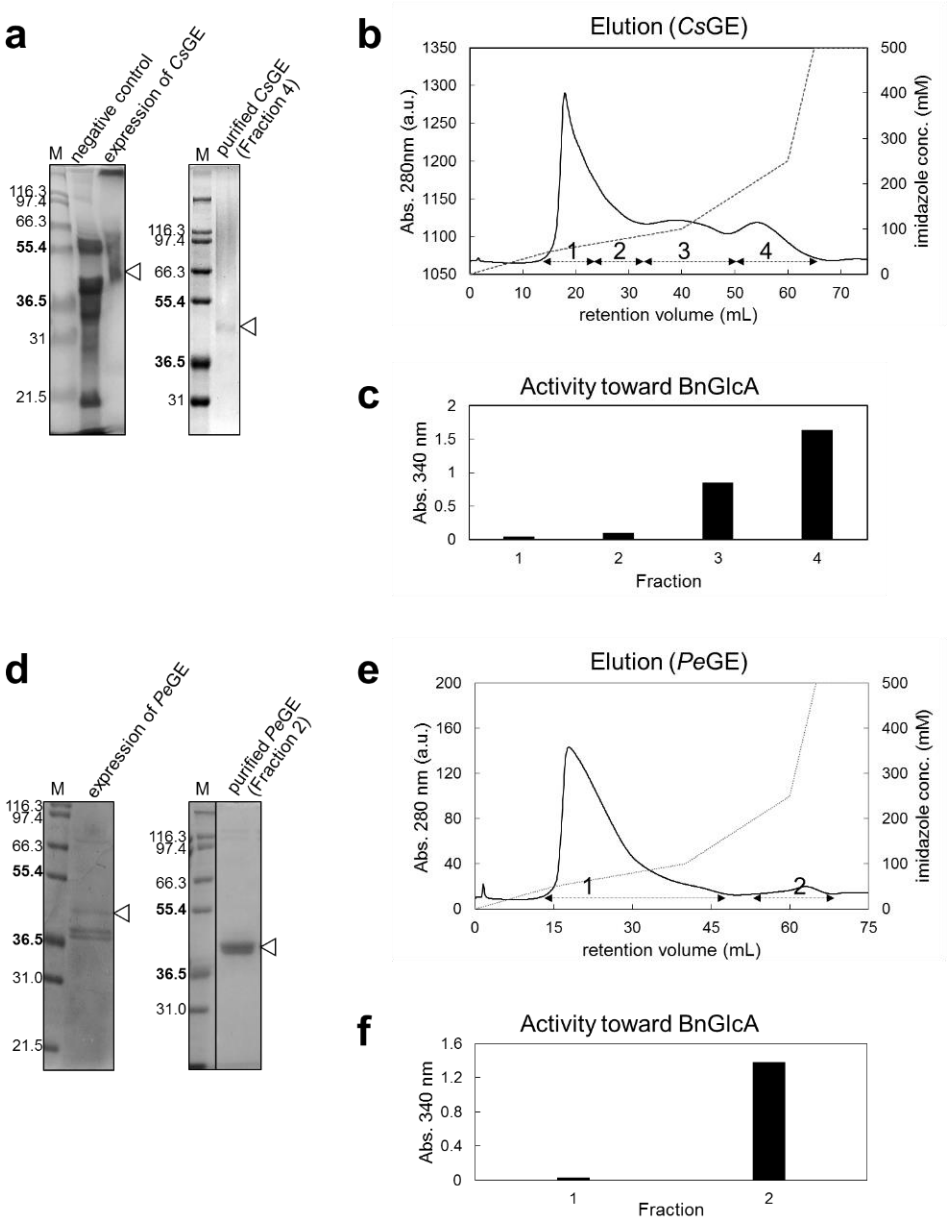

Fig. 6-5. Expression of recombinant *Cs*GE and *Pe*GE using the *P. pastoris* expression system, and their purification.
(a, d) SDS-PAGE analyses of the expression and purification of *Cs*GE (a) and *Pe*GE (d). (b, e) Chromatograms showing the eluted fractions during Ni-affinity chromatography (Histrap HP 5 mL) of *Cs*GE (b) and *Pe*GE (e). Solid lines: protein absorption (280 nm); dotted lines: the imidazole gradient concentrations. (c, f) The FGE activities toward BnGlcA of the selected fractions.

6.2.4 Activity assays

Due to the unstable nature of the substrate BnGlcA, the conditions for the activity assay are limited (80). Here, we used a 50 mM sodium phosphate buffer (pH 6.2) containing 500 mM NaCl and 0.2% CHAPS. The enzyme reactions were performed at 30 °C. The effects of several additives, such as denaturants, inhibitors, and surfactants, were investigated (**Fig. 6-6**). After incubation with a high concentration of EDTA (10 mM) for 20 min, both *Cs*GE and *Pe*GE retained more than 85% activity.

The previous reports on other FGEs have mentioned that the activity was not affected by EDTA (33, 37, 81). Additionally, metal ions were not found in the crystal structures of the other FGEs, *Tr*GE and *St*GE2 (PDB ID: 3pic and 4g4g, respectively) (38, 90). Thus, we inferred that divalent metal ions, such as Mg^{2+} and Ca^{2+}, are not necessary for these enzymes to exert their activity, although the possibility cannot be completely excluded that tightly bound metal ions were not removed even with 10 mM EDTA. 5 mM imidazole affected the activity of *Cs*GE to some extent, which indicates that imidazole should be completely removed after Ni-affinity column purification for the accurate estimation of the activity. Next, we investigated the effect of a reducing agent on FGE's activity. Because the reaction was performed under acidic conditions, we used TCEP instead of frequently used DTT; TCEP is known to exhibit higher reducing ability than DTT under acidic conditions. The addition of TCEP led to an about 30% decrease in the activity of *Cs*GE. PMSF is a commonly used inhibitor for Ser-type esterase; it covalently binds to the active center Ser residue that resides on the surface of proteins. 5 mM PMSF caused a 26% loss of the activity of *Cs*GE. By contrast, *Pe*GE showed higher tolerance to both TCEP and PMSF. Non-ionic detergents such as Tween 20 and Tween 80, and zwitterion detergent CHAPS are widely used to increase the solubility of either substrate or enzyme. The addition of these three detergents did not lead to a distinct improvement in the activity of both *Cs*GE and *Pe*GE toward BnGlcA. Notably, the activities of both *Cs*GE and *Pe*GE decreased by 46% in the presence of 5% glycerol and were almost lost completely with 1% SDS (**Fig. 6-6**).

To determine kinetic parameters, we newly introduced a reaction-quenching step that was not mentioned in the previous reports (80, 82). We added 2% SDS after the first reaction with FGE, which enabled the complete quenching of the reaction with FGE. Then, we applied the second reaction, the UDH-coupling NAD^+-dependent spectrophotometric

assay reaction. The final concentration of SDS for UDH-coupling NAD^+-dependent spectrophotometric assay was 0.1% due to the dilution prior to this assay. We confirmed that 0.1% SDS has no effect on the second reaction (data not shown). The kinetic parameters were determined (**Table 6-1**) for both *Cs*GE and *Pe*GE, *Pe*GE exhibiting superior enzymatic activity toward BnGlcA.

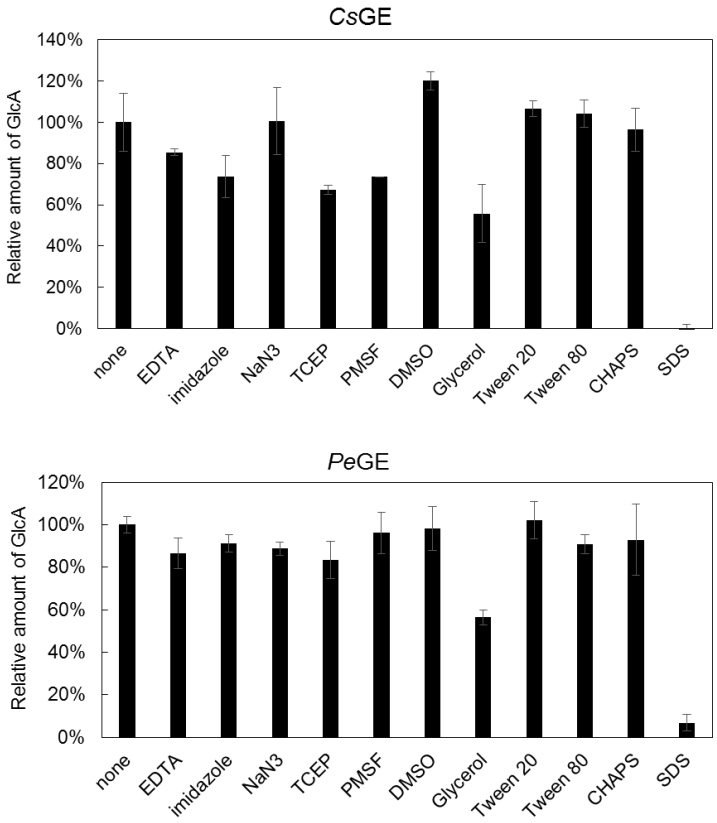

Fig. 6-6. Effects of additives on the activities of *Cs*GE and *Pe*GE toward BnGlcA. Activities were tested with the purified *Cs*GE and *Pe*GE supplemented with none or one of the following reagents, 10 mM EDTA, 5 mM imidazole, 5 mM NaN_3, 5 mM TCEP, 5 mM PMSF, 10% DMSO, 5% glycerol, 2% Tween 20, 2% Tween 80, 1% CHAPS, or 1% SDS. For reaction, samples were incubated at 30 °C for 20 min. The data represent the averages with standard deviations derived from three independent experiments. The activities of the *Cs*GE and *Pe*GE without the addition of the mentioned reagents were taken as 100%.

Table 6-1. Kinetic parameters for *Cs*GE and *Pe*GE with BnGlcA as the substrate.

	K_m (mM)	V_{max} ($\mu mol \cdot mg^{-1} \cdot min^{-1}$)	k_{cat} (s^{-1})	k_{cat}/K_m ($s^{-1} \cdot mM^{-1}$)
*Cs*GE	55.8	30.6	23.6	0.42
*Pe*GE	23.9	150.7	104.6	4.38

6.3 Discussion

We demonstrated that soluble FGEs could also be obtained by using both *E. coli* and *B. choshinensis* expression systems. *E. coli* expression system has been commonly used; it has several advantages such as easy-handling, less time-consuming, and convenient and affordable for making either mutated or isotope-labeled proteins. Fairly new protein expression system of *B. choshinensis* is a gram-positive bacterium, which is able to secrete proteins in large quantity with low protease activity (91). The most attractive property of *B. choshinensis* is that it shows the ability to produce correctly disulfide-bonded proteins with high efficiency (92). It is known that eukaryote secreted proteins, including fungal wood-degrading enzymes, generally contain disulfide bonds to stabilize their structures. Use of *B. choshinensis* as the host for producing wood-degrading enzymes has not been reported yet, so we investigated the possibility whether it can be used as an alternative way for expression of fungal secreting enzymes.

For *E. coli* protein expression system, we tested several different conditions and most of the conditions resulted in the production of *Cs*GE as inclusion bodies. The presence of three putative disulfide bonds and probably a high hydrophobicity are the possible reasons for the formation of inclusion body. Soluble expression was succeeded with the use of the pMAL-p2x and pCold I vectors. The pMAL-p2x vector encodes genes encoding signal peptide and *malE*, which resulted in the expression of maltose-binding protein (MBP) fused *Cs*GE in the periplasm. The solubility of the MBP fused *Cs*GE was high but the cleavage of the MBP led to precipitation of *Cs*GE and significant yield loss. On the other hand, the pCold vector containing a cold shock protein A (cspA) promoter is capable of expressing target protein at a lower incubation temperature, which generally increases the solubility of the target protein. In the case of *E. coli* expression system, lowering the temperature of the medium during the expression reportedly enhance the solubility of the target proteins (61, 62). The solubly expressed *Cs*GE was then purified by the Ni-affinity chromatography. We found many unwanted proteins, which were probably bound to the target protein non-specifically, were eluted together with the target protein. This problem was alleviated by using the buffer solution containing glycerol during purification as glycerol may have diminished the hydrophobic interactions between the target protein and unwanted proteins. To remove imidazole and change buffer conditions after Ni-affinity chromatography step, we found that the desalting column

serves an adequate way to avoid severe precipitation of the purified *Cs*GE. Here we demonstrated the first example of obtaining active FGE by *E. coli* expression system.

We then tested the protein expression system of *B. choshinensis* to see whether it can be used for producing FGEs. The secretion of *Cs*GE by *B. choshinensis* was successful and the secreted *Cs*GE was purified. However, purification was rather inefficient since we lost a significant amount of the target protein during Ni-affinity chromatography step. We assume that either the components in the media or some proteins produced by *B. choshinensis*, or both may exhibit nonspecific binding with the secreted *Cs*GE and/or Ni-beads, thereby interfered with the interaction between *Cs*GE and Ni-beads. As the undesired proteins secreted into the medium by *B. choshinensis* are far less than the undesired proteins expressed by *E. coli* expression system, it is not necessary to add glycerol in the buffer during the Ni-affinity purification step. The activity of the secreted *Cs*GE was confirmed and this expression system could be an alternative way of directly applying to actual biomass degradation process.

However, both *E. coli* and *B. choshinensis* expression systems failed to provide *Pe*GE. We found that both *Cs*Ge and *Pe*GE could be successfully expressed by the frequently used *P. pastoris* secretion expression system and both enzymes could be easily purified by Ni^{2+} affinity chromatography.

Commercially available BnGlcA was used to examine the activity of the recombinant *Cs*GE and *Pe*GE in this study. Here the UDH-coupling NAD^{+}-dependent spectrophotometric assay was applied to measure the activity quantitatively. We found that *Pe*GE is more resistant to the addition of TCEP. Previously, FGEs were classified as Ser-type esterases. Several studies showed, however, that the activity of FGEs was not inhibited completely by PMSF (33, 34, 36, 37, 81). Interestingly, *Pe*GE retained almost 100% of its original activity even in the presence of 5 mM PMSF. Additionally, we found that isopropyl alcohol, which was used to dissolve PMSF, could perceptibly increase the activity of *Pe*GE. Therefore, the compensation effect of isopropyl alcohol on the inhibition of PMSF should be taken into account. Here we could only conclude that the activity of *Pe*GE is slightly inhibited by PMSF under pH 6.2. Protein structure homology-modeling of *Pe*GE suggested that the active center serine residue is exposed on the surface of the protein (data not shown). This indicates that difficulty in access of PMSF to the active center serine cannot be the reason for the weak inhibition. Pokkuluri *et al.*

obtained the crystal structure of *Tr*GE in the presence of PMSF (38). However, the binding between PMSF and the active serine residue remains unclear. Further structure analysis is needed. In any case, *Pe*GE turns out to be more tolerant to the addition of PMSF than *Cs*GE. Apart from PMSF, we observed that in the presence of glycerol, both *Cs*GE and *Pe*GE lost about half of their original activities. This indicates that the hydrophobic interaction may be critical for the enzymatic reactions, as glycerol has been reported to inhibit the binding between hydrophobic compounds and the hydrophobic surface of proteins (93).

As lignin contains a large amount of aromatic groups, detergents may become necessary when FGEs are used to cleave the ester bonds in LCC. Although a great improvement in the activity of *Cs*GE and *Pe*GE toward BnGlcA was not observed by the addition of Tween 20 and Tween 80, non-ionic detergents that are commonly used in enzymatic lignocellulose degradation, the improvement of solubility or accessibility of the substrates by these detergents could play an important role when more complex model substrates or even natural lignocellulose biomass are dealt. As the activity assay buffer contains 0.2% CHAPS, we also examined the effect of CHAPS on the enzymatic reaction. CHAPS is a zwitterionic detergent, which reportedly increases solubility and stability of proteins. For the activity assay used here, CHAPS seems not to affect the activity. Although DMSO is similarly a solvent that is very often used for dissolving and/or stabilizing lignocellulose model substrates, it may also cause denaturation or precipitation of proteins. We demonstrated that both *Cs*GE and *Pe*GE retain their original activity even if the reaction was operated under relatively high concentration of DMSO (10%, about 1.5 M).

Previously, the UDH-coupled spectrophotometric assay system was used for qualitative enzymatic characterization (80). A weak point of this assay system is that the first reaction (BnGlcA hydrolysis reaction by FGE) is not completely quenched, and therefore the first reaction continues even during the second reaction (UDH-coupled reaction). The substrate, BnGlcA, is unstable and easily degraded under several conditions, such as basic (pH>6.5), acidic (pH<4), and high temperature conditions. We intended to find reagents and conditions that can irreversibly denature FGE without inducing the degradation of BnGlcA; this may become a good method to quench the enzymatic reaction. SDS is widely used in protein studies and could denature proteins

effectively. Since we found that 2% SDS can inactivate the activities of both *Cs*GE and *Pe*GE almost completely, we modified this assay system. To quench the first reaction, we added SDS to the final concentration of 2%. Thus, we could quench the FGE enzymatic reaction completely before the second reaction. Additionally, the effect of self-hydrolysis of BnGlcA was eliminated by using heat-inactivated *Cs*GE and *Pe*GE as negative controls. These modifications enabled us to obtain reliable kinetic parameters. It turned out that the *Pe*GE exhibits the highest catalytic efficiency (k_{cat}/K_m) toward BnGlcA among all studied FGEs (37, 80, 82).

6.4 Conclusion

Both *Pe*GE and *Cs*GE were successfully expressed and purified, and showed the ability to hydrolyze commercially available substrate, BnGlcA. We found that 2% SDS can inactivate the enzymatic activities of *Pe*GE and *Cs*GE effectively. As a result, the UDH-coupled spectrophotometric assay system can now be used reliably for quantitative activity assaying by using SDS to quench the FGE reaction completely. This reaction-quenching method should be applicable to all other GEs. Finally, we showed that *Pe*GE exhibits very high catalytic efficiency as to BnGlcA and high tolerance toward various reagents.

6.5 Experimental procedures

6.5.1 Plasmid construction

The genes encoding putative *Cs*GE (JGI protein ID: Cersu1 21396) and *Pe*GE (JGI protein ID: Pleery1 1593200) were synthesized by Thermo Fisher Scientific (Genbank accession number: MH361011 for *Cs*GE and MH361012 for *Pe*GE). The primer pairs for PCR and the selected restriction enzyme sites were listed in **Table 6-2**.

For *E. coli* expression system, the PCR amplified *csge* gene was digested with corresponding restriction enzymes (New England Biolabs Inc.), ligated to pCold I vector (Takara Bio Inc.) using DNA Ligation Kit Mighty Mix (Takara Bio Inc.), and introduced into *E. coli* strain DH5α. Transformed cells were plated on Luria Broth agar plates, containing 200 mg/L ampicillin. The colonies carrying pCold I-*Cs*GE plasmids were selected by colony-directed PCR.

Table 6-2. Vector plasmids and primers used for plasmid construction

	Plasmid	Primer pairs	Restrict-ion site
*Cs*GE	pCold I	5′-GGGAATTCCATATGCCGCAGGCATTTCCGAG-3′	*Nde*I
		5′-CGCGGATCCTCATTACCAATTAATCCACTGGCTC-3′	*Bam*HI
	pNC-HisT	5′-CGCGGATCCCCGCAGGCATTTCCGAG-3′	*Bam*HI
		5′-CCCAAGCTTTCATTACCAATTAATCCACTGGCTC-3′	*Hind*III
	pBIC2, pBIC3	5′-GATGACGATGACAAACCGCAGGCATTTCCGAGC-3′	
		5′-CATCCTGTTAAGCTTTCATTACCAATTAATCCACTGGC-3′	
	pET15b	5′-GGGAATTCCATATGCCGCAGGCATTTCCGAG-3′	*Nde*I
		5′-CGCGGATCCTCATTACCAATTAATCCACTGGCTC-3′	*Bam*HI
	pPICZαA	5′-CGGAATTCCATCATCATCATCATCACAGCAG-3′	*Eco*RI
		5′-CGGGGTACCCCAATTAATCCACTGGCTCTG -3′	*Kpn*I
*Pe*GE	pET15b	5′-GGGAATTCCATATGTGTGCAGCAATTCCGACCTC-3′	*Nde*I
		5′-CGCGGATCCTCATTAGCTCAGGGTCGGCAC-3′	*Bam*HI
	pPICZαA	5′-GCGGAATTCCATCATCATCATCATCACAGCAGCG-3′	*Eco*RI
		5′-ATAAGAATGCGGCCGCTCATTAGCTCAGGGTCGGCAC-3′	*Not*I

Solid under-line: restriction enzyme sites
Dotted under-line: 15-base sequence for insertion of target DNA by homologous recombination

For *B. choshinensis* expression, the plasmids pBIC2 and pBIC3 containing the *csge* gene were constructed according to the manufacture's protocol (Takara Bio Inc.). Briefly, *csge* gene was amplified with the primers having 15-base 5′ overhangs that are homologous to the common cloning sites of the pBIC2 and pBIC3 vectors. The amplified PCR products were mixed with either pBIC2 or pBIC3 vectors and introduced into *B. choshinensis* SP3 competent cells (Takara Bio Inc.). The transformed cells were spread onto the MT plates (1% glucose, 1% casein peptone, 0.5% Ehrlich Bonito Extract, 0.2% yeast extract, 0.001% $FeSO_4 \cdot 7H_2O$, 0.001% $MnSO_4 \cdot 4H_2O$, 0.0001% $ZnSO_4 \cdot 7H_2O$, 0.41% $MgCl_2$, and 1.5% agar) containing 50 mg/L neomycin. The colonies harboring pBIC2-*Cs*GE and pBIC3-*Cs*GE plasmids were selected by colony-directed PCR.

For *P. pastoris* system, the genes encoding *csge* and *pege* were amplified by PCR, and then firstly cloned into pET-15b (Takara Bio Inc.); each gene was inserted between the *Nde*I and *Bam*HI sites located after the sequence encoding the N-terminal 6×His-tag (6H). The obtained plasmids, pET-15b-6H-*csge* and pET-15b-6H-*pege*, were then used as templates for second PCR to amplify the regions containing 6H-*csge* and 6H-*pege*. The amplified 6H-*csge* was then cloned into pPICZαA (Invitrogen, Thermo Fisher Scientific Inc.) using the *Eco*RI and *Kpn*I sites, while the amplified 6H-*pege* was cloned using *Eco*RI and *Not*I sites. The obtained pPICZαA-6H-*csge*-6H and pPICZαA-6H-*pege* plasmids were introduced into the *E. coli* DH5α strain individually. Transformed cells were plated on Luria Broth agar plates, containing 25 mg/L Zeocin. The colonies

containing the pPICZαA-6H-*csge*-6H and pPICZαA-6H-*pege* plasmids were selected by colony-directed PCR. All constructed plasmids were sequenced to confirm the sequences were correct.

6.5.2 Heterologous expression in *E. coli* and purification of *Cs*GE

E. coli BL21 cells carrying the pCold I-*Cs*GE plasmid were inoculated to 1 L LB medium containing 200 μg/mL ampicillin and shaken at 37 °C. When OD_{590} reached 0.4, the flask was placed in a water-ice bath and rapidly chilled to 15 °C, then the flask was kept still at 15 °C for 30 min. Isopropyl β-$_D$-1-thiogalactopyranoside (IPTG) was then added to the final concentration of 0.1 mM and the cells were grown for another 24 hours at 15 °C. The cells were then harvested, and the collected cells were resuspended in 25 mL of 50 mM sodium phosphate buffer (pH 6.8) containing 500 mM NaCl, 0.2% CHAPS, 10 units/mL DNase I and 1.0 μg/mL RNase. Subsequently, the resuspension was sonicated and centrifuged at 50,000 × g for 30 min. The supernatant containing His-tagged *Cs*GE was collected, mixed with 5 mL 60% glycerol to reach final glycerol concentration of 10%, and then applied to HisTrap HP 5 mL column (GE Healthcare Life Sciences), and the column was washed with 50 mM sodium phosphate buffer (pH 6.8) containing 500 mM NaCl, 0.2% CHAPS. His-tagged *Cs*GE was eluted using 0-200 mM imidazole gradient. His-tagged *Cs*GE, having activity, was found in the fractions within the 50-100 mM imidazole concentrations. The collected fractions were applied to a PD-10 desalting column (amersham pharmacia biotech), which was equilibrated with a Buffer 1 (50 mM sodium phosphate buffer (pH 6.2) containing 500 mM NaCl and 0.2% CHAPS), for activity assay.

6.5.3 Heterologous expression and purification of *Cs*GE in *B. choshinensis*

Plasmids pNC-HisT-*Cs*GE, pBIC2-*Cs*GE, and pBIC3-*Cs*GE harboring the *csge* gene were introduced into *B. choshinensis* SP3 by electroporation using the Sc2 program of MicroPulser electroporator (Bio-Rad). The transformants were inoculated to one of the following three media: LB, TM (1% glucose, 1% casein peptone, 0.5% Ehrlich Bonito Extract, 0.2% yeast extract, 0.001% $FeSO_4 \cdot 7H_2O$, 0.001% $MnSO_4 \cdot 4H_2O$, and 0.0001% $ZnSO_4 \cdot 7H_2O$), and 2SY (2% glucose, 4% soytone, 0.5% yeast extract, and 0.015%

$CaCl_2 \cdot 4H_2O$), all of which contain 50 mg/L neomycin. The inoculated media were incubated at either 25 °C or 30 °C for 48-120 hours.

Subsequently, the culture media were centrifuged at 5,000 × g for 5 minutes and the supernatants were collected, since the proteins are secreted. Then the supernatants were filtered over 0.45 µm PES syringe filter (Membrane Solutions). The obtained solutions containing his-tagged *Cs*GE were concentrated ten-fold using an Amicon Ultra-15 centrifugal filter (molecular weight cutoff 10,000) (Millipore), which were then dialyzed against 50 mM sodium phosphate buffer (pH 6.8) containing 500 mM NaCl, and 0.2% CHAPS. After the dialysis, the protein solutions were applied to HisTrap HP 5 mL (GE Healthcare Life Sciences). The column was washed with 50 mM sodium phosphate buffer (pH 6.8) containing 500 mM NaCl, 0.2% CHAPS, and 20 mM imidazole to remove impurities. His-tagged *Cs*GEs were eluted using 10 - 250 mM imidazole gradients, over ten column volumes. His-tagged *Cs*GE was found in the fractions within the 50-100 mM imidazole concentrations.

6.5.4 Heterologous expression in *P. pastoris*, and purification of *Cs*GE and *Pe*GE

The pPICZαA-6H-*csge*-6H and pPICZαA-6H-*pege* plasmids were linearized with a restriction enzyme, *Sac*I. Each linearized plasmid was then purified by phenol-chloroform extraction and ethanol precipitation as described in the EasySelect™ Pichia Expression Kit user manual (Invitrogen, Thermo Fisher Scientific Inc.). The linearized pPICZαA-6H-*csge*-6H and pPICZαA-6H-*pege* plasmids were individually introduced into *P. pastoris* X-33 by electroporation using the Pc program of a MicroPulser electroporator (Bio-Rad). The transformants were grown on YPDS plates (1% yeast extract, 2% peptone, 2% glucose, 1 M sorbitol and 2% agar) containing 100 mg/L Zeocin. The transformants harboring the *csge* and *pege* genes were then inoculated in 100 mL BMGY medium (1% yeast extract, 2% peptone, 100 mM potassium phosphate (pH 6.0), 1.34% yeast nitrogen base with ammonium sulfate without amino acids, 4×10^{-5}% biotin and 1% glycerol), and grown at 30 °C. When the cell density reached OD_{600}=6.0, the cells were collected by centrifugation at 3,000 × g for 5 minutes at room temperature. The precipitated cells were resuspended gently in 600 mL BMMY (1% yeast extract, 2% peptone, 100 mM potassium phosphate (pH 6.0), 1.34% yeast nitrogen base with ammonium sulfate without amino acids, 4×10^{-5}% biotin and 0.5% methanol) to yield cell density OD_{600}=1.0. Then the

inoculated medium was incubated at 15 °C for 3 days, during which methanol was added to 0.5% of the total volume every 24 hours to maintain induction.

The culture medium was centrifuged at 3,800 × g for 40 minutes at 4 °C. Then the supernatant containing secreted His-tagged *Cs*GE or *Pe*GE was filtered (WHATMAN KLARI-FLEX, 500 mL PES 0.45 μm unit), and then subjected to ultrafiltration for concentration and buffer-exchange using a Minimate TFF System (OAPAP110, PALL). The supernatant was concentrated to one-fifth of the original volume with a 10-kDa cut-off membrane (PALL). The retentate, containing concentrated his-tagged *Cs*GE or *Pe*GE, was buffer-exchanged with 50 mM sodium phosphate (pH 7.0) containing 500 mM NaCl and 0.2% CHAPS (Buffer 1). This protein solution was then applied to 5 mL HisTrap HP (GE Healthcare Life Sciences). Impurities were washed out with Buffer 1 and then the concentration of imidazole was increased gradually with a gradient from 0 to 500 mM over fourteen column volumes. All the fractions were collected and buffer-exchanged with 50 mM sodium phosphate (pH 6.2) containing 500 mM NaCl and 0.2% CHAPS (Buffer 2), and then the protein concentrations of all the fractions were adjusted to the same value (10 μM and 2 μM for *Cs*GE and *Pe*GE, respectively). Then the activity of each fraction was examined by the UDH-coupled spectrophotometric assay described in the next section.

6.5.5 Measurement of enzymatic activity by spectrophotometric assaying

To examine the activity and the effects of additives on the activity, the purified 10 μM *Cs*GE and 2 μM *Pe*GE were each dissolved in 10 μL Buffer 2, which was supplemented with one of the following reagents, 10 mM EDTA, 5 mM imidazole, 5 mM NaN_3, 5 mM TCEP, 5 mM PMSF, 10% DMSO, 5% glycerol, 2% Tween 20, 2% Tween 80, 1% CHAPS, or 1% SDS, followed by incubation at room temperature for 20 min. Into each of these solutions, a final concentration of 5 mM BnGlcA was added. The prepared reaction mixtures were then incubated at 30 °C for 20 min. Heat-inactivated (96 °C, 20 minutes) proteins were used as negative controls. The reaction mixtures were then transferred to 96-well flat-bottomed microplates and treated with a K-URONIC kit (Megazyme) following the reported procedure (80). Briefly, the NAD^+ and UDH provided in the kit were added to the above-mentioned reaction mixtures, the final volumes being adjusted to 250 μL. The reaction mixtures were then incubated at 25 °C

for 10 minutes. The amount of the formed nicotinamide-adenine dinucleotide (NADH), which is stoichiometric with that of glucuronic acid, was determined spectroscopically by measuring the absorbance at 340 nm (Infinite® 200 PRO, TECAN).

To determine kinetic parameters, 14.6 µM *Cs*GE and 1.4 µM *Pe*GE were each dissolved in 10 µL Buffer 2, which contained BnGlcA at different concentrations (1-20 mM). These reaction mixtures were incubated at 30 °C for 0-10 minutes. The reaction was quenched by adding final concentration of 2% SDS on ice. The obtained solutions were then applied to a K-URONIC kit using the same procedures as those described above. A standard curve correlating the concentration of glucuronic acid versus the absorbance at 340 nm of formed NADH was generated using glucuronic acid solutions of known concentration beforehand. The K_m and V_{max} values were calculated by using the Graph Pad Prism 7 software.

For all the activity assays, the absorbance obtained for heat-inactivated *Cs*GE and *Pe*GE was used as a negative control.

Chapter 7. General conclusions

Lignocellulose, or wood biomass, is one of the most abundant and renewable materials on earth, but owing to its recalcitrant constituent, lignin, harsh treatments are usually required. Enzymes originating from wood-rotting fungi have been expected to provide a mild and efficient way to either degrade lignin or separate lignin from hemicellulose and cellulose. Fungi manganese peroxidases (MnPs) have long been well-known for degrading lignin, and glucuronoyl esterases (GE) have recently been discovered to cleave the linkage between hemicellulose and lignin. In this study, we focused on these two kinds of lignocellulose-degrading enzymes of a wood-rotting fungus *Ceriporiopsis subvermispora*. Three types of MnPs and two glucuronoyl esterases were heterologously prepared and characterized.

In chapter 1, firstly, a general introduction to renewable energy and wood biomass was given. Then, the categories of wood-rotting fungi and the frequently discussed lignocellulosic enzymes were provided. Finally, the background and the functions of MnPs and GEs were described.

In chapter 2, the soluble expression of three types of MnPs in *E. coli* was described. We have developed a method for preparing active MnPs through soluble expression by *E. coli*, which had long been thought impossible. The genes of the three different types of MnPs were selected, codon-optimized and expressed under the control of a cold shock promoter. A proper level of heme incorporation was achieved by continuous addition of hemin during cultivation. After two steps of purification, as much as 3 mg of purified MnPs was obtained from 100 mL culture, which is an about 20-fold higher yield than that from inclusion bodies through refolding. All obtained MnPs had heme-to-protein ratios as high as those of the native MnPs. Further improvement of the solubility on the expression was achieved by combinatorial coexpression of chaperones.

In chapter 3, the activities of the MnPs obtained using the method described in chapter 2 were characterized. Two common substrates, DMP and ABTS, and one phenolic lignin dimer model compound were used for characterizing the activities of the three MnPs. UV-visible spectroscopy was used to determine the activities of the MnPs toward DMP and ABTS. For oxidative activity toward DMP, all three MnPs show manganese-dependent activities below pH 5, the optimum pH being pH 3.5. For ABTS, all three

MnPs show their activities in the presence of manganese. Surprisingly, we observed manganese-independent activity for one of the MnPs, MnP 124076. Also, different from the other two MnPs, MnP 124076 shows the optimum activity toward ABTS at pH 4.5. To monitor the reaction between the MnP and the phenolic lignin dimer model, NMR, MS, and HPLC were used for analysis. However, a polymerized product was found to be the major product under certain reaction conditions.

In chapter 4, homology modeling and functional mutagenesis were applied to analyze the weak activity toward DMP and the manganese-independent activity toward ABTS of MnP 124076. We demonstrated that the C-terminal differentiation between MnP 124076 and the other two MnPs was not the main reason for the special activity of MnP 124076. We revealed the importance of the hydrophobicity near the activity center by comparing the activities of wild-type MnP 124076 and the A205R H208K mutant. The decreasing manganese-independent activity toward ABTS of the W276A mutant indicated that the tryptophan residue may play an important role. In addition, the ability of MnP 124076 to oxidize a non-phenolic substrate, veratryl alcohol, was also confirmed by UV-visible spectroscopy.

In chapter 5, a phylogenetic tree was built from almost four hundred putative fungal glucuronoyl esterases (FGEs) obtained on BLAST analysis, six main clades being defined. In the phylogenetic tree, all the putative FGEs of Ascomycetes cluster in clades I to IV, and most of the putative FGEs of Basidiomycetes (B-FGEs) cluster in clades V to VI. Interestingly, several B-FGEs were found to cluster in clade II; most FGEs of clade II were found to have higher theoretical isoelectric points than those in the other five clades. To gain an insight into the putative FGEs in the clades that have not been characterized yet, we chose the FGEs of *C. subvermispora* (*Cs*GE) and *Pleurotus eryngii* (*Pe*GE), which belong to clades V and II, respectively, for further studies. The amino acid sequences of *Cs*GE, *Pe*GE, and previously characterized FGEs were aligned and compared.

In chapter 6, expression systems and a method of confirming the activity of *Cs*GE were discussed. We have tried three protein expression systems, *E. coli*, *B. choshinensis*, and *P. pastoris*, for producing *Cs*GE. Among these three systems, the *P. pastoris* system is considered as the most promising one for preparing FGEs. Benzyl glucuronic acid was used as a substrate to confirm the activities of *Cs*GE and *Pe*GE, and the hydrolyzed

product, glucuronic acid, was quantified spectrophotometrically. Both *Cs*GE and *Pe*GE clearly exhibited esterase activity. Additionally, we demonstrated that *Pe*GE exhibits high tolerance toward several denaturing agents, which may make it a potentially more applicable enzyme.

In this study, methods for preparing these enzymes were developed and their activities were characterized. For MnPs, to prevent undesired polymerization, the reaction conditions, such as the enzyme-to-substrate ratio and addition of mediators, are going to be examined. Besides, the effects of combinations of different types of MnPs on either the lignin model or real wood are worth examining. For FGEs, despite being discovered much later than other lignocellulosic enzymes, several reports have been published in the last two years. We constructed a phylogenetic tree of the FGEs, and then characterized two FGEs that have distinct pIs and proposed an easier way for assaying. Instead of using model compounds for enzyme characterization, we are looking forward to analyzing the effects of the FGEs on lignocellulosic materials. The direct treatment of FGEs and the FGEs in combination with either cellulase or lignin degradation enzymes for wood biomass are expected to provide an effective way of lignocellulose utilization.

References

1. RENEWABLES 2018 GLOBAL STATUS REPORT, http://www.ren21.net.
2. Hori C, Ishida T, Igarashi K, Samejima M, Suzuki H, Master E, Ferreira P, Ruiz-Dueñas FJ, Held B, Canessa P. 2014. Analysis of the *Phlebiopsis gigantea* genome, transcriptome and secretome provides insight into its pioneer colonization strategies of wood. PLoS genetics 10:e1004759.
3. Findlay W. 1984. Soft rot of timber—a review. J Ind Acad Wood Sci 15:1-11.
4. Blanchette RA, Held BW, Jurgens JA, McNew DL, Harrington TC, Duncan SM, Farrell RL. 2004. Wood-destroying soft rot fungi in the historic expedition huts of Antarctica. Applied and Environmental Microbiology 70:1328-1335.
5. Filley TR, Blanchette RA, Simpson E, Fogel ML. 2001. Nitrogen cycling by wood decomposing soft-rot fungi in the "King Midas tomb," Gordion, Turkey. Proceedings of the National Academy of Sciences 98:13346-13350.
6. Sista Kameshwar AK, Qin W. 2017. Comparative study of genome-wide plant biomass-degrading CAZymes in white rot, brown rot and soft rot fungi. Mycology:1-13.
7. Vane CH, Abbott GD, Head IM. 2001. The effect of fungal decay (*Agaricus bisporus*) on wheat straw lignin using pyrolysis-GC-MS in the presence of tetramethylammonium hydroxide (TMAH). Journal of Analytical and Applied Pyrolysis 60:69-78.
8. Filley T, Cody G, Goodell B, Jellison J, Noser C, Ostrofsky A. 2002. Lignin demethylation and polysaccharide decomposition in spruce sapwood degraded by brown rot fungi. Organic Geochemistry 33:111-124.
9. Arantes V, Jellison J, Goodell B. 2012. Peculiarities of brown-rot fungi and biochemical Fenton reaction with regard to their potential as a model for bioprocessing biomass. Applied Microbiology and Biotechnology 94:323-338.
10. Arantes V, Milagres AM, Filley TR, Goodell B. 2011. Lignocellulosic polysaccharides and lignin degradation by wood decay fungi: the relevance of nonenzymatic Fenton-based reactions. Journal of industrial microbiology & biotechnology 38:541-555.
11. Yelle DJ, Wei D, Ralph J, Hammel KE. 2011. Multidimensional NMR analysis reveals truncated lignin structures in wood decayed by the brown rot basidiomycete *Postia placenta*. Environmental Microbiology 13:1091-1100.
12. Blanchette RA. 1984. Screening wood decayed by white rot fungi for preferential lignin degradation. Applied and Environmental Microbiology 48:647-653.
13. Hatakka A. 1994. Lignin-modifying enzymes from selected white-rot fungi:

production and role from in lignin degradation. FEMS microbiology reviews 13:125-135.

14. Daniel G. 2003. Microview of wood under degradation by bacteria and fungi. ACS Publications.
15. Cragg SM, Beckham GT, Bruce NC, Bugg TD, Distel DL, Dupree P, Etxabe AG, Goodell BS, Jellison J, McGeehan JE. 2015. Lignocellulose degradation mechanisms across the Tree of Life. Current Opinion in Chemical Biology 29:108-119.
16. Cantarel BL, Coutinho PM, Rancurel C, Bernard T, Lombard V, Henrissat B. 2008. The Carbohydrate-Active EnZymes database (CAZy): an expert resource for glycogenomics. Nucleic acids research 37:D233-D238.
17. Lombard V, Golaconda Ramulu H, Drula E, Coutinho PM, Henrissat B. 2013. The carbohydrate-active enzymes database (CAZy) in 2013. Nucleic acids research 42:D490-D495.
18. Rytioja J, Hildén K, Yuzon J, Hatakka A, de Vries RP, Mäkelä MR. 2014. Plant-polysaccharide-degrading enzymes from basidiomycetes. Microbiology and Molecular Biology Reviews 78:614-649.
19. Manavalan T, Manavalan A, Heese K. 2015. Characterization of lignocellulolytic enzymes from white-rot fungi. Current microbiology 70:485-498.
20. Monclaro AV, Ferreira Filho EX. 2017. Fungal lytic polysaccharide monooxygenases from family AA9: Recent developments and application in lignocelullose breakdown. International journal of biological macromolecules 102:771-778.
21. Thurston CF. 1994. The structure and function of fungal laccases. Microbiology 140:19-26.
22. Bourbonnais R, Paice MG. 1992. Demethylation and delignification of kraft pulp by *Trametes versicolor* laccase in the presence of 2, 2′-azinobis-(3-ethylbenzthiazoline-6-sulphonate). Applied Microbiology and Biotechnology 36:823-827.
23. Bourbonnais R, Paice MG. 1990. Oxidation of non-phenolic substrates: an expanded role for laccase in lignin biodegradation. FEBS letters 267:99-102.
24. Jensen KA, Bao W, Kawai S, Srebotnik E, Hammel KE. 1996. Manganese-dependent cleavage of nonphenolic lignin structures by *Ceriporiopsis subvermispora* in the absence of lignin peroxidase. Applied and environmental microbiology 62:3679-3686.
25. Enoki M, Watanabe T, Nakagame S, Koller K, Messner K, Honda Y, Kuwahara

M. 1999. Extracellular lipid peroxidation of selective white-rot fungus, *Ceriporiopsis subvermispora*. FEMS microbiology letters 180:205-211.

26. Bao W, Fukushima Y, Jensen Jr KA, Moen MA, Hammel KE. 1994. Oxidative degradation of non-phenolic lignin during lipid peroxidation by fungal manganese peroxidase. FEBS letters 354:297-300.
27. Glenn JK, Gold MH. 1985. Purification and characterization of an extracellular Mn (II)-dependent peroxidase from the lignin-degrading basidiomycete, *Phanerochaete chrysosporium*. Archives of biochemistry and biophysics 242:329-341.
28. Paszczyński A, Huynh V-B, Crawford R. 1985. Enzymatic activities of an extracellular, manganese-dependent peroxidase from *Phanerochaete chrysosporium*. FEMS Microbiology Letters 29:37-41.
29. Sundaramoorthy M, Kishi K, Gold MH, Poulos TL. 1994. Preliminary crystallographic analysis of manganese peroxidase from *Phanerochaete chrysosporium*. Journal of molecular biology 238:845-848.
30. Sundaramoorthy M, Youngs HL, Gold MH, Poulos TL. 2005. High-resolution crystal structure of manganese peroxidase: substrate and inhibitor complexes. Biochemistry 44:6463-6470.
31. Sutherland GR, Zapanta LS, Tien M, Aust SD. 1997. Role of calcium in maintaining the heme environment of manganese peroxidase. Biochemistry 36:3654-3662.
32. Hofrichter M. 2002. lignin conversion by manganese peroxidase (MnP). Enzyme and Microbial technology 30:454-466.
33. Špániková S, Biely P. 2006. Glucuronoyl esterase–novel carbohydrate esterase produced by *Schizophyllum commune*. FEBS letters 580:4597-4601.
34. Li X-L, Špániková S, de Vries RP, Biely P. 2007. Identification of genes encoding microbial glucuronoyl esterases. FEBS letters 581:4029-4035.
35. Ďuranová M, Špániková S, Wösten HA, Biely P, De Vries RP. 2009. Two glucuronoyl esterases of *Phanerochaete chrysosporium*. Archives of microbiology 191:133.
36. Topakas E, Moukouli M, Dimarogona M, Vafiadi C, Christakopoulos P. 2010. Functional expression of a thermophilic glucuronoyl esterase from *Sporotrichum thermophile*: identification of the nucleophilic serine. Applied microbiology and biotechnology 87:1765-1772.
37. Huynh HH, Ishii N, Matsuo I, Arioka M. 2018. A novel glucuronoyl esterase from *Aspergillus fumigatus*-the role of conserved Lys residue in the preference for 4-

O-methyl glucuronoyl esters. Applied microbiology and biotechnology:1-11.

38. Pokkuluri PR, Duke NE, Wood SJ, Cotta MA, Li XL, Biely P, Schiffer M. 2011. Structure of the catalytic domain of glucuronoyl esterase Cip2 from *Hypocrea jecorina*. Proteins: Structure, Function, and Bioinformatics 79:2588-2592.
39. Hori C, Gaskell J, Igarashi K, Kersten P, Mozuch M, Samejima M, Cullen D. 2014. Temporal alterations in the secretome of the selective ligninolytic fungus *Ceriporiopsis subvermispora* during growth on aspen wood reveal this organism's strategy for degrading lignocellulose. Applied and environmental microbiology 80:2062-2070.
40. Coconi-Linares N, Magaña-Ortíz D, Guzmán-Ortiz DA, Fernández F, Loske AM, Gómez-Lim MA. 2014. High-yield production of manganese peroxidase, lignin peroxidase, and versatile peroxidase in *Phanerochaete chrysosporium*. Applied microbiology and biotechnology 98:9283-9294.
41. Mayfield MB, Kishi K, Alic M, Gold MH. 1994. Homologous expression of recombinant manganese peroxidase in *Phanerochaete chrysosporium*. Applied and environmental microbiology 60:4303-4309.
42. Conesa A, van den Hondel CA, Punt PJ. 2000. Studies on the production of fungal peroxidases in *Aspergillus niger*. Applied and environmental microbiology 66:3016-3023.
43. Stewart P, Whitwam RE, Kersten PJ, Cullen D, Tien M. 1996. Efficient expression of a *Phanerochaete chrysosporium* manganese peroxidase gene in Aspergillus oryzae. Applied and environmental microbiology 62:860-864.
44. Gu L, Lajoie C, Kelly C. 2003. Expression of a *Phanerochaete chrysosporium* manganese peroxidase gene in the yeast Pichia pastoris. Biotechnology progress 19:1403-1409.
45. Jiang F, Kongsaeree P, Charron R, Lajoie C, Xu H, Scott G, Kelly C. 2008. Production and separation of manganese peroxidase from heme amended yeast cultures. Biotechnology and bioengineering 99:540-549.
46. Doyle WA, Smith AT. 1996. Expression of lignin peroxidase H8 in *Escherichia coli*: folding and activation of the recombinant enzyme with Ca^{2+} and haem. Biochemical journal 315:15-19.
47. Whitwam RE, Gazarian IG, Tien M. 1995. Expression of fungal Mn peroxidase in *E. coli* and refolding to yield active enzyme. Biochemical and biophysical research communications 216:1013-1017.
48. Pérez-Boada M, Doyle W, Ruiz-Dueñas F, Martınez M, Martınez A, Smith A. 2002. Expression of *Pleurotus eryngii* versatile peroxidase in *Escherichia coli* and

optimisation of in vitro folding. Enzyme and Microbial Technology 30:518-524.
49. Fernández-Fueyo E, Ruiz-Dueñas FJ, Miki Y, Martínez MJ, Hammel KE, Martínez AT. 2012. Lignin-degrading peroxidases from genome of selective ligninolytic fungus *Ceriporiopsis subvermispora*. Journal of Biological Chemistry 287:16903-16916.
50. Ufot UF, Akpanabiatu MI. 2012. An engineered *Phlebia radiata* manganese peroxidase: expression, refolding, purification and preliminary characterization. American Journal of Molecular Biology 2:359-370.
51. Wang N, Ren K, Jia R, Chen W, Sun R. 2016. Expression of a fungal manganese peroxidase in *Escherichia coli*: a comparison between the soluble and refolded enzymes. BMC biotechnology 16:87.
52. Mohorčič M, Benčina M, Friedrich J, Jerala R. 2009. Expression of soluble versatile peroxidase of *Bjerkandera adusta* in *Escherichia coli*. Bioresource technology 100:851-858.
53. Bao X, Liu A, Lu X, Li J-J. 2012. Direct over-expression, characterization and H_2O_2 stability study of active *Pleurotus eryngii* versatile peroxidase in *Escherichia coli*. Biotechnology letters 34:1537-1543.
54. Hoshino F, Kajino T, Sugiyama H, Asami O, Takahashi H. 2002. Thermally stable and hydrogen peroxide tolerant manganese peroxidase (MnP) from *Lenzites betulinus*. FEBS letters 530:249-252.
55. Wariishi H, Valli K, Gold MH. 1992. Manganese (II) oxidation by manganese peroxidase from the basidiomycete *Phanerochaete chrysosporium*. Kinetic mechanism and role of chelators. Journal of Biological Chemistry 267:23688-23695.
56. Whitwam R, Tien M. 1996. Heterologous expression and reconstitution of fungal Mn peroxidase. Archives of biochemistry and biophysics 333:439-446.
57. Fernandez-Fueyo E, Ruiz-Dueñas FJ, Ferreira P, Floudas D, Hibbett DS, Canessa P, Larrondo LF, James TY, Seelenfreund D, Lobos S. 2012. Comparative genomics of *Ceriporiopsis subvermispora* and *Phanerochaete chrysosporium* provide insight into selective ligninolysis. Proceedings of the National Academy of Sciences 109:5458-5463.
58. Ambert-Balay K, Fuchs SM, Tien M. 1998. Identification of the veratryl alcohol binding site in lignin peroxidase by site-directed mutagenesis. Biochemical and biophysical research communications 251:283-286.
59. Baynes BM, Wang DIC, Trout BL. 2005. Role of Arginine in the Stabilization of Proteins against Aggregation. Biochemistry 44:4919-4925.

60. Bai C, Bo H, Jiang Y, Hu M, Li S, Zhai Q. 2010. Inactivation of chloroperoxidase by arginine. Process Biochemistry 45:312-316.
61. Schein CH, Noteborn MH. 1988. Formation of soluble recombinant proteins in *Escherichia coli* is favored by lower growth temperature. Nature Biotechnology 6:291-294.
62. Qing G, Ma L-C, Khorchid A, Swapna G, Mal TK, Takayama MM, Xia B, Phadtare S, Ke H, Acton T. 2004. Cold-shock induced high-yield protein production in *Escherichia coli*. Nature biotechnology 22:877-882.
63. Tanabe H, Goldstein J, Yang M, Inouye M. 1992. Identification of the promoter region of the *Escherichia coli* major cold shock gene, cspA. Journal of bacteriology 174:3867-3873.
64. Kondo A, Kohda J, Endo Y, Shiromizu T, Kurokawa Y, Nishihara K, Yanagi H, Yura T, Fukuda H. 2000. Improvement of productivity of active horseradish peroxidase in *Escherichia coli* by coexpression of Dsb proteins. Journal of bioscience and bioengineering 90:600-606.
65. Sudhamsu J, Kabir M, Airola MV, Patel BA, Yeh S-R, Rousseau DL, Crane BR. 2010. Co-expression of ferrochelatase allows for complete heme incorporation into recombinant proteins produced in *E. coli*. Protein expression and purification 73:78-82.
66. Qin X, Sun X, Huang H, Bai Y, Wang Y, Luo H, Yao B, Zhang X, Su X. 2017. Oxidation of a non-phenolic lignin model compound by two *Irpex lacteus* manganese peroxidases: evidence for implication of carboxylate and radicals. Biotechnology for Biofuels 10:103.
67. Reading NS, Aust SD. 2001. Role of disulfide bonds in the stability of recombinant manganese peroxidase. Biochemistry 40:8161-8168.
68. Smulevich G., Miller M. A., Kraut J., Spiro T.G., Conformational change and histidine control of heme chemistry in cytochrome c peroxidase: resonance Raman evidence from Leu-52 and Gly-181 mutants of cytochrome c peroxidase. 1991. Biochemistry 30 9546-9558.
69. Sundaramoorthy M, Gold MH, Poulos TL. 2010. Ultrahigh (0.93 Å) resolution structure of manganese peroxidase from *Phanerochaete chrysosporium*: Implications for the catalytic mechanism. Journal of inorganic biochemistry 104:683-690.
70. Theorell H, Maehly A.C., Untersuchungen an künstlichen peroxydasen. 1950. Acta Chemica Scandinavica 4 422-434.
71. Shannon L, Kay E, Lew J. 1966. Determination of the RZ value for peroxidase. J

Biol Chem 241:2166-2172.

72. Fernández-Fueyo E, Ruiz-Dueñas FJ, Martínez MJ, Romero A, Hammel KE, Medrano FJ, Martínez AT. 2014. Ligninolytic peroxidase genes in the oyster mushroom genome: heterologous expression, molecular structure, catalytic and stability properties, and lignin-degrading ability. Biotechnology for biofuels 7:2.
73. Wang Y, Vazquez-Duhalt R, Pickard MA. 2002. Purification, characterization, and chemical modification of manganese peroxidase from *Bjerkandera adusta* UAMH 8258. Current microbiology 45:77-87.
74. Nelson DP, Kiesow LA. 1972. Enthalpy of decomposition of hydrogen peroxide by catalase at 25 °C (with molar extinction coefficients of H_2O_2 solutions in the UV). Analytical biochemistry 49:474-478.
75. Rytioja J, Hildén K, Hatakka A, Mäkelä MR. 2014. Transcriptional analysis of selected cellulose-acting enzymes encoding genes of the white-rot fungus *Dichomitus squalens* on spruce wood and microcrystalline cellulose. Fungal Genetics and Biology 72:91-98.
76. Sklenar J, Niku-Paavola M-L, Santos S, Man P, Kruus K, Novotny C. 2010. Isolation and characterization of novel pI 4.8 MnP isoenzyme from white-rot fungus *Irpex lacteus*. Enzyme and Microbial Technology 46:550-556.
77. Baborová P, Möder M, Baldrian P, Cajthamlová K, Cajthaml T. 2006. Purification of a new manganese peroxidase of the white-rot fungus *Irpex lacteus*, and degradation of polycyclic aromatic hydrocarbons by the enzyme. Research in Microbiology 157:248-253.
78. Hildén K, Martinez AT, Hatakka A, Lundell T. 2005. The two manganese peroxidases Pr-MnP2 and Pr-MnP3 of *Phlebia radiata*, a lignin-degrading basidiomycete, are phylogenetically and structurally divergent. Fungal Genetics and Biology 42:403-419.
79. Lankinen P, Hildén K, Aro N, Salkinoja-Salonen M, Hatakka A. 2005. Manganese peroxidase of *Agaricus bisporus*: grain bran-promoted production and gene characterization. Applied microbiology and biotechnology 66:401-407.
80. Sunner H, Charavgi M-D, Olsson L, Topakas E, Christakopoulos P. 2015. Glucuronoyl esterase screening and characterization assays utilizing commercially available benzyl glucuronic acid ester. Molecules 20:17807-17817.
81. Huynh HH, Arioka M. 2016. Functional expression and characterization of a glucuronoyl esterase from the fungus *Neurospora crassa*: identification of novel consensus sequences containing the catalytic triad. The Journal of general and applied microbiology 62:217-224.

82. Hüttner S, Klaubauf S, de Vries RP, Olsson L. 2017. Characterisation of three fungal glucuronoyl esterases on glucuronic acid ester model compounds. Applied Microbiology and Biotechnology:1-11.
83. d'Errico C, Jørgensen JO, Krogh KB, Spodsberg N, Madsen R, Monrad RN. 2015. Enzymatic degradation of lignin‐carbohydrate complexes (LCCs): Model studies using a fungal glucuronoyl esterase from *Cerrena unicolor*. Biotechnology and bioengineering 112:914-922.
84. Yin Y, Mao X, Yang J, Chen X, Mao F, Xu Y. 2012. dbCAN: a web resource for automated carbohydrate-active enzyme annotation. Nucleic acids research 40:W445-W451.
85. Gasteiger E, Hoogland C, Gattiker A, Duvaud Se, Wilkins MR, Appel RD, Bairoch A. 2005. Protein identification and analysis tools on the ExPASy server. Springer.
86. Agger JW, Busk PK, Pilgaard B, Meyer AS, Lange L. 2017. A new functional classification of glucuronoyl esterases by peptide pattern recognition. Frontiers in microbiology 8.
87. Xie C, Yan L, Gong W, Zhu Z, Tan S, Chen D, Hu Z, Peng Y. 2016. Effects of different substrates on lignocellulosic enzyme expression, enzyme activity, substrate utilization and biological efficiency of *Pleurotus eryngii*. Cellular Physiology and Biochemistry 39:1479-1494.
88. Petersen TN, Brunak S, von Heijne G, Nielsen H. 2011. SignalP 4.0: discriminating signal peptides from transmembrane regions. Nature methods 8:785-786.
89. Wong DW, Chan VJ, McCormack AA, Hirsch J, Biely P. 2012. Functional cloning and expression of the *Schizophyllum commune* glucuronoyl esterase gene and characterization of the recombinant enzyme. Biotechnology research international 2012.
90. Charavgi M-D, Dimarogona M, Topakas E, Christakopoulos P, Chrysina ED. 2013. The structure of a novel glucuronoyl esterase from *Myceliophthora thermophila* gives new insights into its role as a potential biocatalyst. Acta Crystallographica Section D: Biological Crystallography 69:63-73.
91. Takagi H, Kadowaki K, Udaka S. 1989. Screening and characterization of protein-hyperproducing bacteria without detectable exoprotease activity. Agricultural and biological chemistry 53:691-699.
92. Tojo H, Asano T, Kato K, Udaka S, Horiuchi R, Kakinuma A. 1994. Production of human protein disulfide isomerase by *Bacillus brevis*. Journal of biotechnology

33:55-62.

93. Vagenende V, Yap MGS, Trout BL. 2009. Mechanisms of protein stabilization and prevention of protein aggregation by glycerol. Biochemistry 48:11084-11096.

List of publications

1. High yield production of fungal manganese peroxidases by *E. coli* through soluble expression, and examination of the activities
Meng-I Lin, Takashi Nagata, Masato Katahira
Protein Expression and Purification, (2018) Vol 145, pages 45-52
doi: 10.1016/j.pep.2017.12.012
(Chapter 2 and 3)

2. Classification of fungal glucuronoyl esterases (FGEs), and characterization of two new FGEs from *Ceriporiopsis subvermispora* and *Pleurotus eryngii*
Meng-I Lin, Akiho Hiyama, Keiko Kondo, Takashi Nagata, Masato Katahira
In press, Applied Microbiology and Biotechnology, (2018)
doi: 10.1007/s00253-018-9318-5
(Chapter 5 and 6)

3. Manganese-independent activity and oxidative activity toward non-phenolic lignin model of a short MnP of wood rotting fungus *Ceriporiopsis subvermispora*
Meng-I Lin, Takashi Nagata, Masato Katahira
In preparation
(Chapter 4)

Other publication

1. Characterization of the glutathione S-transferases that belong to the GSTFuA class in *Ceriporiopsis subvermispora*: Implications in intracellular detoxification and metabolism of wood-derived compounds
Wan Hasnidah Wan Osman, **Meng-I Lin**, Keiko Kondo, Takashi Nagata, Masato Katahira
Int. J. Biol. Macromol, (2018) 113, page 1158-1166
doi: 10.1016/j.ijbiomac.2018.03.029.

List of presentations

1. Heterologous expression and structure-activity relationship analysis of the oxidative enzymes involved in lignocellulose degradation from wood rotting fungi

   Meng-I Lin, Takashi Nagata, Bunzo Mikami, Masato Katahira

   The 38th Annual Meeting of the Molecular Biology Society of Japan

   December 01-04, 2015, Hyogo, Japan

2. Heterologous expression and structure-activity relationship analysis of the oxidative enzymes involved in lignocellulose degradation from wood rotting fungi

   Meng-I Lin, Takashi Nagata, Bunzo Mikami, Masato Katahira

   Ajou-Kyoto Joint Symposium on Energy Science

   January 28, 2016, Suwon, Korea

3. Heterologous expression and structure-activity relationship analysis of the oxidative enzymes from wood rotting fungi that are involved in lignocellulose degradation

   Meng-I Lin, Keiko Kondo, Takashi Nagata, Masato Katahira

   The 61st Lignin Symposium

   October 27-28, 2016, Kyoto, Japan

4. Heterologous expression of the ligninolytic enzymes from wood rotting fungi and analysis of peroxidase activity, homology modeling, and lignin model degradation

   Meng-I Lin, Keiko Kondo, Takashi Nagata, Masato Katahira

   The 2017 Annual Meeting of the Japan Society of Bioscience, Biotechnology and Agrochemistry

   March 17-20, 2017, Kyoto, Japan

5. High yield production, activity analysis, and homologous modeling of soluble fungal manganese peroxidases expressed in *E. coli*

   Meng-I Lin, Keiko Kondo, Takashi Nagata, Masato Katahira

   The 17th Annual Meeting of the Protein Science Society of Japan

   June 20-22, 2017, Miyagi, Japan

6. Analysis of peroxidase activity, lignin model degradation of heterologous expressed soluble fungal ligninolytic enzymes

Meng-I Lin, Keiko Kondo, Takashi Nagata, Masato Katahira

2017 Taiwan-Japan Biomedical Symposium on Magnetic Resonance

October 15-17, Tainan, Taiwan

List of honors

1. Ajou-Kyoto Joint Symposium on Energy Science, Best Presentation Award

Heterologous expression and structure-activity relationship analysis of the oxidative enzymes involved in lignocellulose degradation from wood rotting fungi

Meng-I Lin, Takashi Nagata, Bunzo Mikami, Masato Katahira

January 28, 2016, Suwon, Korea

Acknowledgements

Foremost, I would like to show my deepest gratitude to my supervisor, Professor Masato Katahira for providing this precious opportunity of joining his group to me. His kind guidance and positive thinking have continuously encouraged and supported me during these years. I was extraordinarily fortunate in having this opportunity to learn both science and living attitude from him. I am deeply grateful to Prof. Takashi Nagata for his elaborated guidance and I really appreciate and enjoy the time having fruitful discussion with him. I sincerely thank Prof. Tsukasa Mashima for his overall support in experiments and suggestions. I appreciate the technical assistance provided by Prof. Tsutomu Kodaki, Prof. Bunzo Mikami and Dr. Masayuki Saimura.

I convey special acknowledgement to Prof. Takashi Morii and Prof. Tsutomu Kodaki for their time and critical comments to this thesis.

I am heartily grateful to Keiko Kondo for kindness of discussing and sharing experiences on this topic and for selfless helping. Special thanks goes to Keisuke Kamba for instructing me from zero in the beginning. Deeply thank to Ryo Iwaoka and Yudai Yamaoki for their kind advices. I wish to express my special thanks to Li Wan, it was nice to have him here for rooting for each other.

I am grateful for having a nice time in studying in the topic of GE together with Akiho Hiyama. I also want to thank Yuki Ueyama for making the MnP together. I would like to express my thanks to Huyen Nguyen, Wan Hasnidah Wan Osman, Wangsamihardja Andry, Yuta Sakai and Kenneth Teo for sharing their opinions and inspiring results in the similar research field.

I wish to express my sincere appreciation to my reliable tutors, Masato Tsumura and Hironao Sakai, for their openhanded helping. They have brought me a joyful time. I would like to express my gratitude to my dear lab members, Yoshihisa Kagiya, Mamiko Iida, Ayaka Kiyoishi, Kazuma Nagata, Kenshi Takagi, Masayuki Miyake, Nesreen Hamad Abdelgawwad Hamad, Tomohito Igaki, Kuan-heng Lin, Mohammed Oksh Mohammed Mousa, Ning-xin Wang, Shohei Takami, and Wei-hsun Tu, and secretaries Rika Hamada, Reine Saito and Naomi Murakami; their daily company and assistance have colored my life.

I am indebted to my friends for their listening and for being there by my side. My special thanks goes to Yen-chun Lee, Kuan-hsun Huang, and Zhen-jiang Chen for their suggestions and inspiration toward scientific research.

I appreciate the scholarships provided by Japan Student Services Organization for half-year and Japan Taiwan Exchange Association for two-and-half year with no obligation, I understand that I have a duty to devote in improving relationship between our two countries throughout my life.

I am beyond words in gratitude to my family, my lovable parents, sister and her family, for supporting me spiritually in every way. I am extremely blessed to have them always be there for me.

Meng-I Lin
Laboratory of Bioenergy, Department of Fundamental Energy Science
Graduate School of Energy Science, Kyoto University
Sep, 2018